WNSD/HYDRO-90-03

Westinghouse

EFFECTS OF STREAMWISE PRESSURE GRADIENTS ON TURBULENCE STRUCTURE IN THE VISCOUS LAYER

Donald M. McEligot
Hydrothermodynamics Research and Technology
Westinghouse Electric Corporation
Naval Systems Division
(formerly Gould/Ocean Systems Division)
62 Johnnycake Hill
Middletown, Rhode Island 02840 USA

and

Helmut Eckelmann
Max Planck Institut für Strömungsforschung
D3400 Göttingen, BRD

13 July 1990

Annual Technical Report for Period 14 July 1989 to 13 July 1990
Contract Number N00167-89-C-0048

Prepared for
APPLIED HYDRODYNAMICS RESEARCH PROGRAM
OFFICE OF NAVAL RESEARCH (Code 1215)
800 North Quincy Street
Arlington, Virginia 22217-5000

Submitted to
DAVID TAYLOR RESEARCH CENTER
Code 1505
Bethesda, Maryland 20084-5000

REPORT DOCUMENTATION PAGE

Form Approved
OPM No. 0704-0188

1. AGENCY USE ONLY (Leave Blank)	2. REPORT DATE	3. REPORT TYPE AND DATES COVERED
	13 July 1990	Annual Technical Report 14 July 1989 to 13 July 1990

4. TITLE AND SUBTITLE

Effects of streamwise pressure gradients on turbulence structure in the viscous layer

5. FUNDING NUMBERS

Contract
N00167-89-C-0048

6. AUTHOR(S)

Donald M. McEligot (Westinghouse) and Helmut Eckelmann
(Max Planck Institut fuer Stroemungsf., Goettingen, BRD)

7. PERFORMING ORGANIZATION NAME(S) AND ADDRESS(ES)

Westinghouse Electric Corporation
Naval Systems Division, Hydrothermodynamics Research
62 Johnnycake Hill, Middletown, RI 02840

8. PERFORMING ORGANIZATION REPORT NUMBER

WNSD/HYDRO-90-03

9. SPONSORING/MONITORING AGENCY NAME(S) AND ADDRESS(ES)

Office of Naval Research (Code 1215). Arlington, VA 22217-5000
David Taylor Research Center (Code 1), Bethesda, MD 20084-5000

10. SPONSORING/MONITORING AGENCY REPORT NUMBER

None

11. SUPPLEMENTARY NOTES

12a. DISTRIBUTION/AVAILABILITY STATEMENT

Approved for public release
Distribution is unlimited

12b. DISTRIBUTION CODE

13. ABSTRACT *(Maximum 200 words)*

In order to provide bases for hydroacoustic models predicting wall pressure fluctuations in turbulent boundary layers, time series measurements with an X-probe and a wall shear stress sensor were obtained simultaneously in an oil channel both for fully-developed and for laterally-converging flows. Data were concentrated in the viscous layer at y^+ = 5, 7, 10, 15, 25 and centerplane for $K_p = (\nu/\rho u_\tau^3)dp/dx$ = -0.008 to -0.02 (slight to highly favorable pressure gradients). Results presented include comparisons of the profiles of the mean statistics, plus correlations, of u, v, uv and τ_w. The mean profile $u^+(y^+)$ increased and the correlation coefficients $R_{uu}(y^+ \approx 15, \tau^+)$, $R_{uv}(15,\tau^+)$ and $R_{u\tau}(15,\tau^+)$ broadened with an increase in the magnitude of K_p over this range. However, the turbulence statistics $u'(y^+)/u_\tau$, $v'(y^+)/u_\tau$, $S_u(y^+)$ and $F_u(y^+)$ as well as the maximum amplitudes of $R_{uv}(15, \tau)$ and $R_{u\tau}(15, \tau)$ suffered no significant effect.

14. SUBJECT TERMS

Hydrodynamics, hydroacoustics, fluid mechanics, turbulence structure, hot film anemometry, viscous wall layer

15. NUMBER OF PAGES

104

16. PRICE CODE

17. SECURITY CLASSIFICATION OF REPORT	18. SECURITY CLASSIFICATION OF THIS PAGE	19. SECURITY CLASSIFICATION OF ABSTRACT	20. LIMITATION OF ABSTRACT
UNCLASSIFIED	UNCLASSIFIED	UNCLASSIFIED	UNLIMITED

NSN 7540-01-280-5500

Standard Form 298, 880922
Prescribed by ANSI Std. 239-18
299-01

EFFECTS OF STREAMWISE PRESSURE GRADIENTS ON TURBULENCE STRUCTURE IN THE VISCOUS LAYER

by

Donald M. McEligot and Helmut Eckelmann

ABSTRACT

In order to provide bases for hydroacoustic models predicting wall pressure fluctuations in turbulent boundary layers, time series measurements with an X-probe and a wall shear stress sensor were obtained simultaneously in an oil channel both for fully-developed and for laterally-converging flows. Data were concentrated the viscous layer at y^+ = 5, 7, 10, 15, 25 and centerplane for $K_p = (\nu/\rho u_\tau^3)dp/dx$ = -0.008 to -0.02 (slight to highly favorable pressure gradients). Results presented include comparisons of the profiles of the mean statistics, plus correlations, of u, v, uv and τ_w. The mean profile $u^+(y^+)$ increased and the correlation coefficients $R_{uu}(y^+ \simeq 15, \tau^+)$, $R_{uv}(15,\tau^+)$ and $R_{ut}(15,\tau^+)$ broadened with an increase in the magnitude of K_p over this range. However, the turbulence statistics $u'(y^+)/u_\tau$, $S_u(y^+)$ and $F_v(y^+)$ as well as the maximum amplitudes of $R_{uv}(15, \tau^+)$ and $R_{ut}(15, \tau^+)$ suffered no significant effect.

TABLE OF CONTENTS

TABLE OF FIGURES

NOMENCLATURE

A_s	surface area
a_1, a_2, a_3, ..	calibration coefficients
e	voltage signal
f	frequency; f_b, bursting frequency
h	convective heat transfer coefficient
p	pressure
q	heat transfer rate
R	resistance
s	plate spacing
T	temperature
t	time
U	streamwise mean velocity component
u	streamwise velocity component
u_τ	friction velocity, $\sqrt{\tau_w/\rho}$
V	bulk velocity, also V_b
v	normal velocity component
x	streamwise coordinate
y	normal coordinate
z	spanwise coordinate

Greek letters

α	thermal coefficient of electrical resistance
δ	boundary layer thickness
μ	viscosity
ν	kinematic viscosity, μ/ρ
Θ	anemometer overheat
ρ	density
τ	shear stress; also lead time in correlation; τ_w, wall shear stress

Non-dimensional parameters and variables

C_f	skin friction coefficient, $2\tau_w/\rho u_\infty^2$ or $2\tau_w/\rho v_b^2$
F	flatness factor
f	frequency

NOMENCLATURE (Cont'd.)

K_p	streamwise pressure gradient, $(\nu/\rho u_\tau^3)dp/dx$
K_v	acceleration factor, $(\nu/V_b^2)dV_b/dx$; K_u, based on freestream velocity, $(\nu/u_\infty^2)du_\infty/dx$
Re	Reynolds number, $2V_b s/\nu$; Re_s, based on plate spacing, $\bar{u}_c s/\nu$ [Eckelmann, 1974]
R_{ij}	correlation coefficient, $u_i(t) \cdot u_j(t-\tau)/u_i' u_j'$
S	skewness factor
y^+	normal coordinate, yu_τ/ν
τ^+	lead time in correlation, $\tau u_\tau^2/\nu$

Subscripts and other symbols

b	bulk, bursting
c	centerplane
w	wall
∞	freestream
$\bar{(\ )}$	mean value
$\tilde{(\ )}$	instantaneous value
$(\ )'$	mean root square of fluctuation

EFFECTS OF STREAMWISE PRESSURE GRADIENTS ON TURBULENCE STRUCTURE IN THE VISCOUS LAYER

D.M. McEligot and H. Eckelmann

1. BACKGROUND

The structure of a turbulent boundary layer (TBL) determines its radiated noise and self noise characteristics. For most submersibles, if boundary layer control is not employed effectively, the boundary layers near the nose and near hull arrays are turbulent. Along a submersible, the streamwise pressure gradient is typically highly favorable at first (inhibiting transition and stabilizing TBLs after transition) and successively less favorable until the location of $C_{p,min}$ is reached; then it is unfavorable.

"Strong" favorable pressure gradients have been found to reduce viscous drag by altering the structure of the turbulent velocity fluctuations. Reductions in velocity fluctuations and wall shear stress fluctuations are expected to reduce pressure fluctuations. Evidence for this expectation is seen in models of the wave-vector-frequency spectrum of wall pressure fluctuations that vary with the friction velocity, $u_\tau = (\tau_w/\rho)^{1/2}$, such as the one by Chase [1980]. With a favorable non-dimensional pressure gradient K_p on the order of -0.03 an apparent "laminarization" of a turbulent boundary layer can occur [Narasimha and Sreenivasan, 1979; McEligot, 1986].

Leehey [1985] notes that the low wavenumber component of the wall pressure spectrum is a potentially important source of structural excitation and consequent inward radiation of sound to sonar transducers. Landahl [1975] suggested that unsteady shear stresses should contribute significantly both to radiation and to the low wavenumber component of the wall pressure spectrum. Measurements by Martini, Leehey and Moeller [1984] show that the low wavenumber component may be consistent with a shear stress source.

Data on the effects of streamwise mean pressure gradients on wall pressure fluctuations are limited. For example, the extensive, critical review by Willmarth [1975] cites measurements only by Schloemer [1966], Bradshaw [1967],

Lim [1971] and Burton [1973] for the effect of streamwise pressure gradient on wall pressure fluctuations. The more recent review of Simpson, Ghodbane and McGrath [1987] adds only airfoil data for adverse pressure gradients by Hahn [1976] and Brooks and Hodgson [1981] to this short list. Their own data on wall pressure frequency spectra concentrate on a separated turbulent boundary layer; they found that τ_{max} seemed to be a better measure of the stress to use to scale p' than τ_w (however, for a favorable pressure gradient, $\tau_{max} \simeq \tau_w$).

Blake [1986] compared spectra from measurements in adverse pressure gradients without successfully correlating them. He noted that the spectrum shape apparently depends on the upstream history of the boundary layer development, since there is no correlation of the results with Reynolds number, wall shear stress or pressure gradient.

There are three well known models of wall pressure spectra describing the turbulent boundary layer flow noise; they are by Corcos [1963, 1967], Chase [1980] and Ffowcs-Williams [1982]. An excellent review and assessment of the engineering applicability of the above three models was given by Hwang and Geib [1983]. They examined the wavevector-frequency spectrum of the turbulent boundary layer wall pressure in the intermediate and high frequency range. Their intercomparisons showed that both the Corcos and Chase models are suitable for engineering applications; however, computation with the Ffowcs-Williams model could not be pursued due to the still-unknown functions required in that model. In general, the Chase model gave better results and the spectrum corresponding to q_o is sufficiently accurate for engineering applications. Engineering application of this modified spectrum to establish the flow noise over a submersible may be a feasible approach coupled with other correction factors due to pressure gradients, surface curvature, etc.

For negligible pressure gradients, theoretical models due to Kraichman [1956], Meng and Lovett [1985] and others have demonstrated relationships between the wall-pressure frequency spectrum and the integral of the mean square velocity in the boundary layer. From the scaling analysis of Meng and Lovett, one finds that for incompressible flow the wall pressure spectrum may be expressed as

$$p(0,k,\omega) = \frac{\rho\kappa}{2(2\pi)^3} \int_0^\infty e^{-\kappa y} \left[\iiint_{-\infty}^{\infty} u^2 \, e^{i(\vec{k}\cdot\vec{x} - \omega t)} d^2\vec{x} dt \right] dy$$

where κ is the magnitude of the two-dimensional vector wavenumber in the plane of the wall and ω is the frequency. This relation is the basis of a proposal by Meng to determine the wall pressure spectrum via LDA measurements. His order-of-magnitude analysis indicates that high wavenumber variations are due to fluctuations in the linear layer ($y^+<5$), convective peak variations from the viscous layer ($y^+<30$) and low wavenumber contributions from the outer region. However, with favorable pressure gradients these regions are thickened so their related wavenumber spectral regions are shifted, e.g., the viscous layer can begin to affect the low wavenumber component.

For significant transverse curvature, as in a small diameter towed-array, Chase [1981] examined the possible scaling of the axisymmetric component of spectral density of wall pressure with a low-wavenumber expansion in terms of fluctuating Reynolds stresses as sources. A model of the sources was formed based on similarity near the wall (e.g., fixed mixing length function). For low wavenumbers he developed a relationship of the form

$$P_o^o(k,\omega) = C_2 \rho^2 u_\tau^3 \, fn\{k,\omega\}$$

where u_τ is the friction velocity $\sqrt{\tau_w/\rho}$.

Panton and Linebarger [1974] derived wall-pressure wavenumber spectra for zero-pressure gradient and adverse-pressure-gradient equilibrium boundary layers based on Coles' laws of the wall and wake and on turbulence structure being invariant with pressure gradient. There appear to be no models of the wall-pressure wavenumber spectra that take into account the effects of favorable streamwise pressure gradients on the turbulence contributions to the source terms.

Handler, Hansen, Sakell, Orzag and Bullister [1984] obtained predictions of the wall pressure field $p(x,z,t)$ for fully-developed flow in a channel by direct solution of the time-dependent Navier-Stokes equations. Presumeably,

the comparable calculations by Kim, Moin and Moser [1987] could be analyzed to provide the same sort of information; for $tu_\tau/\omega = 10$, this case required O(2 CPU weeks) with a CRAY-XMP computer. How to extend these techniques to turbulent boundary layers with significant pressure gradients is not a trivial question (but the work herein should provide useful tests of some aspects of such predictions).

Hydrodynamic boundary layer predictions can be used to predict the local boundary layer characteristics with pressure gradients, streamwise curvature, etc., so, conceptually, models such as the ones by Chase [1980, 1981] and Panton and Linebarger [1974] could be used to predict wall pressure spectra. The question is whether the turbulence structure is invariant under these phenomena as implied in these models. Measurements of the fluctuating wall shear stress in favorable pressure gradients by Chambers, Murphy and McEligot [1983] indicate it probably is not; for example, the non-dimensional bursting frequency varies with pressure gradient.

Only a few experiments have measured the instantaneous turbulence structure simultaneously with the wall pressure signal, and these have been in zero pressure gradients or fully developed flow. Zakkay, Barra and Hozumi [1979], Thomas and Bull [1983] and Kobashi, Komoda and Ichijo [1984] essentially used wind tunnels and Dinkelacker and Langeheineken [1982; Langeheineken, 1981] at the Max Planck Institut für Strömungsforschung conducted their measurements in fully-developed air flow in a circular tube. All confirmed that the wall pressure fluctuations were related to the turbulent velocity fluctuations. (Since different detection criteria were used these investigations cannot be compared directly.)

Thomas and Bull [1983] measured instantaneous wall pressure and wall shear stress simultaneously, then by conditionally sampling and averaging they were able to examine and compare their characteristic signatures. Thomas and Bull and the other investigators showed that the wall pressure signal was related to the bursting phenomena [Blackwelder and Kaplan, 1976] of turbulent flow.

2. PREVIOUS WORK

As noted above, it is possible to predict the fluctuating pressure field if the turbulence structure of the fluctuating velocity field is known. This section summarizes the studies of the turbulence structure, aimed towards concentration on flows with favorable streamwise pressure gradients.

In an internal flow, a favorable streamwise pressure gradient is induced by a convergence - either lateral or transverse - leading to a spatial acceleration of the flow. For external flows, the body shape near the nose or leading edge induces a favorable pressure gradient and, via Euler's equation, acceleration of the freestream flow.

While the details of many accelerating flows have been extensively studied [Narasimha and Sreenivasan, 1979; Murphy, 1979], only McEligot and colleagues appear to have utilized lateral convergence between parallel plates to examine turbulent flows with positive streamwise pressure gradients [Murphy, Chambers and McEligot, 1983; Chambers, Murphy and McEligot, 1983]. In the idealized problem (Fig. 2.1) the velocity is uniform at an entry at a large distance. The flow develops and may approach a fully established profile. Near the exit of the convergence, acceleration dominates the flow in the center of the duct, causing a flattening of the profile. The profile takes the appearance of an external boundary-layer flow, with a large central core flanked on both sides with thin boundary layers. The boundary layers become successively thinner as acceleration continues. Depending on the entrance length and flow rate, the regime may be laminar or turbulent, or an initially turbulent flow may approach a laminar flow owing to the stabilizing effects of acceleration, i.e., 'laminarization' may occur.

Several authors have proposed various non-dimensional parameters involving either velocity, pressure or shear-stress gradients which purportedly serve as guides to the likelihood of laminarization. Kline et al. [1967] noticed that turbulent bursts ceased when an acceleration parameter $K_u = (\nu/u_\infty^2)du_\infty/dx$ reached a critical value of 3.7×10^{-6}. Jones and Launder [1972] found that the peak Reynolds stress due to turbulence became a progressively smaller fraction of the wall shear stress as K_u increased. They indicated that a turbu-

lent flow could no longer exist when K_u exceeded a critical value somewhere between 2.5×10^{-6} and 3.5×10^{-6}. Blackwelder and Kovasznay [1972] found that, when K_u exceeded the above critical values, the viscous-sublayer thickness increased, the skin-friction coefficient at the wall decreased, and large departures from the turbulent logarithmic law of the wall occurred.

Patel [1965] also noted major departures from the logarithmic law, but correlated his results in terms of a pressure-gradient parameter $K_p = (\nu/\rho u_\tau^3)dp/dx$. Patel and Head [1968] suggested 0.018 for a critical value of K_p. They also suggested that a more appropriate laminarization parameter might be defined by replacing the pressure gradient with the shear stress gradient at the wall $(\partial\tau/\partial y)_w$; we shall call it K_τ. Since the gradient $\partial\tau/\partial y$ is evaluated at the wall, where the convective terms in the boundary-layer momentum equation are zero, $dp/dx = (\partial\tau/\partial y)_w$ for flow between parallel plates, whether fully developed or accelerating; for fully developed pipe flow $dp/dx = 2Mt(y)/My$. For transitional pipe flow Patel and Head found that with the present nomenclature $K_p = 2K_\tau = 0.018$, whereas for transitional flow between parallel plates they found that $K_p = K_\tau = 0.009$. On the basis of consistency, then, they concluded that K_τ was a better guide to the possibility of laminarization and that its critical value was 0.009 or so. They also suggested that the downstream distance required to reverse transition completely must be dependent upon the Reynolds number based on momentum thickness, $R_2 = u_\infty \delta_2/\nu$. Narasimha and Sreenivasan [1973] pointed out that the critical value of K_τ should have been 0.004, owing to algebraic errors. They concluded that laminarization was due to domination of pressure gradients over the Reynolds stresses and, therefore, the parameter K_p incorporating the pressure gradient was recommended. In addition, they pointed out that parameters such as K_u, K_p and K_τ cannot be universally useful for all levels of acceleration. When the acceleration is very low, as in a nearly fully developed duct flow, the flow and its state of turbulence revert to their equilibrium values and the local Reynolds number then provides the best guide to the possibility of laminarization.

From measurement of the local Nusselt number in strongly heated gas flow in a circular tube, McEligot [1963] detected premature transition from turbulent flow towards laminar flow. He proposed the explanation to be a thickening

the viscous sublayer and correlated the flow regimes in terms of a non-dimensional heating rate and inlet Reynolds number. The correlation was later shown by McEligot, Coon and Perkins [1970] to be related to an acceleration parameter $K_v = (\nu/V^2)dV/dx$ based on the bulk velocity. This parameter K_v is a version of K_u appropriate for internal flows. Another Reynolds-number criterion was proposed by Bradshaw [1969], who postulated that a turbulent flow would become directly dependent upon viscosity, i.e., laminarizing, when the energy-containing and the dissipation ranges of eddy size overlap. This led to a critical 'eddy' Reynolds number $R_{eddy} = u_\tau L/\nu = 12$, where L is the dissipation-length parameter u_τ^3/ε and ε is the dissipation rate.

Badri Narayanan and Ramjee [1969] attempted to meld these diverse observations into a unified structure by describing reverse transition in three consecutive states: (i) the disappearance of the turbulent bursts near the wall at $K_u \simeq 3 \times 10^{-6}$; (ii) breakdown of the law of the wall at $K_p = 0.02$; and (iii) the decay of turbulence intensity starting at $R_2 = 300\text{-}400$. While at first glance this description seems to accommodate all the observations reported above, stage (iii) strongly implies that the completion of laminarization is controlled by a critical value of R_2, whereas Launder and Jones [1969] suggested that K_u was the critical parameter. In summary, there still remain significant uncertainties not only in the precise values of the dimensionless parameters to employ as criteria, but also as to which parameter is the best to use in predicting the occurrence of laminarization.

For single phase boundary layers on flat plates with zero pressure gradient or in fully-developed duct flow, a large number of studies have detailed the turbulence structure by flow visualization and hot-wire or hot-film anemometry [Corino and Brodkey, 1969; Kim, Kline and Reynolds, 1971; Eckelmann, 1974; Johansson and Alfredsson, 1982; etc.]. At the Max Planck Institut für Strömungsforschung, Eckelmann [1974] and his colleagues [Wallace, Brodkey and Eckelmann, 1977; Randolph, 1983; Haritonidis and Johansson, 1985, etc.] have developed techniques for structure measurements in their unique oil channel, designed originally by Reichardt to give excellent spatial resolution. The use of oil also leads to higher temporal resolution of fluctuating components than in the common fluids, air and water.

The bursting phenomenon in the viscous layer has been described well by Corino and Brodkey [1969], Kline et al. [1967], Offen and Kline [1974] and others, as well as in reviews by Willmarth [1975] and Cantwell [1981], so only the literature pertinent to the present study will be reviewed here. With Kim, Kline and Reynolds [1971] and Blackwelder and Kaplan [1976], we adopt the term 'bursting' or 'bursting phenomenon' for the overall process. For convenience in description, the phases of the process will be termed (a) a deceleration or ejection, (b) a rapid acceleration or sweep, and (c) a relatively quiescent process, or more gradual deceleration following the sweep. Blackwelder and Kaplan [1976] have demonstrated one version of the typical bursting signal by conditional averaging of the fluctuation in the streamwise velocity component. (Hereinafter we will usually refer to their paper as BK.) With calculations based on a theoretical model for coherent structures in wall turbulence, Landahl [1980] has found qualitative agreement with their conditionally sampled data.

From examination of the simultaneous measurements of $u(t)$ and $\partial u(t)/\partial y$, Eckelmann [1974] showed that the fluctuating shear-stress signal from a wall shear-stress sensor correlates with velocity fluctuations measured with hot wires positioned in the flow at dimensionless distances from the wall of up to $y^+ \simeq 25$. Eckelmann's correlation indicates that the temporal history of either the shear-stress signal or the fluctuating streamwise velocity component (u) should provide a reasonable picture of turbulent events in the viscous layer, $0 < y^+ < 30$ in unaccelerated flows. In addition, Brown and Thomas [1977] have shown that the low-frequency fluctuations of a wall-shear sensor can be correlated with the low-frequency fluctuations of a velocity sensor for the range $0.05 < y/\delta < 0.75$ in a turbulent boundary layer. Eckelmann [1980] notes that the detailed similarity between the two signals decreases with distance from the wall, so one must investigate whether one sees the same burst at $y^+ \simeq 15$, the triggering location of BK, and at the wall.

A second question concerns the appropriate scaling of the bursting frequency f_b in non-accelerated flows. As discussed below, some investigators have suggested non-dimensionalization with respect to a characteristic time for the wall, or inner region, $\nu/(u_\tau)^2$; others advocate a time characteristic of the outer region, δ/U_∞. For a fully developed internal flow, the two resulting

non-dimensional times can be related through their definitions as

$$\frac{(u_\tau)^2}{\nu f_b} = \frac{1}{2} c_f Re_D \frac{V}{D_h f_b} = \begin{cases} \frac{1}{8} c_f Re_D \frac{2V}{s f_b} & \text{for ducts,} \\ \frac{1}{4} c_f Re_D \frac{V}{r_w f_b} & \text{for pipes,} \end{cases}$$

where Re_D is the Reynolds number based on hydraulic diameter D_h and bulk velocity V, and w has been interpreted as s/2, the half-spacing of a duct, or r_w, the radius of a pipe. Thus if a relationship can be found for one, it can be transformed to the other since empirical relationships for $c_f(Re_D)$ exist.

The question has been one of whether either scaling will give a non-dimensional time or frequency which is independent of Reynolds number. The question of scaling is an important one for a better understanding of turbulent behavior because inner scaling implies that the lift-up of the low-speed streak and the subsequent ejection [Offen and Kline, 1974] are derived from a wall-flow instability; theoretical models showing such instabilities have been proposed [Black 1968]. (However, these instabilities cannot be unambiguously accepted as the causes of bursting because the instability models usually require [Black 1968] that the streamwise velocity of the ejected fluid be greater than the local mean velocity corresponding to the y^+ position of the ejection, rather than the velocity deficit actually observed.) Supporting evidence for inner scaling is offered by the flow-visualization data of Offen and Kline [1974], who found that sweeps, low-speed-streak lift-ups, and bursts were intimately connected; indeed, 'sweeps initiate bursts', and 'sweeps originate in the inner layer'.

Outer scaling implies that the bursting process is imposed by large disturbances already present in the outer flow. However, even Rao, Narasimha and Badri Narayanan [1971], early proponents of outer scaling, admitted that the 'origin of the bursting phenomenon cannot be traced directly...to the outer interface'. Outer scaling has its theoretical support, too. The analysis by Schubert and Corcos [1967] attempted to view the inner layer as driven by the outer flow, but failed to predict Reynolds stresses of the right order. Brown and Thomas [1977] inferred from their measurements that the low-frequency fluctuations of the wall shear stress are possibly driven by large-scale structures.

Attempts to resolve the scaling issues experimentally have yielded mixed results. Black [1966] found that the bursting frequencies scaled with wall variables so that $(u_\tau)^2/\nu f_b \simeq 110$. Kline et al. [1967] reported essentially the same finding for a boundary-layer flow, as did Corino and Brodkey [1969] for fully developed flow in a pipe. Sharma and Willmarth [1980] found the non-dimensional bursting frequency to be approximately constant over the range $1 \tilde{<} y^+ \tilde{<} 17$ when based on wall variables (this observation provides further support for the use of a wall-mounted sensor to investigate the bursting process). In contrast, Rao et al. [1971] suggested that outer scaling resulted in Reynolds-number independence for unaccelerated flows, and that $U_\infty/\delta f_b = 5$ or $U_\infty/\delta^* f_b = 32$, where δ^* is the displacement thickness.

A variety of techniques has evolved to identify and measure turbulence and its coherent structures. Among the most popular are the VITA technique [Blackwelder and Kaplan, 1976] and quadrant splitting [Wallace, Eckelmann and Brodkey, 1972]. There has been concern about the various detection techniques and their consequent conditional averages [Johansson and Alfredsson, 1982] and several studies with negligible pressure gradients have been devoted to their comparison [Subramanian et at., 1982; Alfredsson and Johansson, 1984; Luchik and Tiederman, 1987]. Luchik and Tiederman found all they examined to yield the same average time between bursts but different techniques showed different advantages.

Additionally, the finding of Rao et al., was based upon wind-tunnel measurements in which a single hot-wire signal was differentiated and a discrimination level varied to obtain a maximum f_b for each run. (It was stated that, as the discrimination level was set either too low or too high, f_b would decrease.) Offen and Kline [1974] indicate that such burst detection by a single sensor using autocorrelations has little chance of success, except very near the wall, because the individual bursts vary greatly in size. Thus detection techniques based upon spatial rather than temporal coherence are preferred. Flow-visualization studies, such as those by Kline et al. [1967] and Corino and Brodkey [1969], emphasize the more easily detected spatial coherence of bursts. A fixed point sensor can only measure the less organized temporal behavior of the flow. Using the same apparatus as Kline et al., Kim

et al. [1971] determined bursting frequencies for two flows from visualization studies and from the disputed autocorrelation method with a hot wire at $y^+ = 14$. Because the Reynolds numbers of the two flows were nearly equal, the results could be interpreted as supporting either inner or outer scaling.

Strickland and Simpson [1975] measured bursting frequencies in two ways: (i) the time between peaks in the autocorrelation of a wall-mounted shear-stress sensor was taken as a measure of the time between bursts, giving f_{b_1}, and (ii) f_{b_2} was taken to be the frequency at the maximum in the first moment of the curve of power-spectral-density versus frequency. They found agreement of the two frequencies to within 15%. While $U_\infty/\delta f_b$ ranged from 7 to 14, in fair agreement with Rao et al., most of the flows examined were decelerating flows. For the two runs where the flow was mildly accelerated, $U_\infty/\delta f_b$ was approximately 11, twice the value recommended by Rao et al. The Reynolds numbers of the two flows were close enough (Re_θ =2240 and 3520) that, had a Reynolds-number dependence existed, it would not have been easily apparent. Indeed, in related work Strickland [1973] reported a weak Reynolds-number dependence.

Wallace, Brodkey and Eckelmann [1977] attempted to recognize bursts using a pattern-recognition technique based upon the time derivatives of hot-wire velocity sensors. They found that $U_\infty/\delta f_b$ ranged from 5 at $y^+ = 3$ to 2 at $y^+ = 300$. Although the agreement with Rao et al. was apparently good, only a single flow was investigated, so that Reynolds-number independence was not substantiated. Blackwelder and Kaplan [1976], using the variable-interval time-averaging (VITA) technique, also reported that $U_\infty/\delta f_b \simeq 2.8$, but, again, essentially only one Reynolds number was examined.

With a direct numerical simulation, Kim and Spalart [1987] examined the scaling of the bursting frequency for momentum Reynolds numbers, $300 < Re_\theta < 1410$. They concluded that the frequency scaled by inner variables is essentially independent of Reynolds number.

Quantitative turbulence structure measurements with pressure gradients are sparse. In general, they are limited to data with a single sensor (no statis-

tics) due to probe size concerns using air or water as the fluid. Jones and Launder [1972] found that the peak Reynolds stress due to turbulence became a progressively smaller fraction of the wall shear stress as $K_u = (\nu/u_\infty^2)du_\infty/dx$ increased. In a study of large scale motion Blackwelder and Kovasznay [1972] found that, when K_u exceeded "critical" values, the viscous-sublayer thickness increased, the skin-friction coefficient at the wall decreased, and large departures from the turbulent logarithmic law of the wall occurred; to some extent these aspects can be predicted using advanced (and some simple) turbulence models [Rodi, 1980; McEligot, 1986]. Simpson [1979] observed that the spacing of streamwise vortices in the wall region seems to increase with K. Finnicum and Hanratty [1987] measured wall shear stresses in pulsating flows and compared them to steady flow. Recently Tiederman and colleagues have begun the measurement of turbulence structure with adverse pressure gradients [White and Tiederman, 1990].

Analyses predicting the effects of streamwise pressure gradient on turbulent boundary layers are now available from the work of Spalart [1986] and of Finnicum and Hanratty [1988]. Spalart conducted direct numerical simulations of sink-flow boundary layers with acceleration parameters K_u between 1.5×10^{-6} and 3.0×10^{-6}. He solved the three-dimensional, time-dependent Navier-Stokes equations using a spectral method. Predicted effects of the favorable pressure gradients were to extend and displace the logarithmic layer and to alter the energy balance of turbulence near the edge of the boundary layers. Relaminarization was predicted for $K_u = 3.0 \times 10^{-6}$. Reasonable agreement was found with the spatial spectra deduced by Jones and Launder [1972] from their time spectra data at $K_u = 1.5 \times 10^{-6}$ except that Spalart's computed spectra did not collapse versus y. In general his results suggested that the logarithmic behavior of the mean velocity is more universal than the linear behavior of the mixing length.

Finnicum and Hanratty applied the 2-1/2D computational model of Nikolaides [1984] with bursting periods and streak spacing taken to vary as the ratio between the wall shear stress and the mean shear stress at the assumed edge of the viscous layer (y_o^+). Empirical results were used for skin friction coefficients. Phase relations at y_o^+ were assumed to be unchanged by the pressure gradient. For a range $K_u = 0$, 2.0×10^{-6} ("moderate") and 2.8×10^{-6} ("close to relaminarization") they predicted mean statistics of u and v and appropriate

terms for kinetic energy balances. Good agreement was seen with the direct numerical simulations of Spalart [1986].

3. STUDIES BY PRINCIPAL INVESTIGATOR AND COLLEAGUES

For laterally converging laminar flow between parallel plates, Murphy, Coxon and McEligot [1978] extended the numerical approach of Bankston and McEligot [1970], as well as developing a similarity solution. Murphy, Chambers and McEligot [1983] then applied the numerical program to the conditions of an experiment they conducted with turbulent and apparently laminarizing air flow converging between two plates separated by 1.3 cm (1/2 in.). The test section had a sharp-edged entrance to induce a transition to turbulent flow and side rails, whose angle could be adjusted to vary the acceleration parameter and Reynolds number independently (Figure 3.1). With streamwise acceleration the flow was continuously developing through the entry region and downstream. Measurements were restricted to streamwise pressure distributions and wall shear stress, since the spacing necessary was too small to introduce probes into the flow to determine the velocity distribution. By comparison between data and predictions, they found substantial effects to occur with convergence angles as small as 4^{o} and showed that the results could be explained by a thickening of the viscous layer.

In the same apparatus Chambers, Murphy and McEligot [1983] applied conditional sampling, by the VITA technique of Blackwelder and Kaplan [1976], to the instantaneous measurements of wall shear stress (Figure 3.2). They found the typical burst pattern, or conditionally-averaged time history of the wall shear stress, resembled the time history of the streamwise velocity component measured by Blackwelder and Kaplan at $y^{+} = 15$. Families of conditionally-averaged time histories were selected at approximately equal Reynolds numbers and varying acceleration parameters to compare with the results for fully developed flows. Figure 3.2 presents typical results at a Reynolds number of about 12,000. Additional families were compared at Re $\simeq$ 8,000, 18,000 and 23,000 with the same qualitative conclusions.

At a given Reynolds number, there is no large variation in the shape of the time-averaged signals until the acceleration parameter reaches $K_{V} \simeq 2 \times 10^{-6}$.

That is, the sweep pattern is essentially invariant until K_v approaches this value even though the non-dimensional bursting frequency begins to drop considerably for $K_v > 1 \times 10^{-6}$. At higher values than $K_v \simeq 2 \times 10^{-6}$ the recovery or decay of the sweep phase becomes slower than in the fully developed or moderately converging runs.

For fully developed flows (convergence angle = 0) wall scaling of the bursting frequency was found to be essentially independent of Reynolds number. The effects of laterally converging flows upon bursting frequencies are apparent in Figure 3.3. No matter how they are scaled, all the dimensionless frequencies suggest a significant decrease in f_b or increase in its inverse, the average period, as K_v increases.

Focusing upon the inner scaling of f_b, shown to be the most appropriate scaling in the case of fully developed flows, one finds that as K_v decreases towards 10^{-7} the bursting frequency approaches the values observed for fully developed turbulent flows. At $K_v \simeq 1 \times 10^{-6}$, $u_\tau^2/\nu f_b$ is 300, nearly 70% higher than the value at $K_v = 0$; at $K_v \simeq 2 \times 10^{-6}$ one finds a threefold increase, and $K_v = 3.4 \times 10^{-6}$ indicates a fifteenfold increase, with the curve beginning to tend asymptotically towards infinity. This tendency implies that the flow would be effectively laminar for K_v larger than about 3.4×10^{-6}. This finding is in accord with the data of Murphy, Chambers and McEligot [1983] in the same test section and with the data of Moretti and Kays [1965], Kline et al. [1967], Blackwelder and Kovasznay [1972] and Jones and Launder [1972] in different geometries using other techniques. For laterally converging flows, the measurements of bursting characteristics essentially confirmed the deductions of Murphy, Chambers and McEligot [1983]; the apparent modification of turbulent behavior inferred from comparison of predictions and pressure measurements corresponded with a reduction in the non-dimensional bursting frequency.

For this flow problem, the results of Murphy, Chambers and McEligot can be summarized as follows: 1) for $K_v > 4 \times 10^{-6}$, laminar predictions are adequate for pressure distributions and friction factors, 2) for $K_v < 10^{-7}$, the simple van Driest [1956] model provides reasonable predictions, 3) the temporal wall shear signal was consistent with these observations, and 4) as K_v

increased, the non-dimensional bursting frequency decreased but the conditionally-averaged signal remained approximately constant until large K_V.

In summary there is evidence that the turbulence structure is modified by streamwise pressure gradients and there is a need to determine which features remain relatively invariant and to quantify the variation of the others in order to provide the turbulence structure information needed in hydroacoustic models accounting for their effects.

4. GOAL AND OBJECTIVES

The ultimate goal of this study is to develop practical models of wall pressure spectra in turbulent boundary layers where significant drag reducing phenomena may alter the turbulence structure that is the basis of such models. The next steps are (1) to analyze the turbulence structure for measurements with favorable streamwise pressure gradients, (2) to compare the results to data with drag-reducing additives, and (3) to derive a model for the effects of these phenomena on wall pressure spectra based on the significant variations in turbulence structure deduced in steps (1) and (2). The present objective is to accomplish the first step.

5. APPARATUS

The experiments performed utilized the familiar oil channel at the Max Planck Institut für Strömungsforschung (Figure 5.1a). This unique facility was designed originally by Reichardt to give high spatial and temporal resolution in the viscous layer and has since been developed by Eckelmann [1974] and his colleagues [Wallace, Eckelmann and Brodkey, 1972; Wallace, Brodkey and Eckelmann, 1977; Blackwelder and Eckelmann, 1978; Randolph, 1983; etc.]

The oil channel and procedures employed in its use have been described in detail by Eckelmann [1970, 1974]. In this section we will concentrate on the differences in apparatus and techniques applied for the present study; only a brief overview will be given for the aspects which are common with the earlier work.

The channel is 22 cm wide and 1 m deep with an 8 m length. In contrast to the 1.3 cm spacing in the experiment of Murphy, Chambers and McEligot [1983], the plates forming this oil channel have much larger separation, so area blockage by the probes is negligible. Also, at a Reynolds number of 11,000 a distance of 1 cm corresponds to $y^+ = 17$, permitting high spatial resolution. The use of oil as working fluid leads to higher temporal resolution of fluctuating components than in the common fluids, air and water. Velocity measurements are with commercial hot film probes which are calibrated via a time-of-flight technique moving the support cart along the channel.

For measurements with laterally-converging flow, the channel floor was modified to a convergence angle of 2^o (Figure 5.1b) giving a potential intermediate range of acceleration parameters $1 \times 10^{-6} < K_v < 3 \times 10^{-6}$ as desired to examine conditions where the turbulence structure was expected to be modified. The channel was straightened and reinforced and a new traversing mechanism was designed and constructed for measurements in the entrance half of the channel. Data acquisition programs were modified for digital application of the hot film calibration as a function of the oil temperature at low overheat ratios. Experimental studies of flow-induced vibrations were conducted in order to design probe supports for measurements deep in the channel.

The lateral convergence is induced by a ramp-shaped insert of 2^o which has been placed in the bottom of the open channel, as shown in Figure 5.1b. The oil passes along a return channel of the same length and approximate wall spacing(s) giving $L/s \sim 30$ for flow development before passing through a series of curved vanes in the 180^o bend, which forms the entrance to the test channel. With a typical depth of 80 cm the aspect ratio is about 3.6 for the open channel; with the free surface approximating a zero shear surface, this configuration is comparable to a closed channel with an aspect ratio of seven. This geometry gives mildly three-dimensional velocity distributions away from the edge region (i.e., bottom).

In the test channel the entrance region is $\Delta x/s \sim 15$ for flow development ahead of the convergence section of length $\Delta x/s \sim 17$ to the minimum cross section ("throat"). The main measurements in the converging section are taken

at x/s ≃ 31 (or Δx ≃ s ahead of the throat), where a wall sensor is also mounted.

For direct comparison, measurements approximating fully-developed conditions ($K_V \simeq 0$) were obtained by removing the ramp from the bottom of the channel. Otherwise, locations remained the same.

6. TECHNIQUES AND CALIBRATIONS

The techniques and calibrations employed were essentially those of Eckelmann [1974] except as noted.

6.1 Data acquisition

At the maximum oil velocity of 23 cm/sec, giving Re ≃ 11,000, the hot film signals are sampled for over one hour at 50 Hz to obtain mean values within one per cent. Maximum significant turbulence frequencies are less than 5 Hz and bursting frequencies are estimated to be of the order of 0.1 Hz or less.

Time series data were acquired via a DEC PDP-15 system from four hot-film sensors simultaneously; an X-probe for u(t,y) and v(t,y), a wall element for $\tau_w(t)$ and a single, fixed upstream sensor to serve as a reference. Measurements were taken in the viscous layer ($y^+ \sim 5, 7, 10, 15, 25$) and at the centerplane for $K_V = 1.6 \times 10^{-6}$ and $K_V = 2.4 \times 10^{-6}$ for the cases with streamwise acceleration. These data are stored on digital magnetic tape in the compact format produced by the VAX "backup" utility. Some additional measurements of mean turbulence quantities for fully-developed flow in the same channel are available at the same Reynolds numbers for comparison [Eckelmann, 1974; Randolph, 1983].

The mean signals are approximately suppressed by a constant voltage and then are amplified to improve the accuracy (so-called "buck and gain" technique) before analog-to-digital conversion and storage. Oil temperature is measured manually with a glass thermometer and by "cold" resistance measurements. For the X-probe the overheat ratio is set at about five percent (rather than the more common one or two percent) in order to reduce sensitivity to gradual

temperature variations. Despite control of the room temperature, these precautions are necessary to reduce the uncertainties in the velocities to below one percent.

In data reduction, a subroutine is employed to apply a correction for the (small) difference between operating temperature and calibration temperature, to calculate the velocity across the sensor and, for the X-probe, to apply a calibrated relation for angular dependence to deduce the instantaneous velocity components. These time series of velocity components are integrated to yield the various mean statistics desired.

6.2 Velocity calibration

For both velocity probes the sensors were calibrated by the time-of-flight technique of Ecklemann [1970, 1974]. The support cart for the main station was linked to the one for upstream measurements with a sturdy bar linkage, so the calibration runs were conducted simultaneously.

Microswitches 1 meter apart were connected to an electronic timer to measure the time-of-flight over a calibrated distance. Acceleration to a steady velocity was accomplished before the cart reached the first switch and deceleration occurred after the last. During the motion of the cart between the microswitches the sensor voltages were measured with integrating digital voltmeters.

Oil temperature was measured with a glass thermometer. Although it took two to three hours to obtain the desired ten to fifteen calibration points, the temperature drift during this period was negligible. Therefore, the calibration temperature was taken as the reference temperature for the resulting velocity calibration curves $V_{cal}(e)$ for each sensor.

A least squares approximation procedure, developed by Randolph [1983], was employed to determine the coefficients a_i in fourth-order calibration curves of the form

$$V = a_1 + a_2 e + a_3 e^2 + a_4 e^3 + a_5 e^4$$

Weighting of the calibration points was adjusted to yield agreement within 1/2 percent or better for the difference between the resulting curve and any measured point.

6.3 Temperature correction

During the measurements with flow, the oil temperature was close to the calibration temperature but not necessarily the same, so a correction was applied for the slight difference. Development of the correction factor is summarized in section 7.3 concerning the wall shear sensors.

The oil temperature and/or equivalent cold resistance of the sensor was measured before and after the data acquisition for the run. For the correction the instantaneous measured voltage was adjusted to the value it would have been at the same velocity if the oil had been at the reference temperature. This first order correction was of the form

$$\frac{e_{ref}}{e_{op}} = 1 + \frac{1}{2}\frac{R_{c,op} - R_{c,ref}}{R_{op} - R_{c,op}}$$

Where R_c stands for cold resistance and the subscript op denotes the measuring or operating conditions of the actual run. The correction is actually introduced by adjusting the values of the gain and bucking voltage which the data reduction programs employ to convert the integer digital sample records into equivalent (floating point) voltages.

6.4 Velocity calculation

In some preliminary measurements a single sensor probe was used to measure the streamwise component u. In that case, the velocity was calculated directly from its calibration relation $V_{cal}(e)$ after measuring the anemometer voltage. For the X-probe a cosine approximation was applied via an algorithm employed by Randolph [1983],

$$\tilde{u} = V_{cal,1}\cos^2\alpha_1 + V_{cal,2}\cos^2\alpha_2$$

$$\tilde{v} = (V_{cal,1} - V_{cal,2})\cos\alpha_1\cos\alpha_2$$

where $V_{cal,i}$ represents "calibration velocity" after correcting for temperature, converting to voltage and applying the calibration function $V_{cal}(e)$. The angles of the two wires were measured to be $\pm$ 45.0 degrees by Herr Nortemann who constructed and repaired hot film sensors as appropriate.

In the present work the normal mean velocity $\bar{v}$ was not adjusted to zero, whereas earlier workers with fully developed flows did "correct" the sensor angles to yield $\bar{v} = 0$ before further processing [Randolph, 1983; Brodkey, 1990]. We retained the non-zero result since $\bar{v}$ is not necessarily zero in flows with streamwise acceleration. The deduced fluctuation v is taken around $\bar{v}$ in the same manner that the streamwise fluctuation is determined. Since $\tilde{v}$ is calculated as a small difference between larger quantities, its percent uncertainty is considerably more than that of $\tilde{u}$. The non-zero values of $\bar{v}$ calculated for the fully developed flows (i.e., without ramp) are consequences of that uncertainty and an apparent wall interaction observed by Randolph [1983]. Therefore, for the accelerating flows, in order to decide whether non-zero values of $\bar{v}$ are meaningful, it is necessary to compare to the fully-developed results.

6.5 Wall distance, y

The theodolite technique of Eckelmann [1970, 1974] was employed to set the reference location of the crossing of the sensors of the X-probe to within about $\pm$ 0.1mm. For y < 30mm, a dial indicator with an estimated reading uncertainty of $\pm$ 0.002mm was used to determine transverse locations relative to this reference. Beyond that distance a vernier rule was employed; it could be read to $\pm$ 0.1mm.

The wall distance y (or y^+) is typically used as a coordinate on the profile plots and to identify approximately equivalent locations when comparing accelerated flows with fully developed flows. For these purposes high accuracy is not necessary. While Eckelmann [1974] determined the location y = 0 by linear extrapolation of his near wall data, the present report uses physical measurement of the length of the pin which served for the reference location in the theodolite measurements. A slight correction for displacement of the wall surface (due to pressure differential between the two parallel flow channels, Fig. 5.1) is also included.

Precision is required for the location of the one-point velocity measurement [McEligot, 1984] applied to determine mean wall shear stress (to calculate y^+ and to calibrate the wall sensor). Sensitivity studies showed a typical influence coefficient of the order of unity (see Figure 7.2 later), i.e. a one percent error in y^+ would cause a one percent error in the value of τ_w deduced. For the worst case in this determination, the uncertainty in y^+ was about 0.04 percent so the uncertainty in the velocity measurement dominates the wall shear stress determination.

6.6 Measurement of pressure gradient

With oil, the pressure gradient corresponding to a significant value of K_p is miniscule. Thus, it was difficult to obtain an accurate measurement of dp/dx for determining τ_w and K_p. Several methods were considered and/or attempted.

Static pressure taps were designed and installed by Reichardt along the wall in the original channel. These were no longer useful.

Two pitot-static probes were installed in the channel approximately in the same manner as the X-probe, but displaced longitudinally. The difference between the static pressure taps on the two probes was measured with an MKS Baratron Differential Pressure Meter. We used the most sensitive transducer, one with a span of 1 mm Hg. Unfortunately, the differences in the sizes of the transducer plenums, the length of the necessary tubing (volume considerably greater than transducer) and slight variation in the room temperature led to slow oscillations of the measured differential pressure. The amplitude of these oscillations was greater than the magnitude of the pressure drop so the approach proved to be impractical.

Ultimately a hook gage technique was applied. Essentially, the drop in the oil surface elevation due to flow was measured at several locations for the flow rates of interest. The pressure gradient dp/dx was then approximated as $\Delta z/\Delta x$ with flow. Precision of the individual measurements was about 0.05 mm which propagated to an estimated experimental uncertainty of 0.14 mm for Δz (the per cent uncertainty of Δx was negligible). Since measurements of Δz varied from 0.15 to 0.5 mm for the range of interest, the estimated experi-

mental uncertainty in dp/dx and K_p is large (100 to 30 per cent, respectively!).

The consequent estimates of K_p can be considered to be little better than order-of-magnitude estimates. However, their consistency gives confidence that meaningful comparisons of the various results can be made in order to examine the effects of significant increases in the (non-dimensional) streamwise pressure gradient. Fortunately, the determination of τ_w is insensitive to the estimated experimental uncertainty in dp/dx.

6.7 Amplifier gain

The amplifier gain was calibrated in situ. That is, it was determined for the same circuitry and settings as were used for the actual measurement runs. With the instrumentation ready for a run, the leads from the anemometers were disconnected and replaced by calibrated voltage sources. The digital data acquisition program was then run as if it were a normal run and the amplifition factors were calculated from the mean signals recorded.

The same procedure was employed to deduce the slight zero error that remained after the initial adjustments of the amplifiers. The inputs to the amplifiers were shorted and the normal digital data acquisition plus integration of the recorded signals then yielded the amplifier zero error. Typically, it was less than one or two digits in 1024, but it was accounted for in the data reduction.

A short program (DINP.FOR) calculated the temperature correction and then the input values of gain and bucking voltage used by the main data reduction programs, DUVTR.FOR, DCORR.FOR and DSPEC.FOR.

6.8 Channel width

The channel width was measured along its length by Herr Nörtemann with a large dial indicator. The estimated experimental uncertainty was $\pm$ 0.05 mm. Before the experiment was conducted the spacers above the oil surface were reset to give equal spacing along the channel. At the measuring position, the deflec-

tion near the oil surface was approximately 1.5 mm from no flow to maximum flow. This effect was included in the calculation of the probe location y and its uncertainty.

The orientation of the channel wall relative to the track of the calibration cart was also checked by mounting a dial indicator to the probe support structure (Figure 5.1) and moving it along the channel.

7. WALL SHEAR STRESS

The one-point technique suggested by McEligot [1984; 1985] was extended slightly and was applied to determine the wall shear stress. The wall sensor calibration was done essentially in situ. With the X-probe at $y^+ \simeq 10$ it was away from significant wall interaction but close enough that the uncertainty due to choice of a turbulence model was minimal.

Typically a non-linear polymonial was employed to relate the instantaneous wall shear stress to the instantaneous voltage signal

$$\tau_w = a_1 + a_2 e + a_3 e^2 + \ldots\ldots\ldots$$

at the temperature ("cold resistance") chosen for the reference calibration. The slight difference between the reference temperature and temperature measured during a run was corrected when the calibration was applied to deduce $\tau_w(t)$.

7.1 Determination of τ_w for calibration

The one-point technique deduces the mean wall shear stress from the measured mean streamwise velocity u at a measured distance from the wall, via a turbulence model for the viscous layer (Figure 7.1). McEligot [1984] presented the details including sensitivity to turbulence model and measurements (Figure 7.2), resulting experimental uncertainties (Figure 7.3), and the Couette flow analysis upon which it was based. For fully developed flows the assumption that the convective terms are negligible in the governing momentum equation,

$$\bar{u}\,\frac{\partial \bar{u}}{\partial x} + \bar{v}\,\frac{\partial \bar{u}}{\partial y} = -\frac{1}{\rho}\frac{d\bar{p}}{dx} + \frac{1}{\rho}\frac{\partial \bar{\tau}}{\partial y}$$

is ideally approached. However, for spatially accelerating flows the relative magnitude of these terms depends on the applied pressure gradient and the distance y from the wall [Hanratty, 1988].

To account for the convective terms, we adopted a suggestion of Finnicum and Hanratty [1988] based on earlier work of Julien et al. [1969]. For Couette flow the local shear stress $\tau(y)$ is given as

$$\tau^+(y) = 1 + K_p\, y^+$$

where $\tau^+(y) = \tau_{(y)}/\tau_w$ here and $K_p = (\nu/\rho u_\tau^3)dp/dx$. Given a reasonable turbulence model, the one-point technique effectively determines the value of τ_w which satisfies

$$u_m = \int_o^{y_m} \frac{\tau(y)}{\mu_{eff}(y)}\, dy$$

where the subscript m refers to the measuring point and μ_{eff} represents the turbulence model.

For sink flows, Julien et al. [1969] developed the relation

$$\tau^+(y^+) = 1 + K_p y^+ \left[1 - \frac{c_f}{2}\,\frac{1}{y^+}\int_o^{y^+} (u^+)^2\, dy^+\right]$$

to account for the convective terms. We implemented this revision by multiplying the term $K_p y^+$ in existing program TAU.FOR [McEligot, 1984] by the grouping in brackets above. For fully-developed flow this change is suppressed. The integral which makes the procedure implicit was evaluated by successive substitution during the iterative process for τ_w or u_τ. The revised program, TAU2.FOR, is listed in Appendix C.

The effect of the convective terms was evaluated for several accelerated flows of interest by conducting the calculations with and without the correction. Typical results were

K_p	$\simeq 0.011$	$\simeq 0.011$	$\simeq 0.02$	$\simeq 0.02$
y^+	10	25	10	15
Δu_τ	0.1%	0.8%	0.5%	0.9%
ΔK_p	0.3%	2.5%	1.5%	2.6%

Since values with the X-probe at $y^+ \simeq 10$ are used to determine τ_w for calibration and for calculating wall coordinates, the inclusion of the convective terms led to no great change.

7.2 In situ calibration

As explained in the section above, during calibration of the wall sensor the mean wall shear stress is determined by the one-point method [McEligot, 1984] as revised. Actually, the calibration data are extracted from normal measuring runs. Thus, the flow is turbulent with the same fluctuating field present during calibration as during application.

The calibration relation for the fluctuating wall shear stress is taken to be

$$\tau_w(t) = a_1 + a_2 e + a_3 e^2 + \ldots .$$

where e is the instantaneous voltage signal from the sensor. By integration with respect to time, one finds the relation for mean values to be

$$\bar{\tau}_w = a_1 + a_2 \bar{e} + a_3 \overline{e^2} + \ldots .$$

The data reduction program for mean velocities, DUVTR, was modified slightly so that with suitable choices of calibration coefficients it would calculate the mean voltage statistics of the wall sensor, $\bar{e}$, $\overline{e^2}$, $\overline{e^3}$ and $\overline{e^4}$ as part of the data reduction for a normal run.

In order to calculate the calibration coefficients a_i for an n-th order polynomial, one needs calibration data at n + 1 (or more) levels of $\bar{\tau}_w$. The

values a_i are then determined by solving the n + 1 simultaneous equations for $\bar{\tau}_{w,i}$ or by a least-squares fit.

7.3 Temperature correction

Although the temperature of the room was closely regulated by thermostatic control, there were slight variations from run to run during the overall period of the measuring program, say $\pm$ 0.1 C. During an individual run the fluctuation was a few hundredths of a degree at most. Since the overheat ratio used for the wall sensor operation was relatively low (equivalent to about 10 C), a first order temperature correction was developed. The approach is comparable to one suggested by S.J. Kline a number of years ago [reference citation now forgotten].

We choose a standard or calibration temperature to which the data will be referred. The calibration relation $\tau_w(e)$ is then developed for that temperature. In converting calibration data to this temperature and in applying the calibration, the key question is -- for the shear stress existing at the operating temperature, what voltage signal would the same shear stress cause at the standard reference temperature?

Figure 7.4 describes the conceptual process graphically. The individual curves represent the functional behavior u(e) expected for different fluid temperatures (or temperature differences or overheat ratios) while the sensor operating resistance is held constant. The variable u is the wall shear stress or the velocity, as appropriate, and e is the required sensor voltage. For example, T_1 and T_2 may be considered the fluid temperatures at which measurements are made while T_3 is the temperature chosen for the reference condition. If we have data at T_1 for a given value of u (and e_1), we wish to determine the value e_3 which would be required for the same value of u at T_3. A Taylor series approximation would give

$$e_3 \simeq e_1 + \frac{\partial e}{\partial T}\bigg|_u \Delta T + \ldots .$$

or

$$e_3 \simeq e_1 + \left.\frac{\partial e}{\partial \Theta}\right|_u \Delta\Theta + \ldots.$$

where Θ represents a temperature difference, overheat, or other convenient function of temperature. In practise, we ultimately form the ratio e_3/e_1 so the correction is a multiplier for the measured voltage.

The first order correction takes the steady state energy balance of the sensor to be

$$i^2 R_{op} = \frac{e^2}{R_{op}} = q_{conv} = hA_s(T_{op} - T_\infty)$$

and attributes the primary temperature effect to the term $(T_{op} - T_\infty)$ and neglects the variation of other quantities due to temperature.

The resistance R_{op} is held constant in "constant temperature" operation of the anemometer. With the temperature coefficient of resistance, one can write

$$R_{op} = R_o\,[1 + \alpha\,(T_{op} - T_o)] = R_c\,[1 + \alpha\,(T_{op} - T_\infty)]$$

where the subscript o represents a reference condition. In our case we let

$$R_o = R_c = R(T_o) = R(T_\infty)$$

where R_c is called the cold resistance.

The energy balance can then be rearranged to

$$e^2 = \frac{hA_s R_{op}}{\alpha R_c}\,(R_{op} - R_c)$$

or, with a definition for Θ,

$$e^2 = fn\{u,\ constants\}\ \frac{R_{op} - R_c}{R_c} \triangleq fn\{u\}\ \Theta$$

Further rearrangement gives

$$e = \sqrt{fn\{u\}}\ [\Theta]^{-1/2}$$

and

$$\frac{\partial e}{\partial \Theta} = \frac{1}{2}\sqrt{fn\{u\}}\ [\Theta]^{-1/2}$$

For the first order approximation

$$\frac{e_3}{e_1} = 1 + \frac{\partial e_1}{\partial \Theta}\frac{\Delta\Theta}{e_1} \simeq 1 + \frac{1}{2}\frac{\Delta\Theta}{\Theta_1}$$

or

$$\frac{e_3}{e_1} \simeq 1 + \frac{1}{2}\frac{R_{op}}{R_{c3}} \cdot \frac{R_{c1} - R_{c3}}{R_{op} - R_{c1}}$$

For the correction of velocity signals to the chosen calibration reference temperature, we approximated $R_{op}/R_{c3} \simeq 1$ (along with Kline); this introduced a small percent error in a small percent correction (typically less than one percent). For the wall sensor calibration R_{op}/R_{c3} was included.

For more convenient application, the correction may be recast into terms of temperatures via the relation

$$R_{c1} \simeq R_{c3} + \frac{\partial R_c}{\partial T}(T_1 - T_3)$$

The result is

$$\frac{e_3}{e_1} \simeq 1 + \frac{B}{2} \frac{1}{1 - (R_{c3}/R_{op})(1 + B)}$$

where

$$B = (T_1 - T_3) \frac{1}{R_{c3}} \frac{\partial R_c}{\partial T}$$

7.4 Application of wall shear stress calibration

For the fully-developed conditions, measurements are available at four wall shear stress levels corresponding to runs at four flow rates (or pump speeds). A temperature of 24.8 C was chosen to serve for the calibration curve; this temperature was in the midst of the range of operating temperatures. The mean voltages $\bar{e}$, $\overline{e^2}$, $\overline{e^3}$ and $\overline{e^4}$ for each run were converted to the values that would have been at 24.8 C via the approach of the previous section.

Due to the limited range of τ_w values available for calibration purposes, a second order polynomial was used for the actual curve,

$$\tau_w = a_1 + a_2 e + a_3 e^2$$

The coefficients were determined by fitting the relations

$$\bar{\tau}_{wi} = a_1 + a_2 \overline{e_i} + a_3 \overline{e_i^2}$$

through the data for u_τ = 0.52, 0.80 and 1.04 cm/sec, spanning the range of measurements to be reported.

The mean $\bar{\tau}_w$ data and the resulting calibration curve $\tau_w(e)$ are plotted on Figure 7.5. It is seen that $\tau_w(e)$ is near linear over this range. Further, it does not differ significantly from $\bar{\tau}_w(\bar{e})$, although the second order term $a_3 e^2$ is not negligible.

For the calculations of mean statistics, correlations and spectra involving τ_w for runs at the various X-probe locations, y^+, the temperature correction to 24.8 C was introduced by correcting the input gain and bucking voltage to account for e_3/e_1. Then the coefficients a_1, a_2 and a_3 (with $a_4 = a_5 = 0$) were employed

in the data reduction program to convert each voltage sample for the wall sensor to its equivalent instantaneous wall shear stress.

For normalization of wall shear stress quantities in correlations, spectra, skewness, flatness, etc., the mean value $\bar{\tau}_w$ was determined by integration of the instantaneous values of τ_w in the data reduction program. However, wall coordinates such as y^+ and t^+ were calculated from $\bar{\tau}_w$ (or u_τ) deduced from the one-point velocity technique of McEligot [1984]. The differences in $\bar{\tau}_w$ involved were slight (and at $y^+ \simeq 10$ essentially nil since it was the basis of the calibration).

7.5 Treatment of wall shear stress signal for accelerated flows

The same wall sensor was used in the same position in the laterally converging configuration as in the fully developed version. Therefore, the basic thermal behavior of the sensor should be the same for the two cases and the calibration determined for fully developed flow should be the same as for the accelerated flows. However, the operating resistance of the sensor and its cold resistance were slightly different in the two cases. Since, for the accelerated case, complete details of the gain, bucking voltage and cold resistance at the measuring temperature are now available for only one strain rate or wall shear stress level (thanks to Lufthansa baggage handling in Frankfurt), it is necessary to combine these data with the calibration from the fully developed runs.

For steady or quasi-steady state, the energy balance for the wall sensor can be written as

$$e^2/R = hA_s\,(T_w - T_c)$$

where the heat transfer coefficient represents heat transfer to the fluid by three modes,

$$h = h_{NC} + h_{eff,\,cond} + h_{fc,\tau}$$

buoyancy, conduction via the substrate and forced flow effects which vary with

the wall shear stress. It is the variation of the last which provides the usual calibration of voltage signal versus wall shear stress. If the Leveque solution [1928] describes the forced flow contribution and the temperatures (or resistances) are held constant, the relation can be rearranged to

$$\tau_w^{1/3} \sim c_1 e^2 - c_2 h_{NC} - c_3 h_{eff,cond} = c_1 e^2 - A'$$

with the c_i representing constant coefficients. Over the range of the present experiments this relation may be approximated as

$$\tau_w = a_1 + a_2 e + a_3 e^2$$

as shown in section 7.4 above.

It is expected that, aside from the change in temperature difference or overheat ratio (which is treated as in section 7.3) the main effect of a change in sensor operating resistance R_{op} is to modify the "constant" contributions from buoyancy effects and substrate conduction. For application to the accelerated data, the values of a_2 and a_3 are taken from the three point calibration (section 7.4) and coefficient a_1 is calibrated via the data with the probe at $y^+ \simeq 10$ and the lower flow rate (corresponding to a pump speed of 1200 rpm).

The time series for the data at this point are integrated to give the mean, voltage quantities for the relation

$$\bar{\tau}_w = a_1 + a_2 \bar{e} - a_3 \overline{e^2}$$

and the mean wall shear stress is determined from the mean velocity $u(y^+ \simeq 10)$ in accordance with the procedure of section 7.1. Thus, the desired coefficient is given as

$$a_1 = \bar{\tau}_w - a_2 \bar{e} - a_3 \overline{e^2}$$

from the calibration measurements.

For the laterally converging flows, the temporal wall shear stress is normalized by its mean value for application, thereby reducing the effects of uncertainties in this calibration procedure. For wall coordinate scaling as in determining u^+, y^+, etc., the one point velocity method (section 7.1) is used to obtain $\bar{\tau}_w$.

When the coefficients a_2 and a_3 from from the fully-developed calibration were used to deduce a_1, it was found that the resulting calculated value of τ_w was reasonable. However, the rms fluctuation of τ_w appeared to be much too small (about 1.2 percent of τ_w). This difficulty was traced to the second order polynomial in the calibration. While the variation of τ_w was within its calibrated range, the voltages were lower than those in the fully-developed calibration. The values of a_2 and a_3 led to a minimum in the calibration curve $\tau_w(e)$ near the mean value $\bar{e}$ for the accelerated flow. Thus, significant fluctuations in e_τ yielded only slight variations in the calculated τ_w calculated and a low rms value of τ_w was deduced.

To counter this difficulty a linear calibration

$$\tau_w = a_1 + a_2 e$$

was ultimately employed. The coefficient a_2 was deduced from the slope of the fully-developed correlation between its lowest and highest values of τ_w. As noted earlier, the relation $\tau_w(e)$ was approximately linear over this range (Figure 7.5). The constant a_1 was then adjusted to fit the data at $y^+ \simeq 10$ for the measurements at $K_p \simeq -0.02$ as

$$a_1 = \tau_w - a_2 e$$

The deduced value of rms τ_w then was approximately twenty percent of τ_w and the skewness and flatness factors S_τ and F_τ showed magnitudes comparable to S_u and F_u.

7.6 Determination of pressure gradient parameter, K_p

The pressure gradient parameter is defined as

$$K_p = \frac{\nu}{\rho u_\tau^3} \frac{dp}{dx}$$

The friction velocity u_τ was determined via program TAU2.FOR along with τ_w as described above. The pressure gradient dp/dx was estimated with the "hook gauge" measurements as mentioned in section 6.6 and its experimental uncertainty is relatively large. However, even though dp/dx is an input in the determination of u_τ, the resulting value of u_τ is insensitive to the uncertainty of dp/dx or K_p (Figure 7.2). Consequently, the estimated experimental uncertainty of K_p is approximately that of dp/dx.

8. RESULTS

The primary experimental results are the simultaneous measurements with the wall sensor for τ_w and X-probe for u and v. Velocity data were concentrated in the viscous sublayer at $y^+ \simeq 5$, 7, 10, 15 and 25 plus the centerplane. Typically, 200,000 samples of each signal were acquired for the time series. Four sets of operating conditions were selected as follows:

Ramp Angle	$K_p = \frac{\nu}{\rho u_\tau^3} \frac{dp}{dx}$	$Re_s = \frac{u_c s}{\nu}$	$K_v = \frac{\nu}{V_b^2} \frac{dV}{dx}$
"Fully-developed" flows			
0	- 0.0083	7400	$\simeq 0$
0	- 0.011	5600	$\simeq 0$
Streamwise accelerating flows			
2^o	- 0.011	8300	1.6×10^{-6}
2^o	- 0.02	5600	2.4×10^{-6}

This selection of conditions permits separating effects of K_p from Re_s and from K_v. For example, at one (approximately constant) Reynolds number there are data at two different values of K_p, and vice versa.

Mean turbulence statistics are tabulated in Appendix A. Additional mean velocity profile measurements are listed in Appendix B; these are required for the estimation of V_b in the calculation of K_v. Results calculated to date are

these mean statistics, selected auto- and cross-correlations plus preliminary power spectra of the signals. This chapter presents those results with discussion as appropriate. Usually our presentation is in terms of wall coordinates.

8.1 Mean velocity profiles

The streamwise mean velocity profiles are presented in Figure 8.1 in terms of wall coordinates. These data confirm the trends predicted in Figure 7.1; as K_p increases in magnitude the curves $u^+(y^+)$ also have higher values away from the wall. This is one effect of streamwise pressure gradient on mean turbulence structure. It corresponds to a thickening of the layer dominated by viscous effects as in the mixing length wall models of McEligot, Ormand and Perkins [1966], Huffman and Bradshaw [1972], Launder and Jones [1969] and others. The trend is also predicted by the direct numerical simulations of Spalart [1986]. Comparable data have been obtained by Jones and Launder [1972] and Loyd, Moffat and Kays [1970] for transversely converging flows, by Perkins and McEligot [1975] and Shehata [1984] for strongly heated gas flows in tubes and in turbulent flows with drag reduction by polymer additives [Berman, 1977; Harder and Tiederman, 1989].

The deduced values of the transverse mean velocity v^+ are tabulated in Appendix A for the viscous layer and the centerplane. These data can be subject to a variety of difficulties. The calculation of v from the X-probe signals involves determining the small difference between two much larger signals. (For a fully-developed flow, v is ideally zero and consequently percent experimental uncertainties are infinite.) In a fully developed flow in the same oil channel Randolph [1988] found that as his X-probe approached the wall, the measurements yielded flow angles which were not parallel to the wall -- a possible indication of wall-probe interaction. Moin and Spalart [1988] modeled the behavior of a typical X-probe via direct numerical simulations of a turbulent flow; they found that neglecting the spanwise component w led to larger errors in v than in u and the separation of the two films can have strong effects. Moin and Spalart did not present calculations of the expected measured value for the mean $v^+(y^+)$, but in general the predicted errors in-

creased as y^+ approached zero with dependence on w and the calibration relations employed.

Thus, the statistics involving v are best considered in a comparative or relative manner rather than placing too much confidence in their absolute values. That is, we recommend examining the effects of K_p by using the data for the lowest value as a reference (fully-developed flow, $K_p \simeq -0.008$) and then comparing the data for other K_p to it. Other investigators have arbitrarily adjusted their sensor angles to force $\bar{v} = 0$ in order to avoid the appearance of this type of problem. As mentioned earlier, for a laterally converging flow $\bar{v}$ is not identically zero so we carry the values actually calculated (and look for relative effects at the same locations).

The mean values $v(y^+)$ are all towards the wall except centerplane values for the fully-developed flows. The largest values appear at $y^+ \simeq 7$ to 10 and then the magnitudes decrease as y^+ increases. However, they are generally less than about five percent of the value of u at the same y^+. Although there are differences between the values of $v^+(y^+)$ for the various runs, there is no clear trend as K_p varies and the difference at a given y^+ is generally within the experiental uncertainty. The major variation observed is with y^+ and is likely to be a consequence of the difficulties discussed above.

8.2 Root mean square fluctuations

The normalized values of the r.m.s. velocity components are plotted in Figures 8.2 and 8.3. For u' the maximum value approaches three at y^+ near 15 in agreement with the data of Eckelmann [1974] and others. Also, v' is much less than u' and continues to increase within the viscous layer rather peaking there as u' does. The magnitude of $v'(y^+)$ is approximately the same as the data of Eckelmann but does fall slightly lower.

Eckelmann compared the data at two Reynolds numbers, corresponding to our two fully-developed conditions. When non-dimensionalized with wall coordinates (his Fig. 13) the data collapsed, i.e., there was no apparent effect of Reynolds number. Our Figures 8.2 and 8.3, using comparable wall scaling, also show no significant trends with variation of K_p. That is, for these measures of the

turbulence structure there appears to be no important effect of the streamwise pressure gradient.

8.3 Reynolds shear stress

With the dimensions of the channel and the flow rates yielding centerline values of y^+ in the range of 140 to 210, the total shear stress varies observably across the viscous layer. Therefore, the popular constant shear layer approximation is not valid, even for the fully-developed flows.

Near the wall the total shear stress variation is given approximately as

$$\frac{\bar{\tau}(y)}{\tau_w} = \frac{\partial u^+}{\partial y^+} - \frac{\overline{uv}}{u_\tau^2} \simeq 1 + K_p y^+$$

neglecting the convective contribution in the x-momentum equation. For fully-developed flow between parallel plates this relation is exact while for accelerating flows it will diverge as y^+ increases (see the earlier discussion in section 7.1 for further details).

At the wall $u = v = 0$ so $\overline{uv}$ is likewise zero there. Since

$$\bar{\tau}(y) = \mu\frac{\partial \bar{u}}{\partial y} - \rho\overline{uv},$$

the Reynolds shear stress increases with y approaching the total shear stress relation as the turbulent transport becomes dominant relative to viscous effects.

Figure 8.4 presents the approximate asymptotic values for $\tau(y^+)$ versus K_p plus the measured Reynolds shear stress $-\rho\overline{uv}$ obtained by integrating the time series signals for $u(t)\cdot v(t)$. While there is some scatter, it may be seen that the variation of $\bar{\tau}(y^+)$ is large enough to impose an effect of K_p on the behavior of $\overline{uv}/u_\tau^2$ in the viscous layer. Since the estimated experimental uncertainties in K_p are large, the uncertainties in the locii of the curves $\bar{\tau}(y^+)/\tau_w$ are large as well.

In the viscous layer the data increase from zero towards these "asymptotes".

While the data for the lower values of K_p do not differ from one another substantially, some trends may be discerned. The lowest value of K_p generally leads to the highest values of the Reynolds stress (except for the first points near the wall), corresponding to the higher asymptotic relation. On the other hand, the higher K_p yields definitely lower non-dimensional Reynolds stress in the viscous layer, consistent with its approximate asymptotic curve. (For this latter case, K_p is so large that $\tau(y^+)$ would become zero at y^+ near 50 if the convective terms were indeed negligible.)

8.4 Skewness and flatness

The skewness and flatness factors were calculated from the time series for u and v and are presented as Figures 8.5 through 8.8. For u these higher order moments are reasonably well behaved whereas for v they appear to suffer a bit more experimental scatter.

These factors for u agree with the data of Kreplin [Eckelmann, 1984] and of Randolph [1983] for fully-developed flow in the same channel. No significant dependence on K_p is evident.

The skewness and flatness data for τ_w or $(\partial u/\partial y)_w$ show some variation. However, a contributor to the variation may be experimental scatter arising from low sensitivity of the sensor in combination with digital round-off error. With the lowest value of K_p, realizations with the X-probe at $y^+ \approx 10$ and 15 gave $S_\tau \approx 0.55$ and 0.44 and $F_\tau \approx 3.16$ and 2.95, respectively. These values are lower than those of Kreplin (0.75 and 3.7) which are, in turn, lower than the values for S_u and F_u as y^+ approaches zero. At the highest pressure gradient K_p, two realizations yielded $S_\tau \approx 0.22$ and 0.24 and $F_u \approx 2.62$ and 2.62, lower yet.

For the normal fluctuations plotted one might envision some trends with K_p within the experimental scatter. For example, $S_v(y^+)$ may be shifted a bit to the right for the highest K_p relative to the lowest in the viscous layer. There is a general pattern evident for S_v with a maximum near $y^+ = 10$ and a

zero crossing a lower y^+. Maximum magnitudes are somewhat smaller than for S_u, implying more symmetric probability density distributions. The negative values at low y^+ indicate that large negative values of v (sweeps?) are more frequent than large positive values (ejections?) near the wall. There does not seem to be a clear trend evident in F_v. However, its values are much greater than F_u; this would imply that v frequently takes on values much greater than the mean (which is near zero).

8.5 Correlations

Since the mean structure showed only a gradual variation with K_p, when it showed any significant effect at all, the rest of the present study concentrates on the two extremes. Results for the highest streamwise pressure gradient, $K_p \simeq -0.02$, are compared to those for $K_p \simeq -0.008$, the lowest. The latter is the condition at which much of the earlier structure results have been presented; fully developed flow at the maximum flow rate of the oil channel [Eckelmann, 1970, 1974; Wallace, Eckelmann and Brodkey, 1972; Randolph, 1983, 1988]. The location of $y^+ \simeq 15$ was chosen since it corresponds to the most popular (and most energetic) location for conditional analyses [Blackwelder and Kaplan, 1976; etc.].

The cross correlation coefficients are defined as

$$R_{u_i u_j}(y^+,\tau) = \frac{1}{T} \int_0^T \frac{u_i(y^+,t) \cdot u_j(y^+,t-\tau)}{u_{i,rms}\, u_{j,rms}}\, dt$$

where u_i or u_j represents any of the deduced signals and y^+ is the location of the X-probe if involved. Typically, u_i was taken as the streamwise velocity fluctuation, u. With i = j the result reduces to the autocorrelation for the quantity.

The data reduction program to calculate the correlations was based on one written by Randolph [1988]. It was modified (slightly) to handle four input signals and calculate the "instantaneous Reynolds stress" or uv product. Input control parameters allowed correlating any two resulting time series

against a third. All correlations are presented for 401 sample points at 50 samples per second, giving a total period of about eight seconds in real time. Another short program was written to convert the independent variable from physical time to a non-dimensional lead time τ^+ ($\simeq \tau u_\tau^2/\nu$) in terms of wall coordinates. While τ has also been used as a symbol to represent shear stress, there should be no confusion when taken in context.) Thus the results are plotted and presented as correlation coefficients, non-dimensionalized by the root mean square values of the fluctuations about their mean quantities, versus τ^+ in Figures 8.9 to 8.13.

The correlation coefficients for fully-developed turbulent flow at y^+ are compared on Figure 8.9. The autocorrelation of the streamwise component peaks at about one (= 0.99988) as it should and shows the expected symmetry. There does seem to be a slight change in the trend of the slope in the range $50 \lesssim \tau^+ \lesssim 70$ indicating a (very) slightly increased correlation with some phenomenon at y^+ near 60. The normal component v shows less correlation with u, both in peak value and period of significant correlation. The u.v correlation is negative, indicating that v tends to be negative when u is positive and vice versa -- a sweep towards the wall corresponds to increase in u and an ejection to a retardation of u. These quantities are essentially uncorrelated until $\tau^+ \gtrsim -15$, but the show some small level of correlation to $\tau^+ \simeq +70$. The greatest u.v correlation is slightly after the peak in the u-auto correlation, say, at $\tau^+ \simeq 3$ or so.

The best correlation of τ_w with u is over 0.8 and occurs at $\tau^+ \simeq -10$. The $u.\tau_w$ correlation shows a greater correlation between u at $u^+ \simeq 15$ and τ_w than between u at $y^+ = 15$ and v at the same location! The peak magnitude is almost twice as large and the time period is considerably longer. In fact, for most of the correlation period the correlation of u with τ_w is as large or larger than u with itself (if the difference in the times of the peak correlation is taken into account). These observations help explain the success Chambers, Murphy and McEligot [1983] had in using the temporal wall shear stress in a VITA sampling technique to deduce average bursting periods for laterally-converging flows. This result also implies that it should be possible to use

the wall sensor as a detector to relate the signals from the single X-probe for different y^+ locations.

Figure 8.10 presents the same correlations for $K_p \simeq -0.02$. Qualitatively, the observations are the same. Since the same number of points (same real time) was used in the correlations, the lower value of u_τ leads to a smaller range of τ^+. The individual correlations will now be compared directly for the two flow conditions in Figures 8.11 to 8.13; here the circles represent the flow with the larger pressure gradient ($K_p \simeq -0.02$) and the square symbols give the fully-developed results for reference.

The u-autocorrelations are displayed by Figure 8.11. By definition both peak at unity at zero lead, $\tau^+ = 0$. The autocorrelation at $K_p \simeq -0.02$ is broader, i.e., greater correlation over a longer non-dimensional time. This corresponds to the observation of Chambers, Murphy and McEligot that, as the magnitude of K_p increases, the bursting frequency decreases or bursting period increases in terms of wall coordinates. The longer average time between randomly occurring bursts would allow eddies to remain coherent longer in the vicinity of the measuring instrument.

Figure 8.12 compares the u.v correlations. The peak value is almost the same for both as is its lead; there are miniscule differences but they are likely less than the typical experimental uncertainty. Again the correlation is broader for the larger pressure gradient. The fully-developed results are nearly uncorrelated for $\tau^+ \lesssim -15$ whereas the values for $K_p \simeq -0.02$ are just approaching zero at the limit of the calculation at $\tau^+ \simeq -45$. After the peak u and v remain slightly more correlated for $K_p \simeq -0.02$ than for the fully-developed run.

The values of R_{uv} at $\tau = 0$ reveal consistencies in the data and implications for v' (and $\overline{uv}$) that are not obvious from direct examination of v'/u_τ alone. The quantity $R_{uv}(y^+,\tau^+ = 0)$ is sometimes called the correlation coefficient itself; it may be calculated directly from the mean statistics as $\overline{uv}/u'v'$ without forming the more complete correlation. From Figure 8.12 we see it is almost exactly the same for the two extreme cases plotted (the tabulated difference is less than one percent). The Reynolds shear stress

$\overline{uv}$ decreases about fifty percent from the fully-developed flow to the accelerated one. This decrease is shared somewhat equally between the rms values, u' and v', in yielding the same value of R_{uv}. However, treating these results in wall coordinates gives a different picture. The quantity $\overline{uv}/u_\tau^2$ decreases (as expected since the total τ/τ_w decreases at this location) but only about 14 percent. The corresponding change in non-dimensional rms values is almost all in the normal component; v'/u_τ decreases about 14 percent and u'/u_τ decreases less than one percent. In other words, if $u'(y^+)/u_\tau$ does not have a significant effect of K_p, $v'(y^+)/u_\tau$ must in order to remain consistent with the effect on $\tau(y^+)/\tau_w$; however, the small value of v'(<<u') makes it difficult to separate this trend from the experimental uncertainty in the graph of $v'(y^+)/u_\tau$.

The peak value of the correlation between u and τ_w is approximately the same for both flows (Figure 8.13) but it is slightly later (more negative lead time) in the accelerated case. This observation may be a first indication that the inclination of the fronts of the sweep events [Kreplin and Eckelmann, 1979] changes with variation of the pressure gradient. As with the other two correlations discussed, in this flow the $u.\tau_w$ correlation is broader.

The general effects of increasing K_p appear to be increases in the correlations over longer non-dimensional times. This seems reasonably consistent with the idea that increase of the bursting period with K_p leads to a better organized flow in the wall region. Longer non-dimensional time scales can be expected to relate to larger non-dimensional length scales, such as the increase in "linear" layer thickness or the van Driest "constant" A^+ required in mixing length predictions of the mean velocity profile. That is, the average structures must become larger in terms of wall variables.

8.6 Relation to measurements with drag-reducing additives

The effects of polymer injection have been studied for several decades [Hoyt and Fabula, 1964; Wells and Spangler, 1967; White and McEligot, 1970; Donohue, Tiederman and Reischman, 1972; Tiederman, Luchik and Bogard, 1985; Hendricks, 1988, etc.] and a number of studies have examined the turbulence

structure via velocity measurements, flow visualisation and wall sensors. It has been shown that polymer additives in the viscous layer (say $10<y^+<100$) modify the structure and bursting rate (e.g., Tiederman, et al. [1985]).

Recently Harder and Tiederman [1989] have measured fully-developed flows in two-dimensional channels with low polymer concentration via laser Doppler velocimetry. Drag reduction of up to forty percent was obtained. A two-component system was used to obtain u, v and their statistics.

The turbulence structure quantities deduced by Harder and Tiederman varied with the amount of drag reduction rather than wall strain rate, polymer concentration and channel height, per se. The ratio of the average period of the turbulence production cycle for a drag-reduced flow to the average period for a water flow at equal wall shear stress increases in a manner comparable to the increase in bursting period observed with streamwise pressure gradients by Chambers, Murphy and McEligot [1983] and others. Likewise, the mean velocity profile $u^+(y^+)$ increased as the present data do (e.g., our Figure 8.1) but the magnitude of the increase appears considerably greater for the polymer flow. The increase is reminiscent of the laminarizing data of Perkins and McEligot [1975] and Shehata [1984]; this same observation has been made by Brodkey earlier [1975]. The Reynolds shear stress distribution with polymer additives (their Figure 3.21) shows the same trend as our measurements with streamwise acceleration presented in Figure 8.4.

Differences from the data of Harder and Tiederman are evident in the root mean square values of the velocity fluctuations and in the correlation coefficients. The present measurements revealed no large variation of u'/u_τ or v'/u_τ with K_p. With typical levels of drag reduction Harder and Tiederman have no big effect on v'/u_τ, particularly in the viscous layer, but in their case with strongly non-Newtonian drag reduction there appears to be a decrease beyond their estimated experimental uncertainty. For u'/u_τ there is a substantial increase, peaking at $y^+ \simeq 30 \rightarrow 40$; this shift outward may correspond to the thickening of the viscous layer.

In our terms Harder and Tiederman present $R_{uv}(y^+,\tau^+ = 0)$ for correlation coefficients while our current data emphasize $R_{ij}(y^+ \simeq 15, \tau^+)$. Thus we can compare $R_{uv}(y^+ \simeq 15,\tau^+ \simeq 0)$. In our case we show no significant effect of K_p (or K_v) whereas Harder and Tiederman have a decrease of fifty to near 100 percent with the addition of polymers. Theirs is consistent with the large increase in $u'(y^+)/u_\tau$ and may be equivalent to a laminarized flow with passive fluctuations.

8.7 Import for hydroacoustic modelling

As noted above, Thomas and Bull [1983] and Landahl's colleagues [Johansson, Her and Haritonidis, 1987] demonstrated that the instantaneous wall pressure and instantaneous wall shear stress are related to one another, as indicated earlier by Landahl [1967, 1975] who suggested that unsteady shear stresses should contribute significantly both to radiation and to the low wave number component of the wall pressure spectrum. Related data have been presented by Zakkay, Barra and Hozumi [1979], Dinkelacker and Langeheineken [1982; Langeheineken, 1981] and Kobashi, Komoda and Ichijo [1986]. All have been with zero pressure gradients or fully developed flow of air. The most direct correlation appears to be between the fluctuations of the normal velocity component and the wall pressure.

Knowledge of the turbulence structure is required to derive models of wall pressure spectra as by Panton and Linebarger [1974], Chase [1980] and Ffowcs Williams [1982], but no such models appear to have been developed which include modification of the turbulence structure by drag reducing phenomena. Only the study of Panton and Linebarger has treated effects of streamwise pressure gradients.

For hydroacoustic models typical turbulence structure quantities needed are source distribution functions for the mean shear-turbulence component of the wall pressure, turbulence - turbulence interaction, etc. The former may be approximated as $(dU/dy)^2 \cdot \overline{v^2}$. A key hypothesis of Panton and Linebarger [1974] is that the intensity of the normal velocity component scales with the Reynolds shear stress and normalized wall distance, $\overline{v^2}/\overline{uv} = fn\{y^+\}$, but does not depend on pressure gradient.

The idea that $v'(y^+)/u_\tau$ is independent of streamwise pressure gradients is tested by our Figure 8.3 as well as being addressed in the analysis of Finnicum and Hanratty [1988, Figure 7] and the direct simulations of Spalart [1986, 1990]. A trend is seen towards a reduction in $v'(y^+)/u_\tau$ with increase in the magnitude of K_p, more favorable pressure gradients. The question is how large is the effect. For the range of the present data, ($-0.008 < K_p < -0.02$, $0 < K_v < 2.4 \times 10^{-6}$) the reduction is about thirty percent at $y^+ \simeq 25$, but our comments on experimental uncertainty of $\tilde{v}$ must be reiterated. Finnicum and Hanratty predict a drop of about forty percent from $K_u = 0$ to 2.0×10^{-6} while Spalart's results suggest about twenty five percent for K_u increasing from 1.5×10^{-6} to 2.5×10^{-6}, both at $y^+ \simeq 25$.

9. CONCLUDING REMARKS AND RECOMMENDATIONS

To provide bases for incorporating the effects of streamwise pressure gradients into hydroacoustic models for the wave vector-frequency spectrum of wall pressure fluctuations in turbulent boundary layers, the turbulence structure has been studied. Efforts were concentrated on the viscous layer which often dominates momentum, energy and mass transfer from the wall. (Here we define the viscous layer with Bradshaw [1969] as the region of a turbulent flow where viscous effects are significant though not necessarily dominant, typically $0 < y^+ \lesssim 30$ in a fully-developed flow.)

Earlier measurements of the temporal wall shear stress by Chambers, Murphy and McEligot [1983] in a laterally-converging flow had led to the conclusions that

- o non-dimensional bursting frequencies decrease greatly as the acceleration parameter increases
- o the time history of the conditionally-averaged wall shear stress was less affected
- o results presented in terms of wall scaling were less sensitive to acceleration than those normalized by outer scaling.

These observations came from experiments in an air flow where the half-inch

(about 13mm) plate spacing and thin shear layer prohibited fluid velocity measurements.

The present studies were conducted in the 22cm wide Reichardt/Eckelmann oil channel at the Max Planck Institut für Strömungsforschung to obtain good spatial and temporal resolution. Simultaneous time series data were obtained with an X-probe and a wall sensor to determine u(t), v(t) and $\tau_w(t)$. Measurements with the X-probe at $y^+ \simeq 5, 7, 10, 15, 25$ and the centerplane concentrated on four sets of conditions:

- o $K_p \simeq -0.02$, $K_\nu \simeq 2.4 \times 10^{-6}$, $Re_s \simeq 5600$
- o $K_p \simeq -0.011$, $K_\nu \simeq 1.6 \times 10^{-6}$, $Re_s \simeq 8300$
- o $K_p \simeq -0.011$, $K_\nu \simeq 0$, $Re_s \simeq 5600$
- o $K_p \simeq -0.008$, $K_\nu \simeq 0$, $Re_s \simeq 7400$

In terms of wall layer scaling, the following effects were found when the (non-dimensional) streamwise pressure gradient increased:

- o the mean velocity profile, $u^+(y^+)$, increased, corresponding to a thickening of the layer dominated by viscous effects
- o at $y^+ \simeq 15$, correlation coefficients, $R_{uu}(\tau^+)$, $R_{uv}(\tau^+)$ and $R_{u\tau}(\tau^+)$ broadened, consistent with the decrease in bursting frequencies observed by Chambers, Murphy and McEligot

The following aspects of the turbulence structure showed no significant effects in the viscous layer:

- o $u'(y^+)/u_\tau$, root mean square of the streamwise velocity fluctuations
- o $S_u(y^+)$, skewness factors of the streamwise velocity fluctuations
- o $F_u(y^+)$, flatness factors of the streamwise velocity fluctuations
- o maximum amplitudes of the correlation coefficients $R_{uv}(\tau^+)$ and $R_{u\tau}(\tau^+)$ (and R_{uu} by definition) at $y^+ \simeq 15$

Experimental uncertainties in determining the instantaneous normal velocity component $\tilde{v}$ (i.e., calculation of a small difference between larger quantities) hamper conclusions on the statistics of v. But it appears a tentative con-

clusion is warranted that there is no major effect on $S_v(y^+)$ or $F_v(y^+)$.

Calculations of the non-dimensional spectra are in process. It is recommended that they be completed. Modification of the versatile pattern recognition program of Brodkey, to correspond to the details of the present measurements, has also been initiated. In addition to pattern recognition, this program applies the VITA technique [Blackwelder and Kaplan, 1976] with a variety of detection schemes suggested in the literature plus a number of quadrant-splitting approaches [Wallace, Eckelmann and Brodkey, 1972]. It is likewise recommended that this aspect of the study be completed to determine further in which ways streamwise pressure gradients affect the turbulence structure in the dominant viscous layer.

These data and the comparable measurements of Randolph [1983] show signs of interaction between the probe and the wall as the probe approaches the wall. It is believed that relative or comparative results are not significantly affected although the mean wall shear stress and the mean flow angle vary somewhat. Therefore, it is recommended that these data be supplemented by non-intrusive measurements with laser Doppler velocimeters in the oil channel. Such instrumentation could offer the further benefit of more direct measurement of the normal velocity and, possibly, more accurate determination of its statistics.

ACKNOWLEDGEMENTS

The present work has been supported by the Applied Hydrodynamics Program of the Office of Naval Research, with Mr. James A. Fein as Program Manager and Mr. V.J. Monacella of David Taylor Research Center as Scientific Officer. Earlier incarnations were financed by the National Science Foundation (Dr. Win Aung, Program Manager), the U.S.-Deutschland Fulbright Commission, the Max Planck Gesellschaft, the University of Arizona and Westinghouse Naval Systems Division (earlier Gould Ocean Systems Division). To all we are extremely grateful.

The data reduction to date has principally been via extension of computer programs developed and kindly provided by Dr. Michael Randolph, now of DFVLR/AVA, Göttingen. At the Max Planck Institut für Strömungsforschung

friendly assistance was given by Herrn Eduard Bawirzanski, Holger Eisenlohr, Paul Habermann, Ullrich Isermann, Hans-Werner Kompart, Thomas Kowalski, Frank Ohle und Burkhard Thiele and by Herrn Karl-Heinz Nörtemann und Hansjuergen Shäfer with the experiment construction, modifications and preparations. Throughout, the support of Julie McEligot increased the cost effectiveness of DM's efforts. At Westinghouse Naval Systems Division, timely, expert and warm help came from Lee Desrosiers, Roland Thibodeau and their merry colleagues in the Graphics Department of the Field Service Organization, Newport, RI. And Dr. Philipe R. Spalart of NASA Ames Research Center gave us direct, large scale graphs of the mean statistics predicted by his direct simulations. Likewise we thank them all.

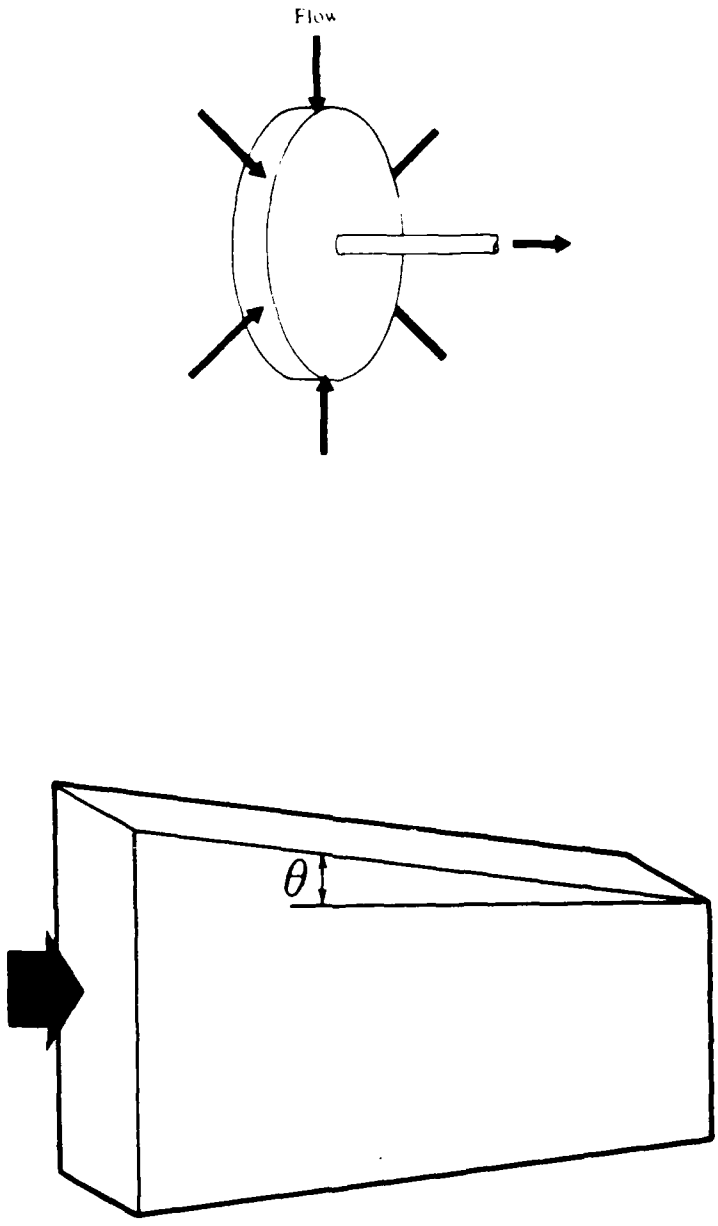

Fig. 2.1 Idealized models of laterally converging flows.

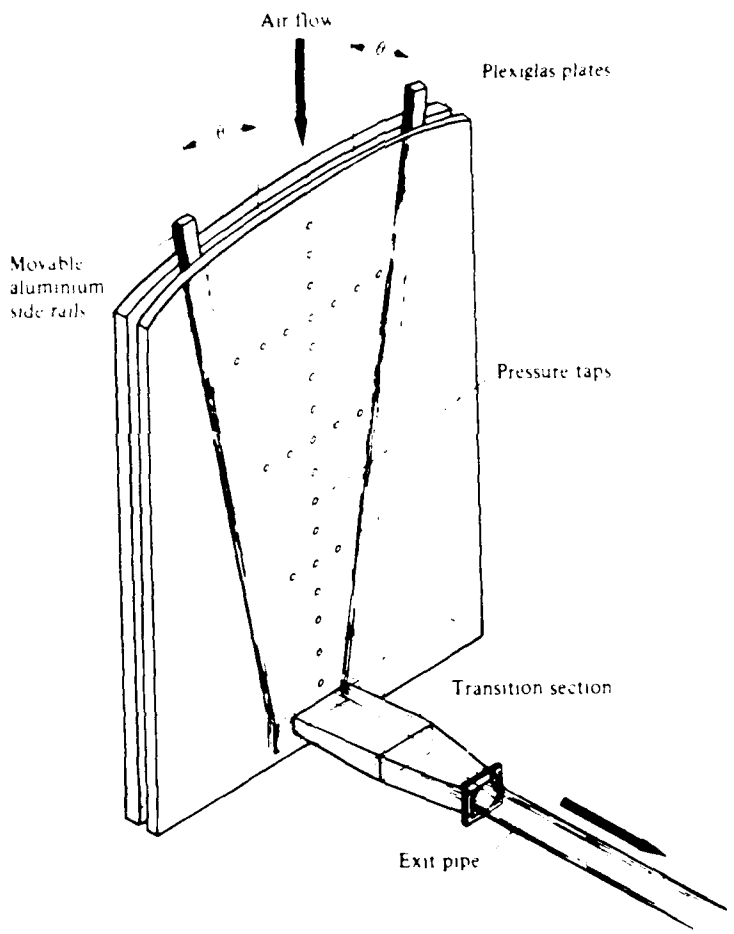

Fig. 3.1 Turbulent flow test section of Murphy, Chambers and McEligot [1983].

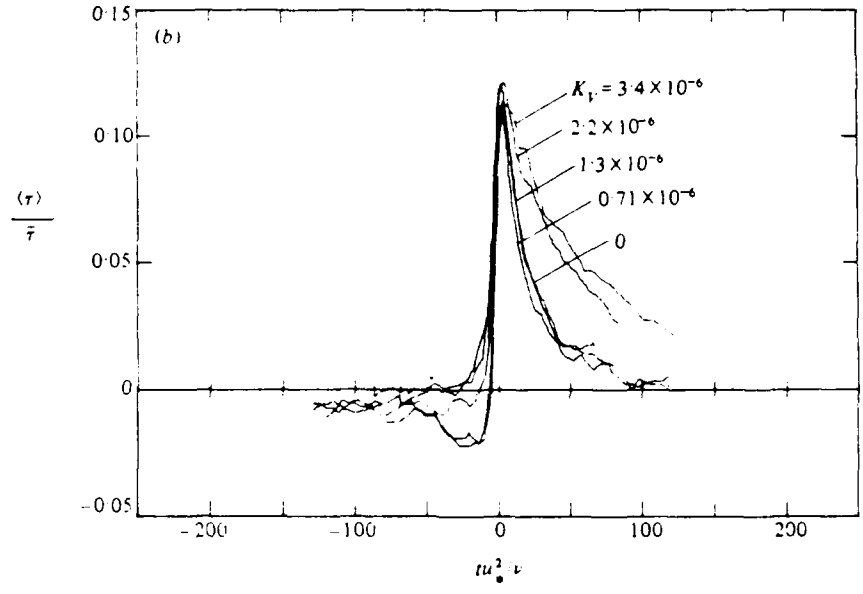

Fig. 3.2 Conditionally-averaged wall shear-stress fluctuations in laterally converging flow; 11,000 < Re_D < 13,800; $0 \leq K_V \leq 3.4 \times 10^{-6}$ [Chambers, Murphy and McEligot, 1983].

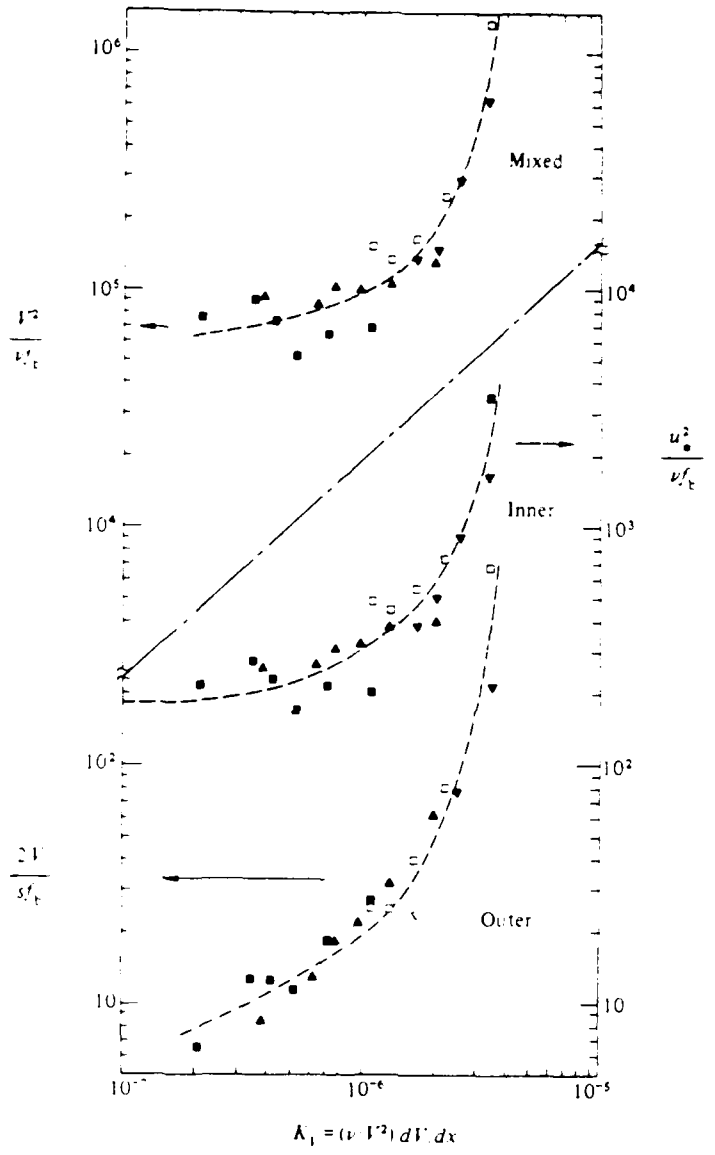

Fig. 3.3 Average bursting periods (inverse of bursting frequency) for laterally converging flows [Chambers, Murphy and McEligot, 1983].

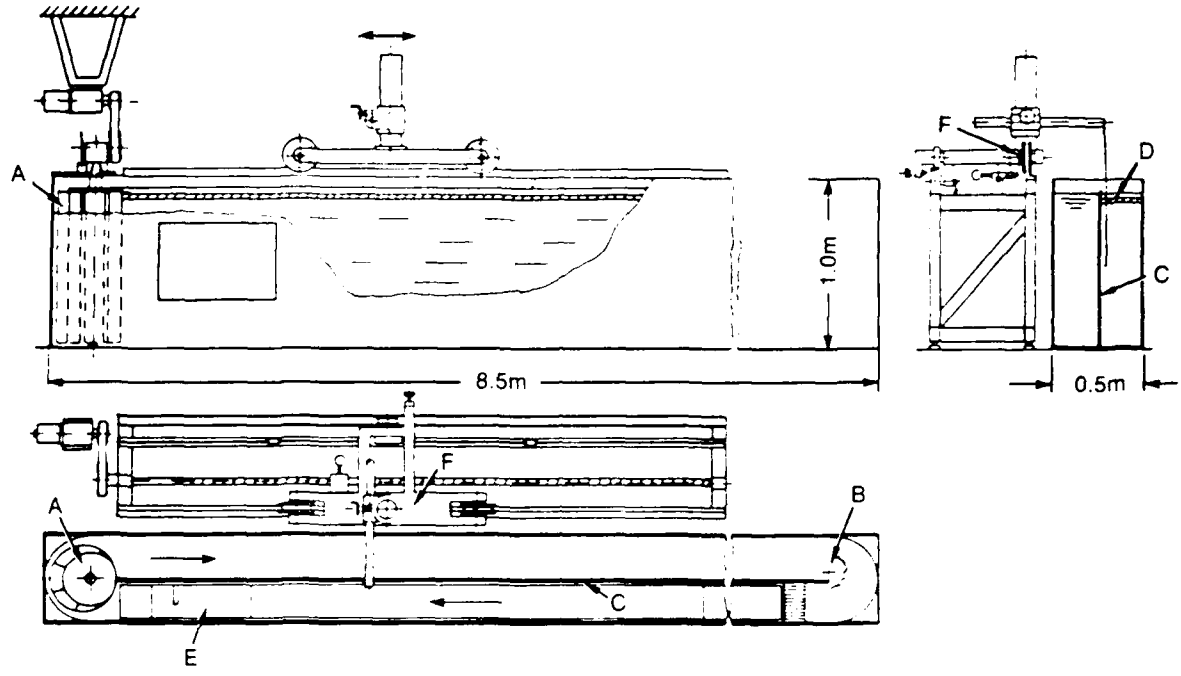

a. REICHARDT OIL CHANNEL [ECKELMANN. 1974]

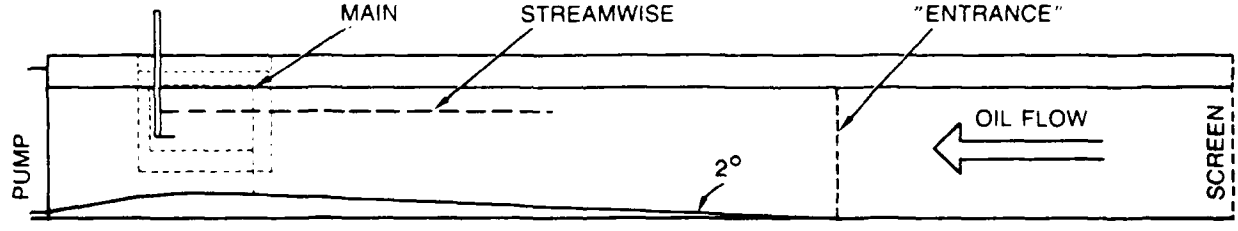

b. MODIFICATIONS AND PRIMARY MEASURING POSITIONS

Fig. 5.1 Schematic diagram of open channel, oil flow apparatus.

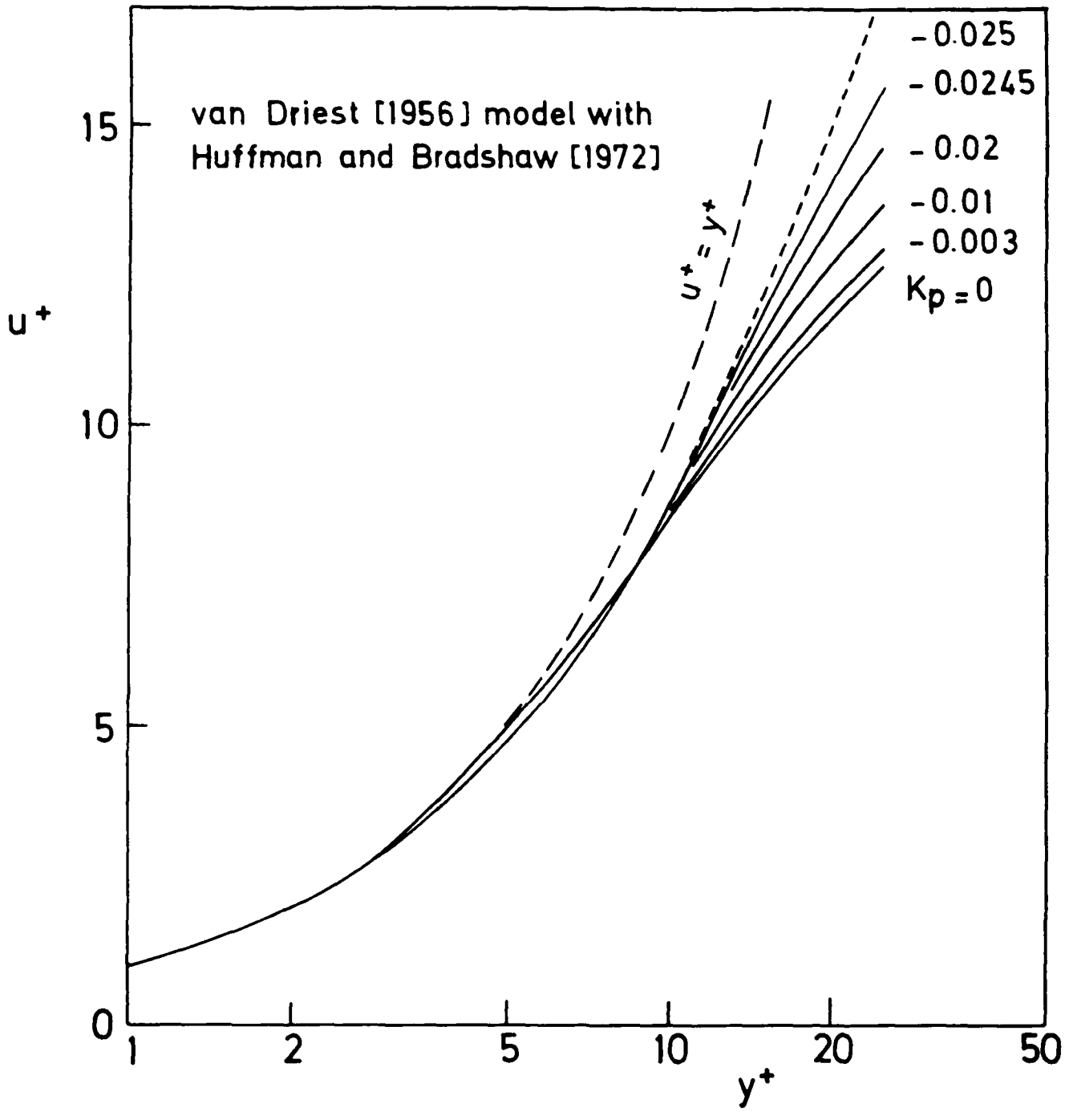

Fig. 7.1 Mean velocity predictions using function $A(K_p)$ deduced from Huffman and Bradshaw [1972] in van Driest mixing length model [1956].

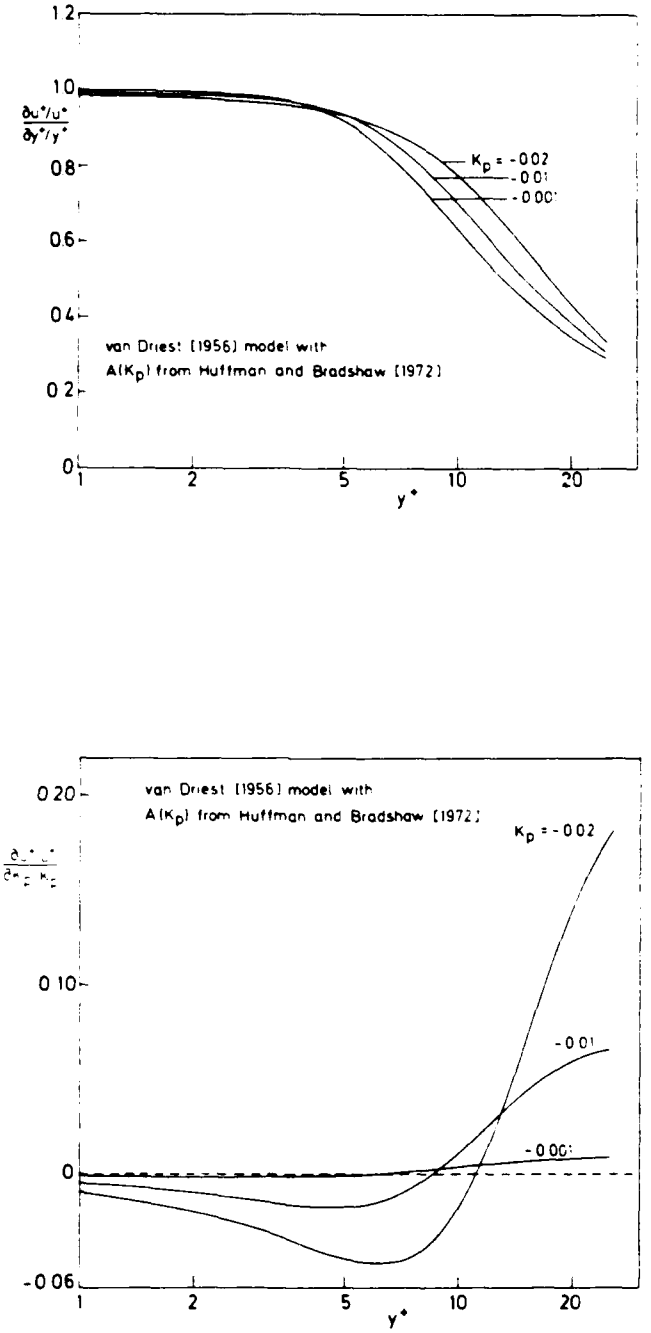

Fig. 7.2 Influences of measurements of X-probe location and estimates of pressure gradient parameter [McEligot, 1984].

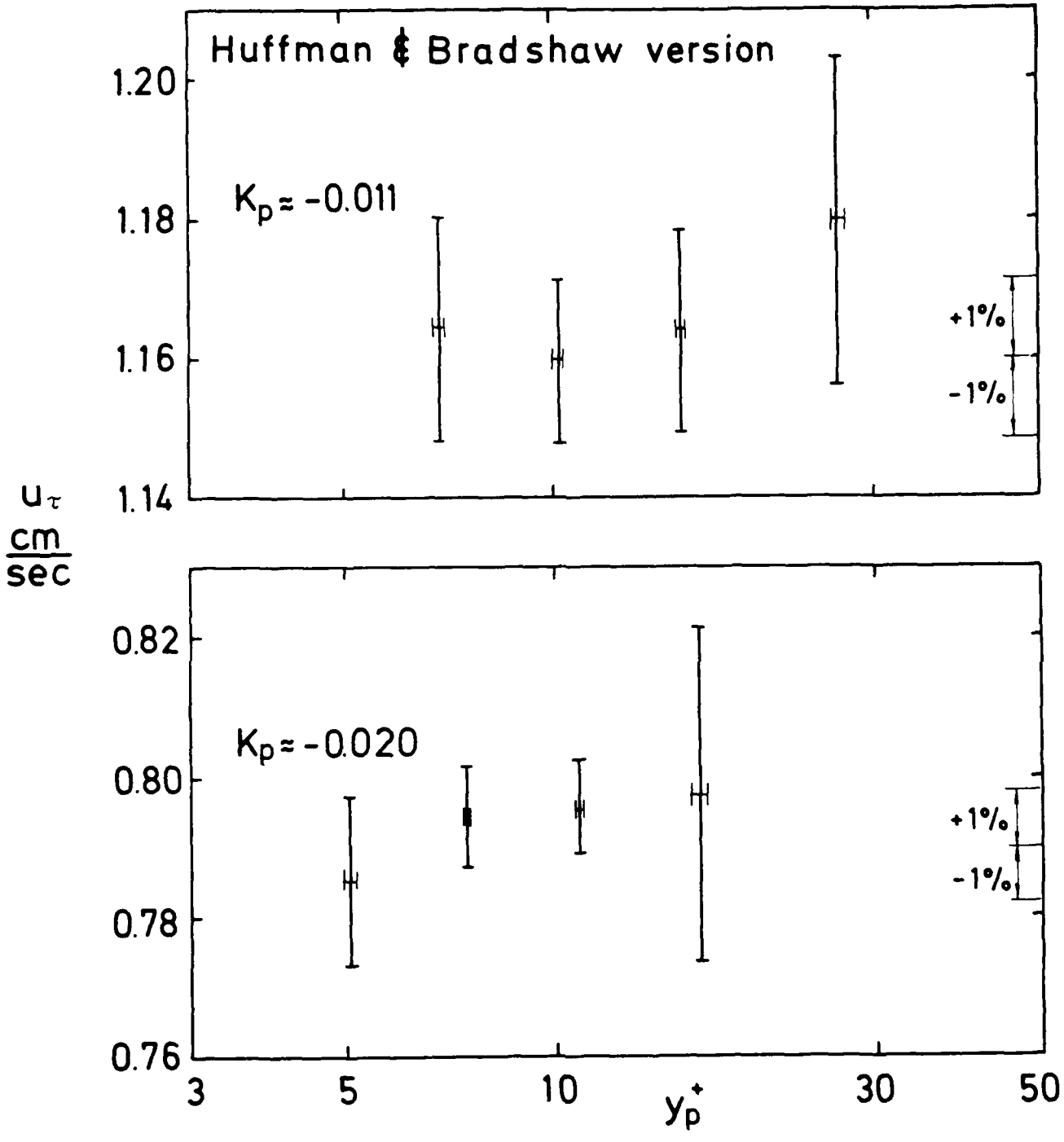

Fig. 7.3 Independent estimates of friction velocity in accelerated oil flow deduced from mean velocity measurements at positions indicated [McEligot, 1984].

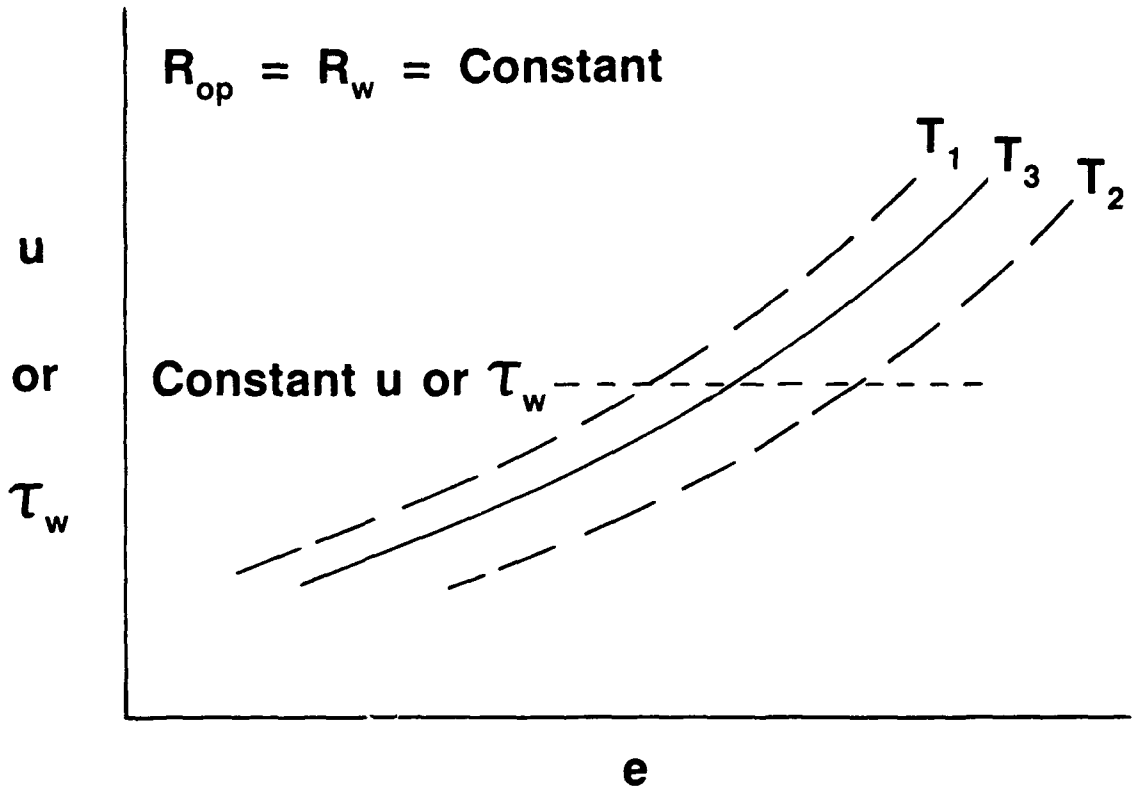

Fig. 7.4 Graphical representation of correction process for effect of fluid temperature.

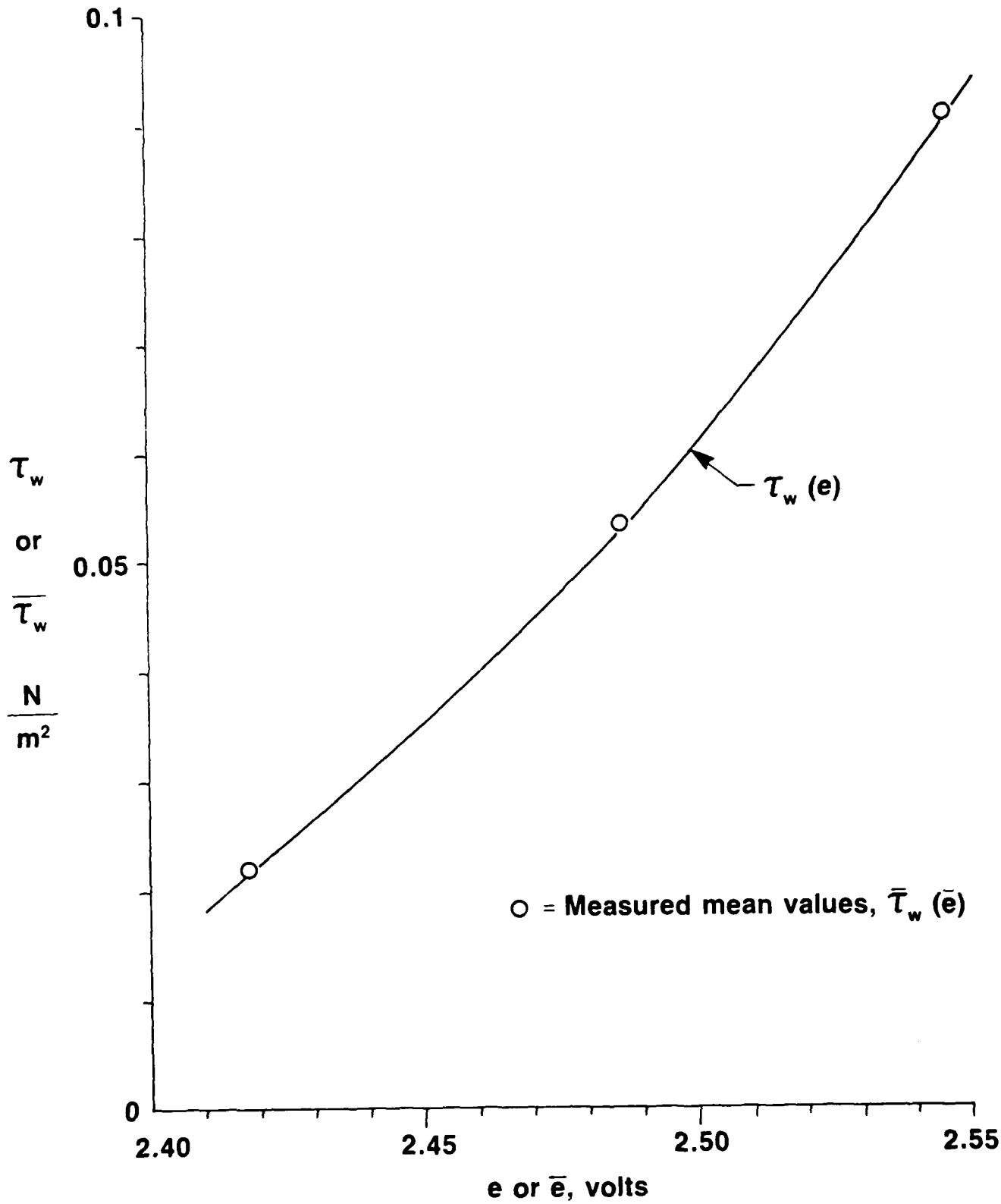

Fig. 7.5 Instantaneous wall shear stress calibration ($u_\tau(e)$) compared to mean measurements, $\bar{u}_\tau$ vs $\bar{e}$.

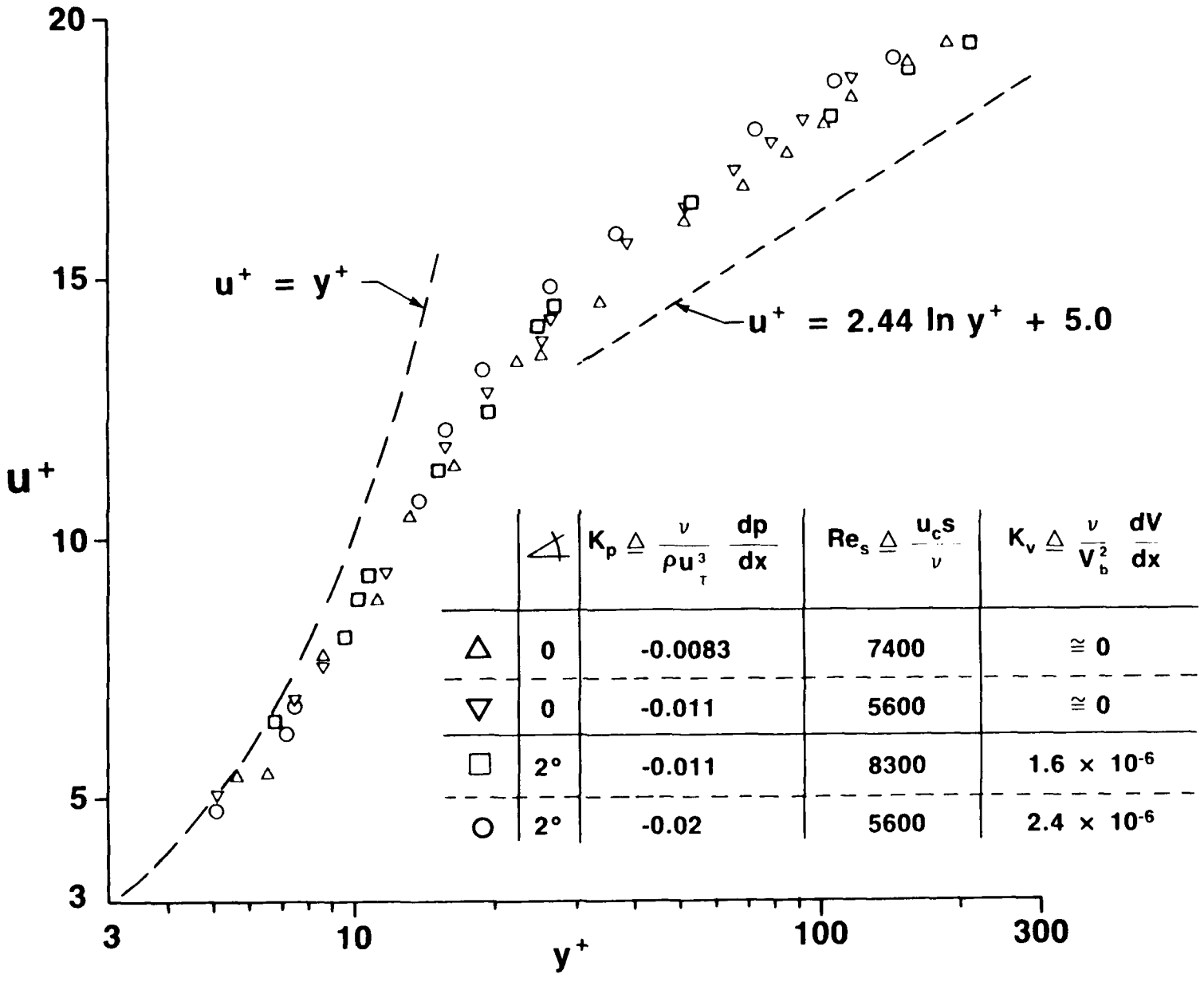

	α	$K_p \triangleq \frac{\nu}{\rho u_\tau^3} \frac{dp}{dx}$	$Re_s \triangleq \frac{u_c s}{\nu}$	$K_v \triangleq \frac{\nu}{V_b^2} \frac{dV}{dx}$
△	0	-0.0083	7400	$\cong 0$
▽	0	-0.011	5600	$\cong 0$
□	2°	-0.011	8300	1.6×10^{-6}
○	2°	-0.02	5600	2.4×10^{-6}

Fig. 8.1 Streamwise mean velocity profiles.

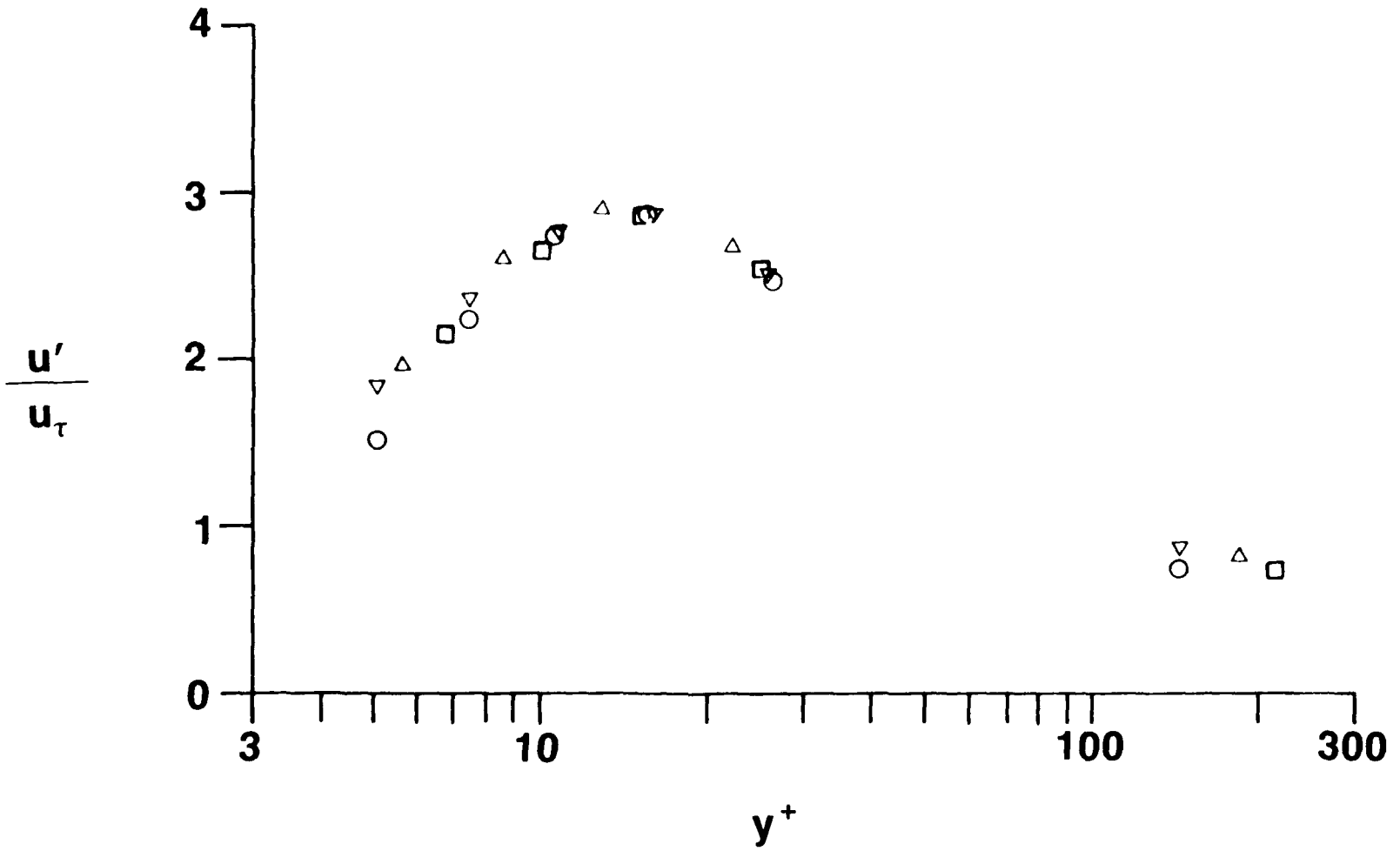

Fig. 8.2 Root mean square values of streamwise velocity component fluctuations. Symbols as in Fig. 8.1.

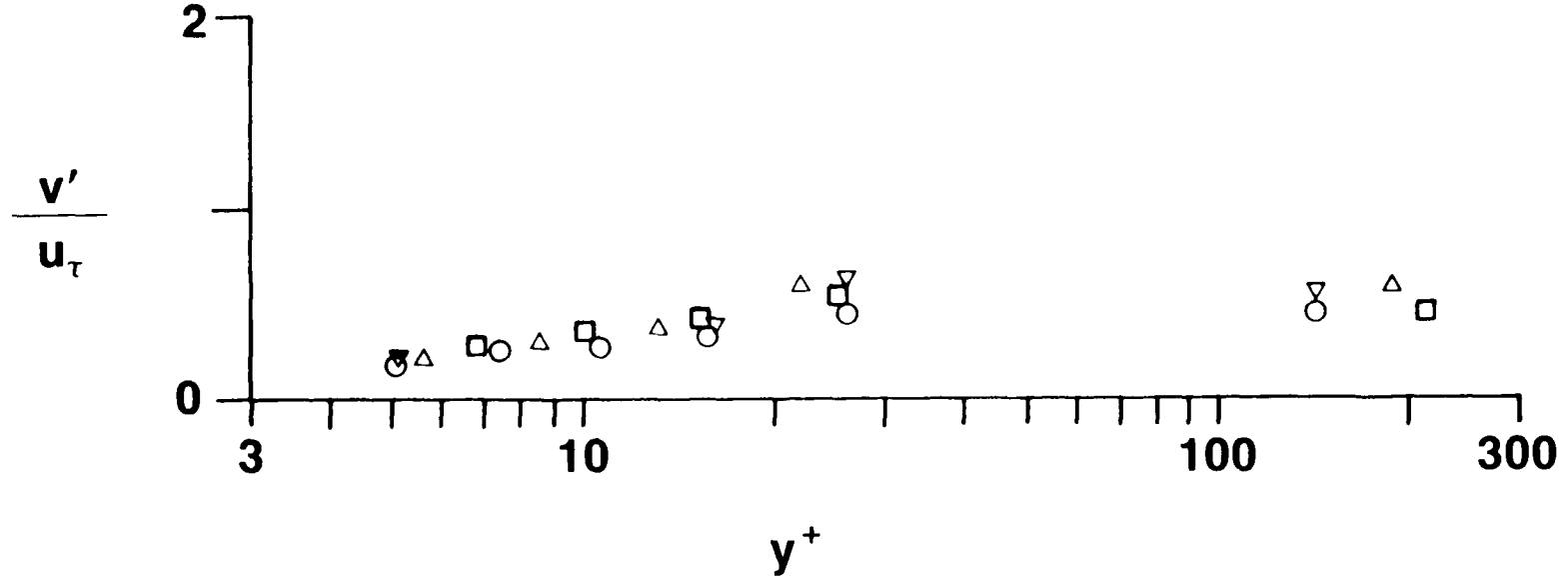

Fig. 8.3 Root mean square values of normal velocity component fluctuations. Symbols as in Fig. 8.1.

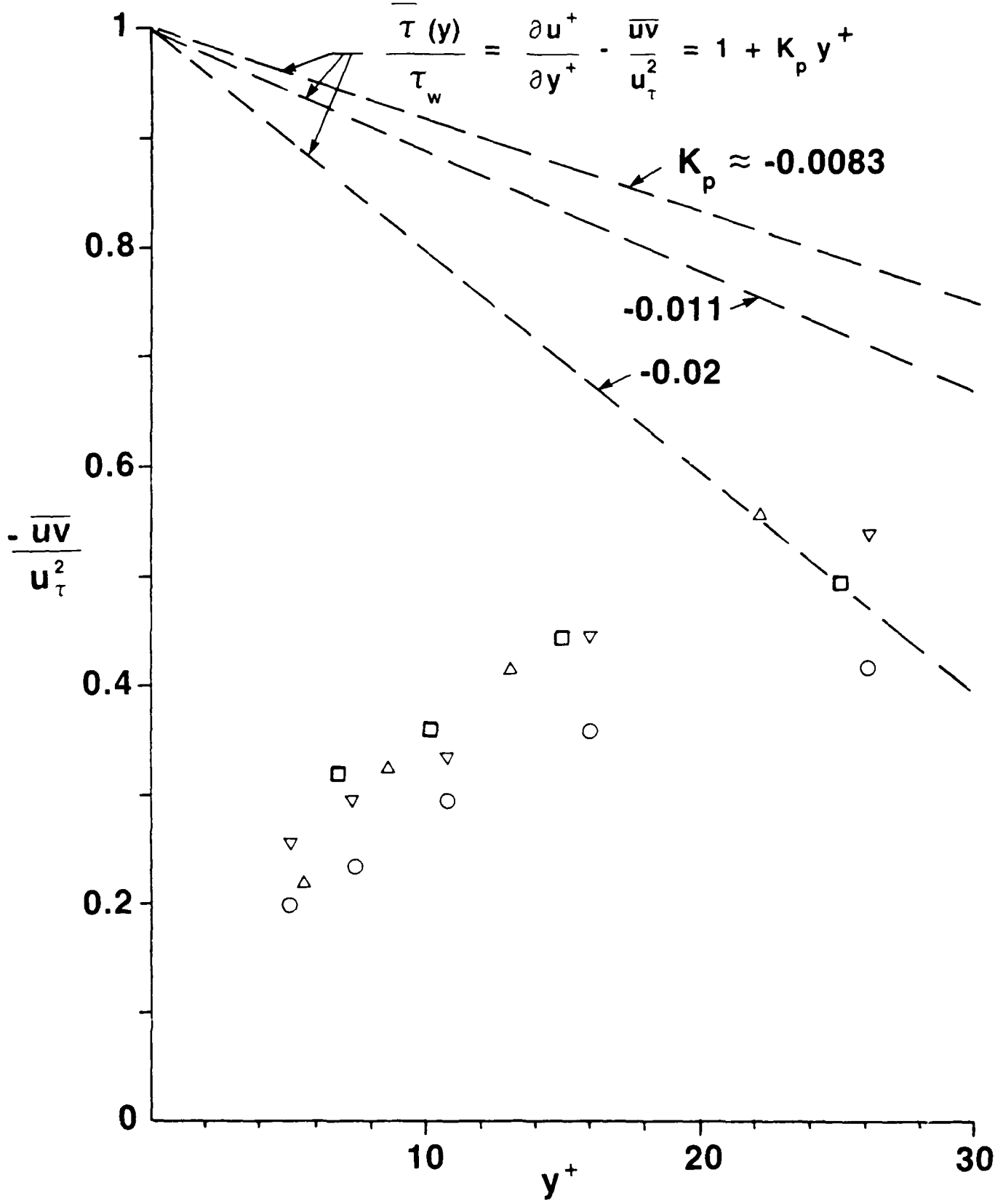

Fig. 8.4 Variation of Reynolds shear stress.

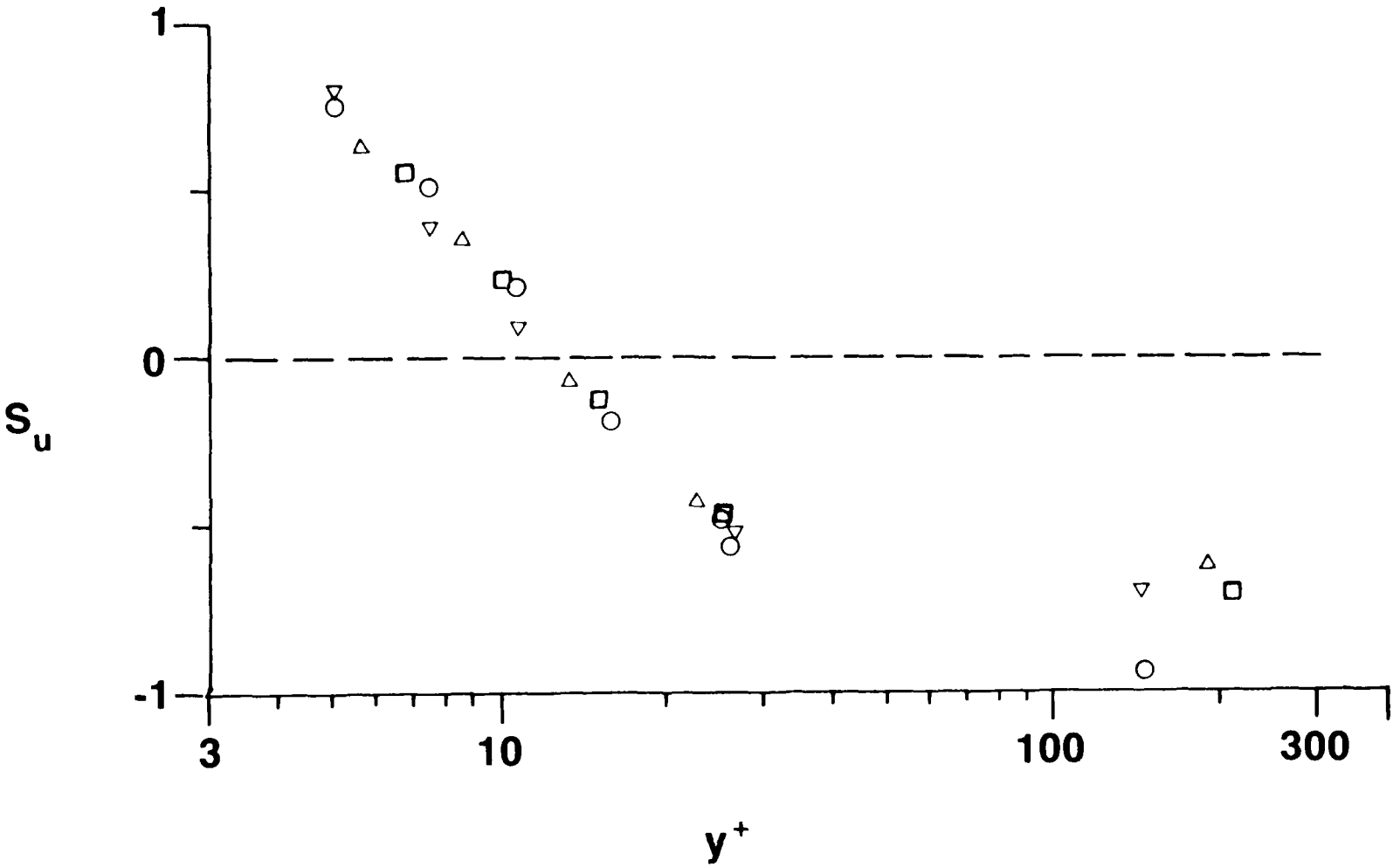

Fig. 8.5 Distribution of skewness factors of streamwise velocity fluctuations. *Symbols as in Fig. 8.1.*

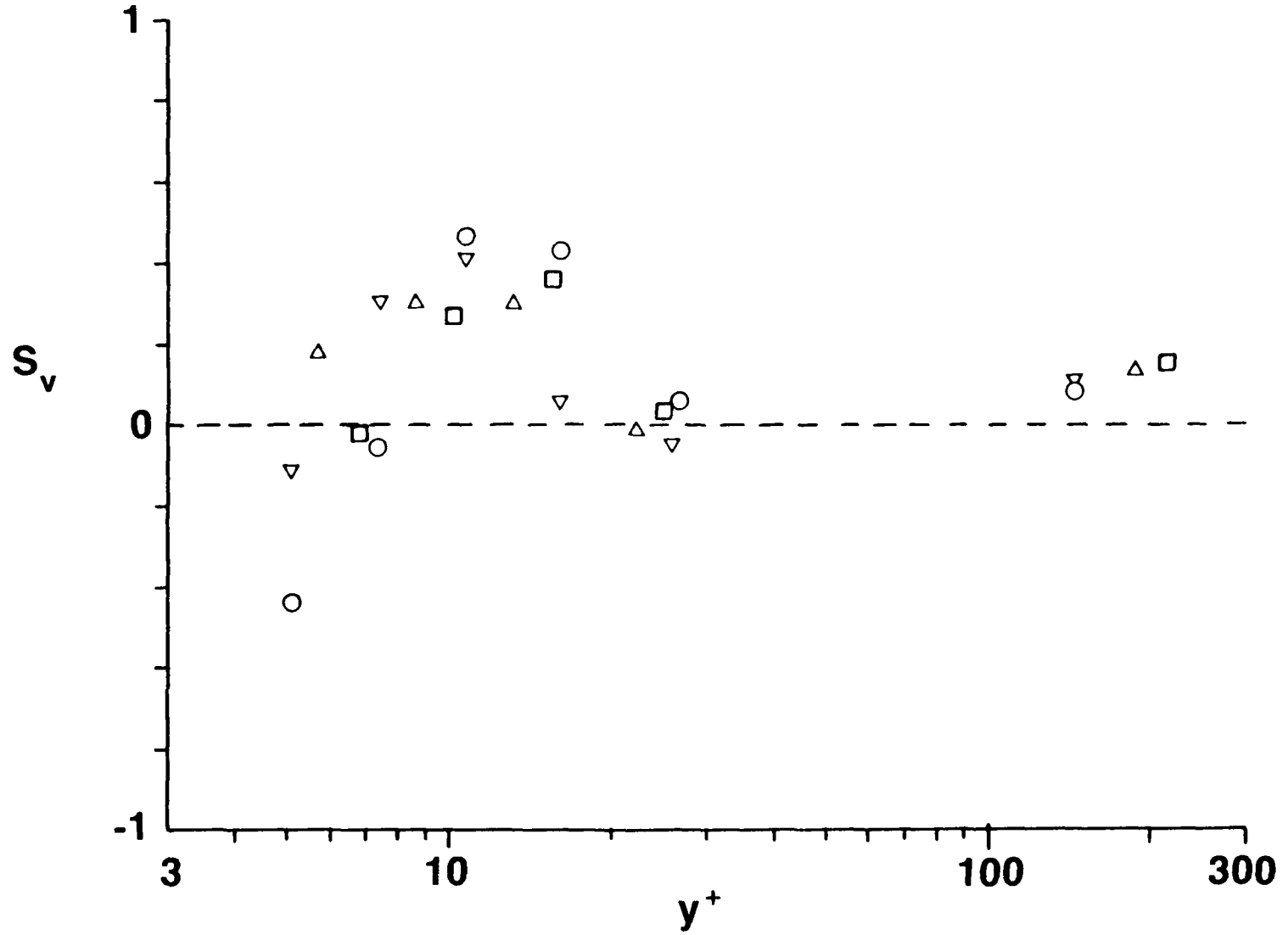

Fig. 8.6 Distribution of skewness factors of normal velocity fluctuations. Symbols as in Fig. 8.1.

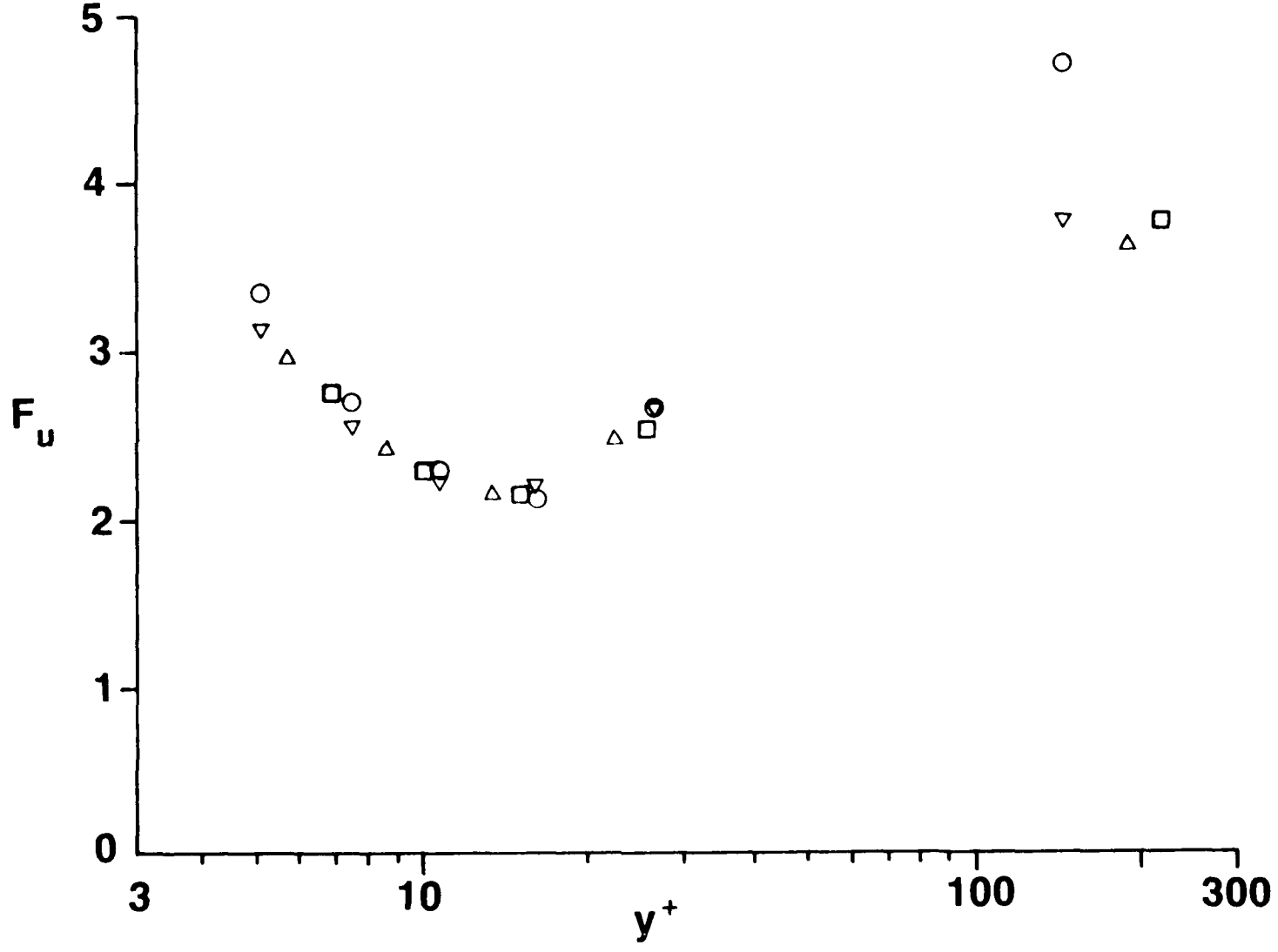

Fig. 8.7 Distribution of flatness factors of streamwise velocity fluctuations.

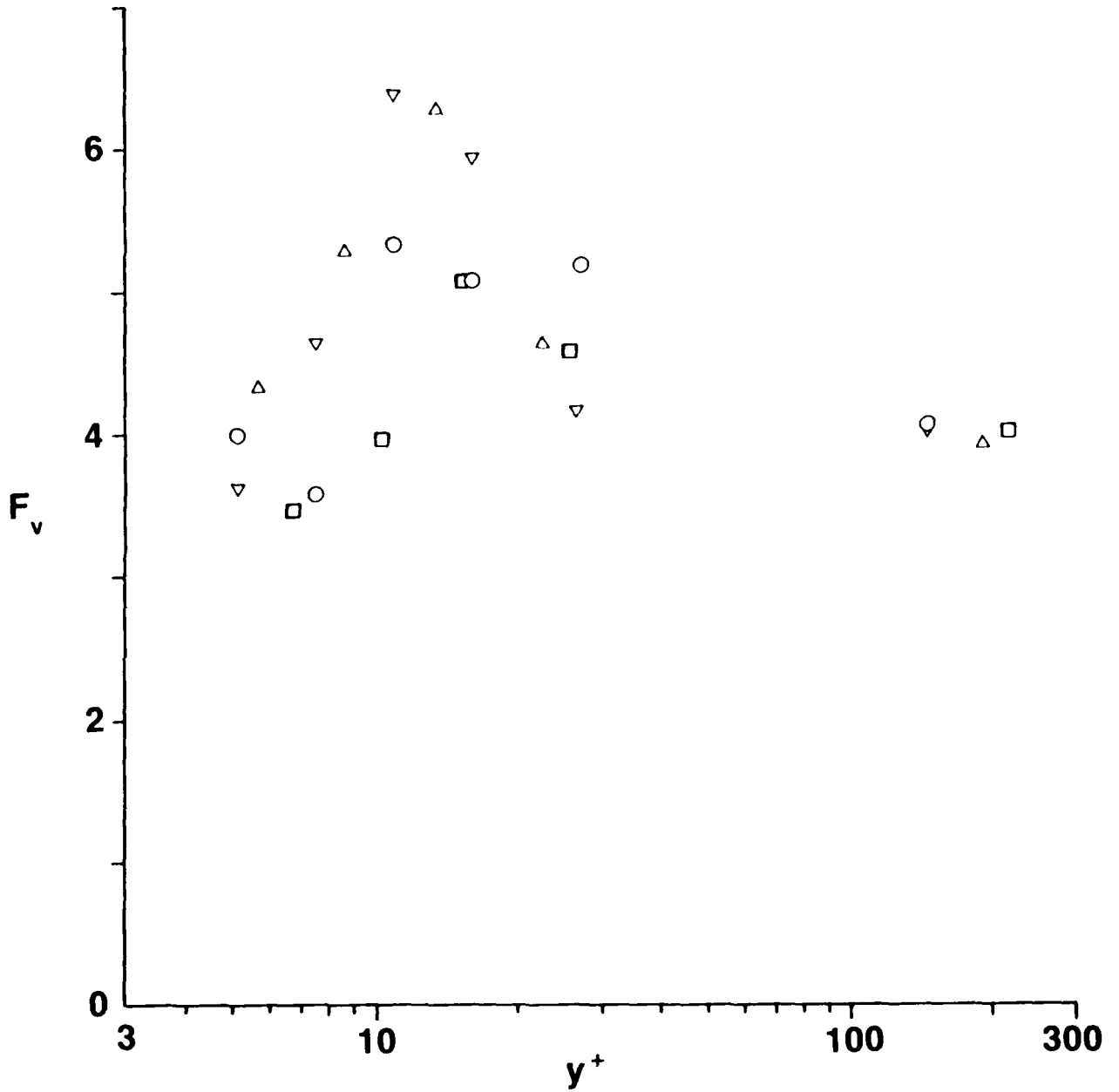

Fig. 8.8 Distribution of flatness factors of normal velocity fluctuations.

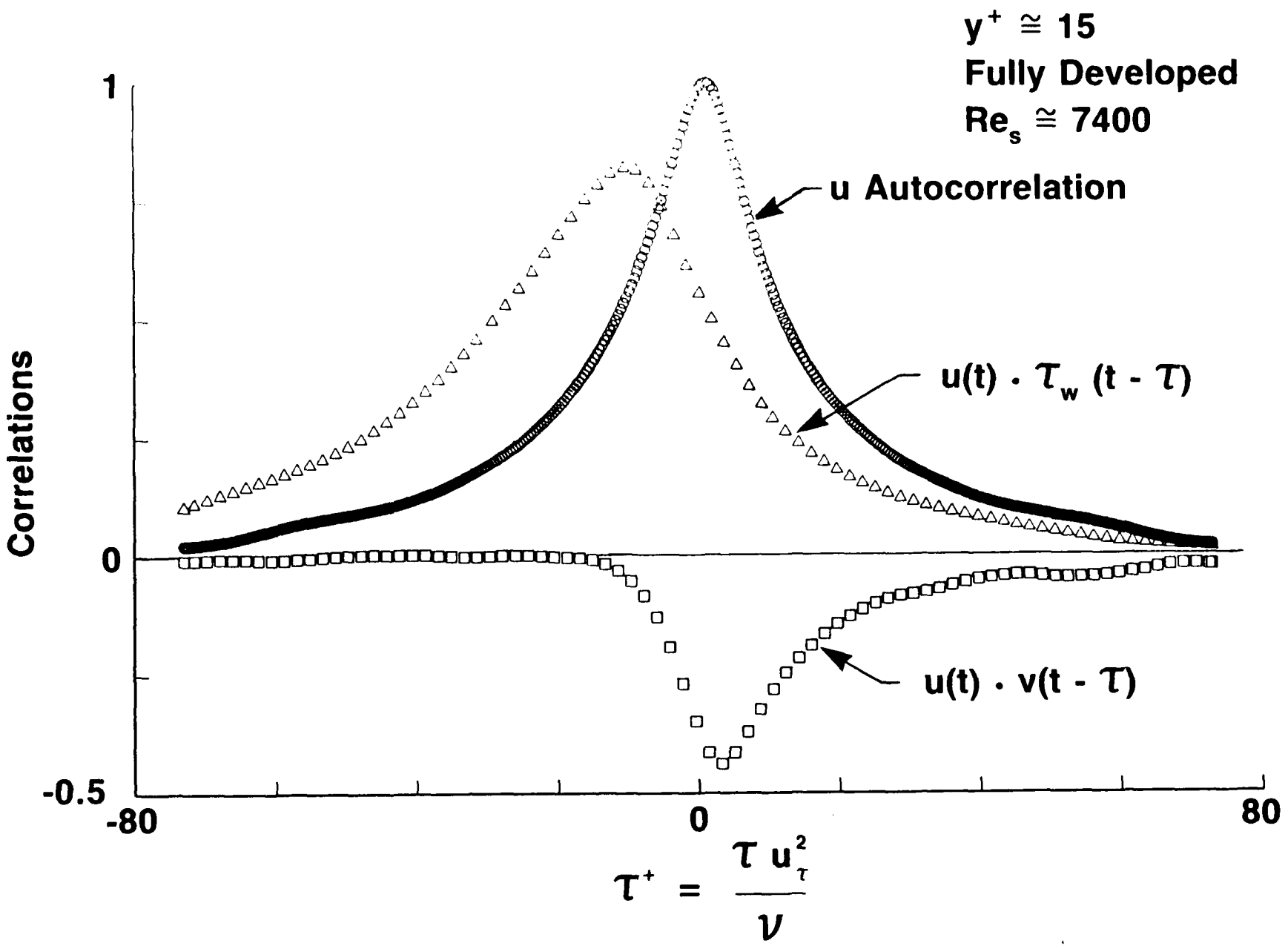

Fig. 8.9 Typical correlation coefficients for fully-developed flow, $K_p \simeq -0.008$, $y^+ \simeq 15$.

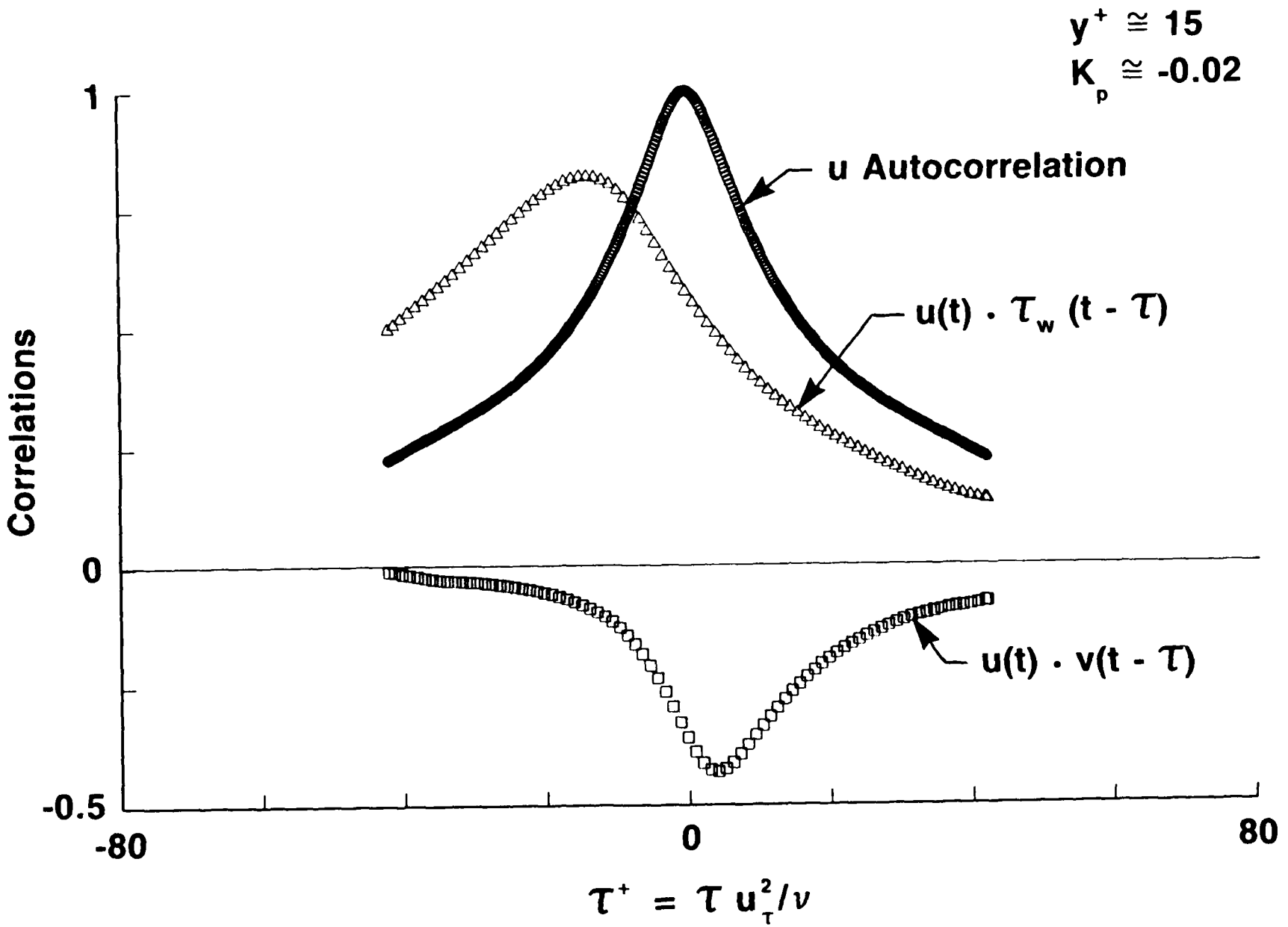

Fig. 8.10 Typical correlation coefficients for laterally-converging (streamwise-accelerating) flow, $K_p \simeq -0.02$, $y^+ \simeq 15$.

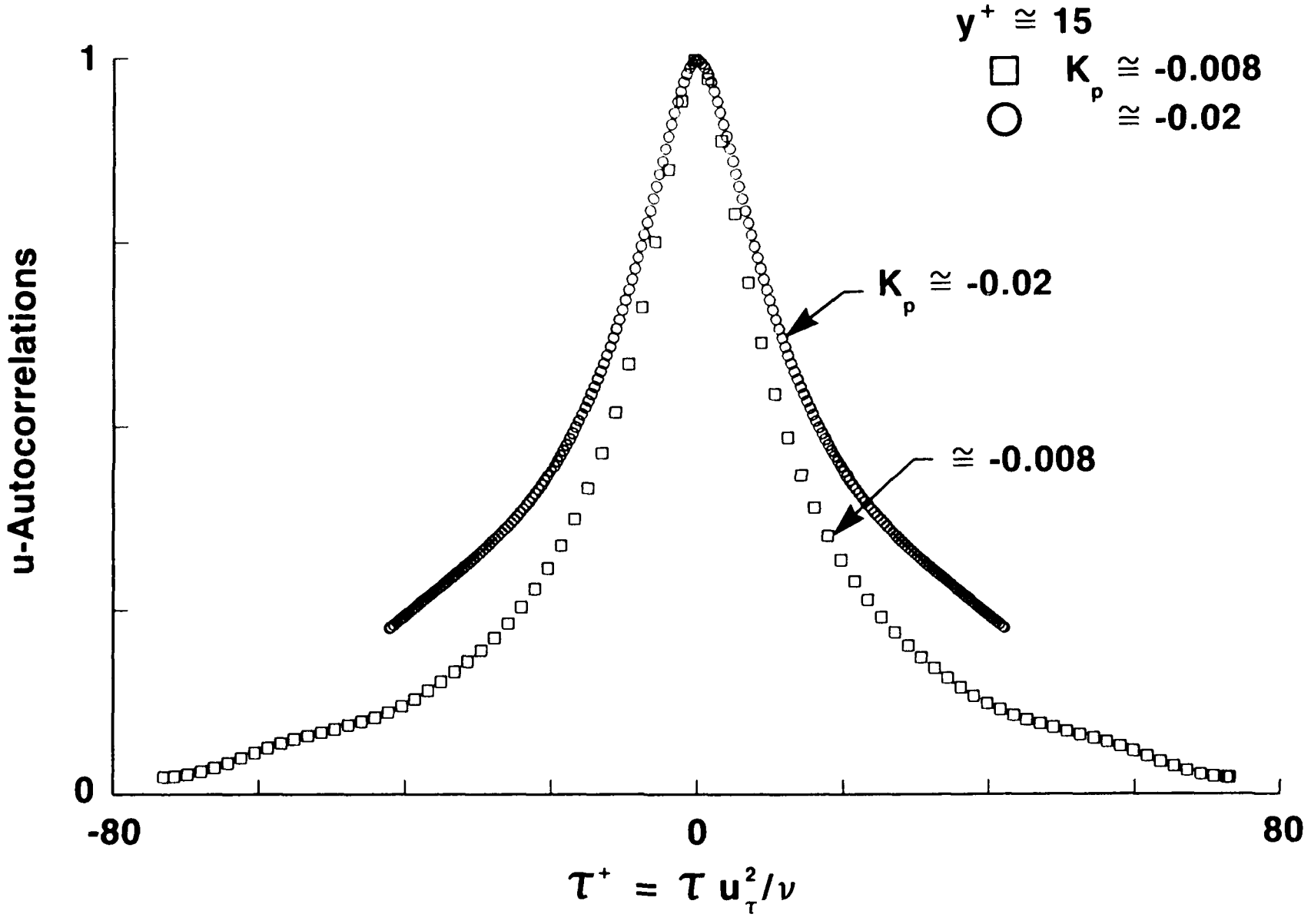

Fig. 8.11 Comparison of autocorrelation coefficients of streamwise fluctuations.

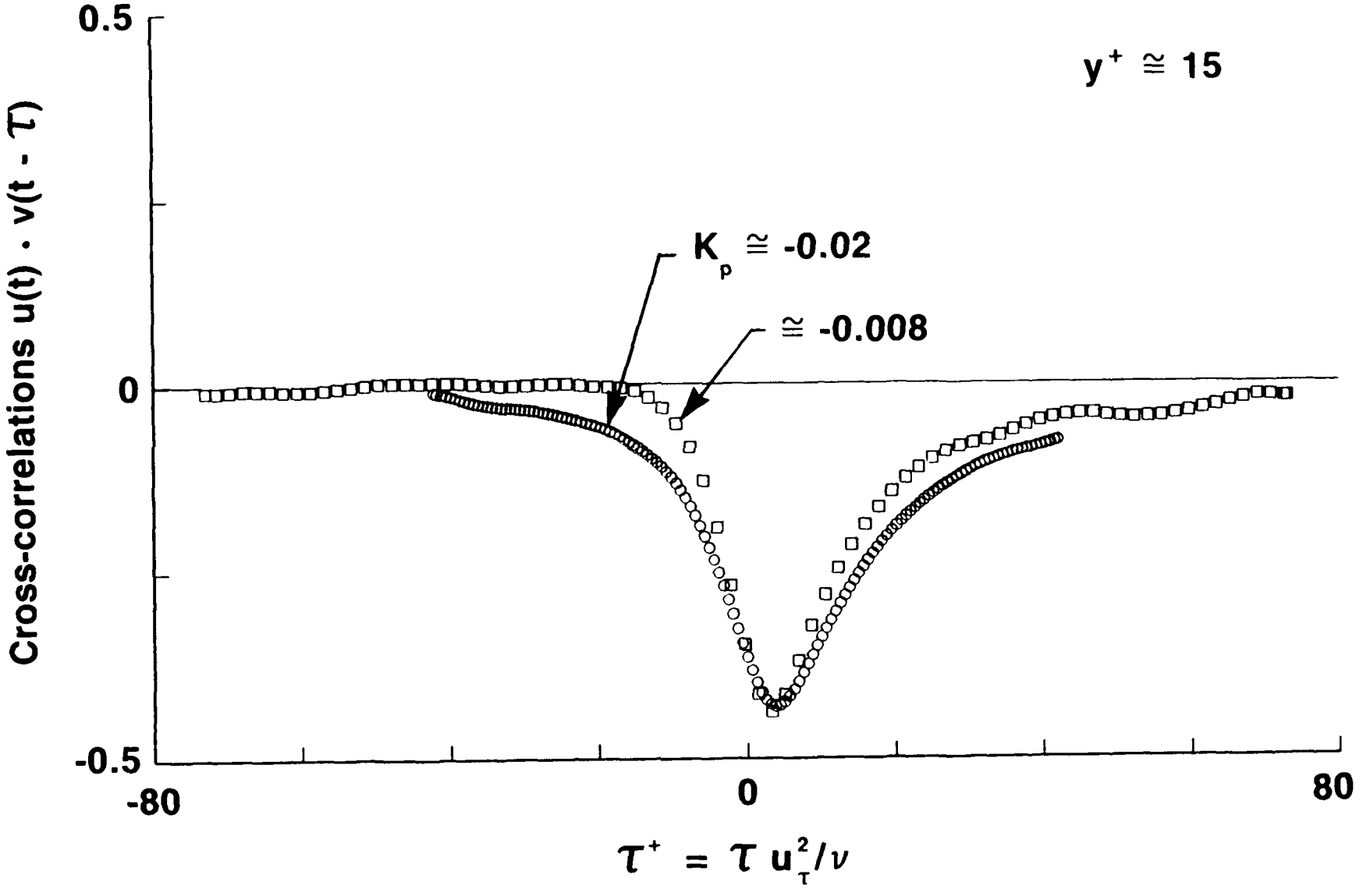

Fig. 8.12 Comparison of cross correlation coefficients for streamwise and normal fluctuations.

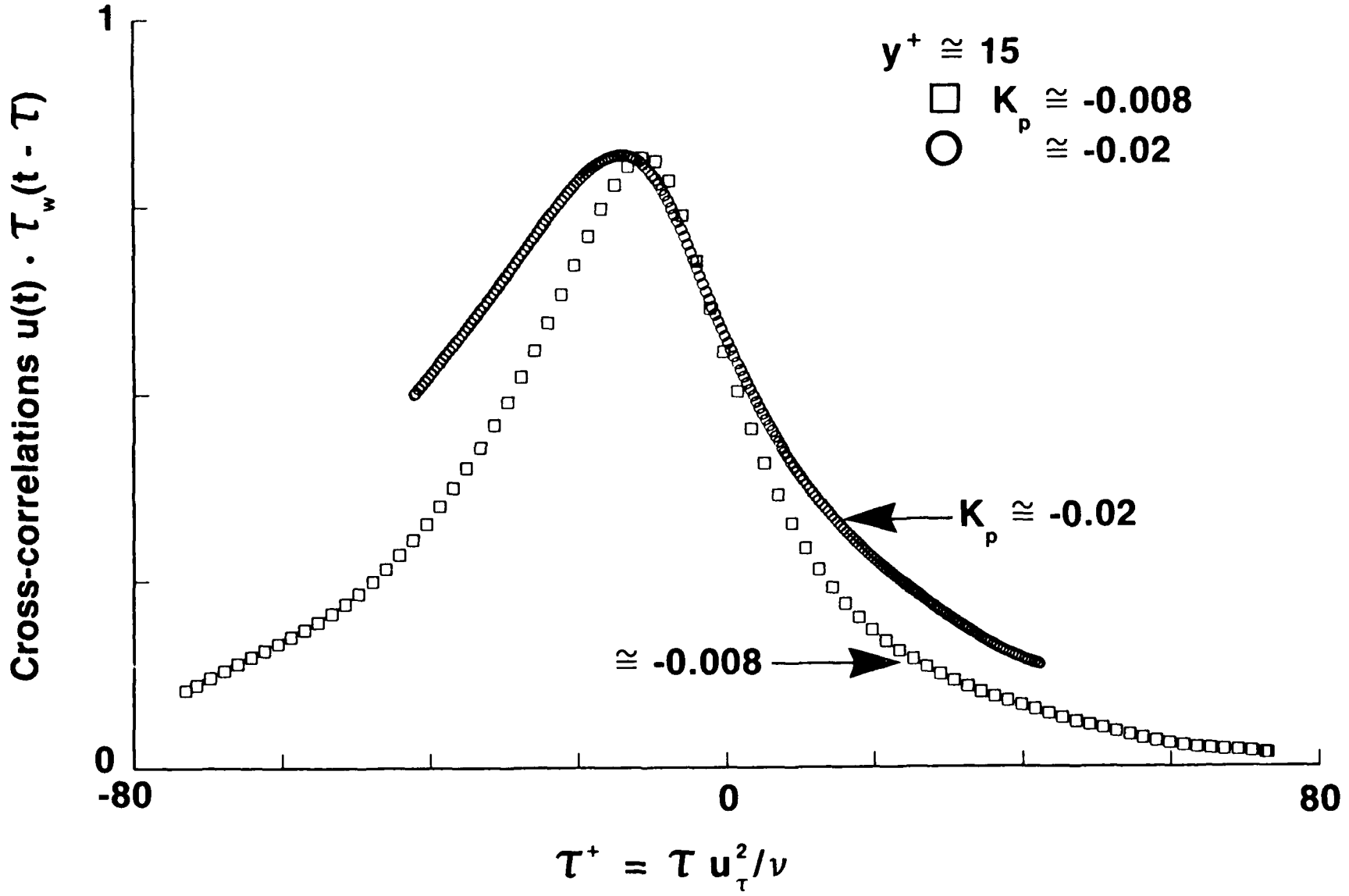

Fig. 8.13 Comparison of cross correlation coefficients for streamwise velocity and wall shear stress fluctuations.

Appendix A. MEAN STATISTICS OF VISCOUS LAYER

"Fully-developed" flow

$K_p = -0.00831$, $u_\tau = 1.05$ cm/s, pump speed ≃ 1790 rpm

Approximate y^+	7	10	15	25	Centerplane
T, °C	25.02	25.0	24.98	24.95	24.72
ν, cm²/sec	0.05977	0.05980	0.05984	0.05988	0.06024
y, mm	3.224	4.922	7.529	12.702	109.3
$\bar{u}$, cm/sec	5.79	8.12	10.91	14.04	20.32
$\bar{v}$, cm/sec	-0.295	-0.314	-0.200	-0.0499	0.0861
u', cm/sec	2.06	2.71	3.04	2.79	0.884
v', cm/sec	0.222	0.290	0.408	0.615	0.622
$\overline{uv}$ (cm/sec)²	-0.244	-0.352	-0.450	-0.607	-0.0404
S_u	0.606	0.331	-0.0673	-0.432	-0.614
S_v	0.179	0.316	0.286	-0.0228	0.139
F_u	2.97	2.43	2.16	2.52	3.63
F_v	4.34	5.31	6.28	4.64	3.93
y^+	5.64	8.60	13.15	22.17	189.6
u^+	5.54	7.77	10.43	13.43	19.44
v^+	-0.282	-0.301	-0.191	-0.0477	0.0824
u'^+	1.98	2.59	2.91	2.67	0.846
v'^+	0.214	0.278	0.390	0.589	0.595
$\overline{uv}/u_\tau^2$	-0.223	-0.322	-0.412	-0.555	-0.0370
$\bar{v}/\bar{u}$	-0.0509	-0.0387	-0.0183	-0.00356	+0.00424
$u'/\bar{u}$	0.356	0.334	0.279	0.199	0.0435
$v'/\bar{u}$	0.0384	0.0358	0.0374	0.0438	0.0306

Appendix A. MEAN STATISTICS OF VISCOUS LAYER (Cont'd.)

"Fully-developed" flow

$K_p = -0.0111$, $u_\tau = 0.801$ cm/sec, pump speed ≃ 1350 rpm

Approximate y^+	5	7	10	15	25	Centerplane
T, °C	24.9	24.9	24.82	24.82	24.85	24.74
ν, cm²/sec	0.05996	0.05996	0.06009	0.06009	0.06004	0.06021
y, mm	3.831	5.585	8.136	12.001	19.717	109.4
$\bar{u}$, cm/sec	4.02	5.54	7.49	9.41	11.41	15.39
$\bar{v}$, cm/sec	-0.203	-0.224	-0.195	-0.123	-0.0195	0.0798
u', cm/sec	1.47	1.89	2.19	2.30	1.96	0.701
v', cm/sec	0.157	0.179	0.235	0.325	0.483	0.468
$\overline{uv}$ (cm/sec)²	-0.165	-0.190	-0.214	-0.285	-0.345	-0.0326
S_u	0.653	0.398	0.0988	-0.210	-0.521	-0.688
S_v	-0.105	0.305	0.409	0.0501	-0.0518	+0.111
F_u	3.13	2.55	2.22	2.21	2.66	3.79
F_v	3.66	4.68	6.39	5.95	4.18	4.04
y^+	5.12	7.46	10.85	16.00	26.31	145.5
u^+	5.02	6.92	9.36	11.74	14.25	19.22
v^+	-0.253	-0.280	-0.244	-0.154	-0.0243	0.0996
u'^+	1.84	2.36	2.74	2.87	2.45	0.875
v'^+	0.196	0.224	0.294	0.406	0.603	0.584
$\overline{uv}/u_\tau^2$	-0.257	-0.296	-0.333	-0.445	-0.537	-0.0407
$\bar{v}/\bar{u}$	-0.0504	-0.0405	-0.0261	-0.0131	-0.00171	+0.00518
$u'/\bar{u}$	0.366	0.341	0.293	0.245	0.172	0.0455
$v'/\bar{u}$	0.0391	0.0324	0.0314	0.0346	0.0423	0.0304

Appendix A. MEAN STATISTICS OF VISCOUS LAYER (Cont'd.)

Laterally converging (spatially accelerated) flow

$K_p = -0.0108$, $u_\tau = 1.16$ cm/s, pump speed ≈ 1790 rpm

Approximate y^+	7	10	15	25	Centerplane
T, °C	25.07	25.05	25.0	24.98	24.72
ν, cm²/sec	0.05970	0.05973	0.05980	0.05984	0.06024
y, mm	3.50	5.20	7.801	13.001	110.0
$\bar{u}$, cm/sec	7.46	10.17	13.10	16.32	22.37
$\bar{v}$, cm/sec	-0.379	-0.386	-0.289	-0.178	-0.191
u', cm/sec	2.51	3.09	3.32	2.93	0.822
v', cm/sec	0.341	0.391	0.471	0.615	0.517
$\overline{uv}$ (cm/sec)²	-0.427	-0.486	-0.597	-0.666	-0.103
S_u	0.544	0.220	-0.124	-0.468	-0.697
S_v	-0.0293	0.270	0.356	0.0308	0.150
F_u	2.78	2.28	2.17	2.57	3.79
F_v	3.49	3.96	5.08	4.60	4.06
y^+	6.80	10.10	15.13	25.20	211.8
u^+	6.43	8.77	11.30	14.07	19.29
v^+	-0.327	-0.333	-0.249	-0.153	-0.165
u'^+	2.16	2.66	2.86	2.53	0.709
v'^+	0.294	0.337	0.406	0.530	0.446
$\overline{uv}/u_\tau^2$	-0.318	-0.361	-0.444	-0.495	-0.0766
$\bar{v}/\bar{u}$	-0.0508	-0.0380	-0.0221	-0.0109	0.00854
$u'/\bar{u}$	0.337	0.304	0.253	0.180	0.0367
$v'/\bar{u}$	0.0457	0.0384	0.0360	0.0377	0.0231

Appendix A. MEAN STATISTICS OF VISCOUS LAYER (Cont'd.)

Laterally converging (spatially accelerated) flow

$K_p = -0.0201$, $u_\tau = 0.793$ cm/s, pump speed ≃ 1200 rpm

Approximate y^+	5	7	10	15	25	Centerplane
T, °C	25.08	25.0	25.05	25.08	25.09	25.05
ν, cm²/sec	0.05968	0.05980	0.05973	0.05968	0.05966	0.05973
y, mm	3.84	5.592	8.121	12.019	19.719	110.0
$\bar{u}$, cm/sec	3.75	5.39	7.36	9.58	11.75	15.25
$\bar{v}$, cm/sec	-0.213	-0.215	-0.187	-0.139	-0.0917	-0.0280
u', cm/sec	1.21	1.79	2.15	2.29	1.96	0.572
v', cm/sec	0.165	0.195	0.219	0.2680	0.347	0.336
$\overline{uv}$ (cm/sec)²	-0.125	-0.186	-0.186	-0.225	-0.262	-0.0349
S_u	0.757	0.563	0.205	-0.197	-0.551	-0.942
S_v	0.437	-0.0506	0.470	0.433	0.0559	0.0824
F_u	3.37	2.69	2.24	2.15	2.64	4.75
F_v	4.04	3.57	5.33	5.09	5.20	4.07
y^+	5.11	7.43	10.80	15.99	26.25	146.3
u^+	4.72	6.793	9.27	12.06	14.80	19.20
v^+	-0.268	-0.271	-0.235	-0.175	-0.116	-0.0352
u'^+	1.53	2.26	2.71	2.88	2.47	0.720
v'^+	0.208	0.246	0.276	0.338	0.437	0.423
$\overline{uv}/u_\tau^2$	-0.200	-0.234	-0.295	-0.356	-0.416	-0.0553
$\bar{v}/\bar{u}$	-0.0568	-0.0399	-0.0254	-0.0145	-0.00780	-0.00184
$u'/\bar{u}$	0.324	0.332	0.292	0.239	0.167	0.0375
$v'/\bar{u}$	0.0440	0.0362	0.0298	0.0280	0.0296	0.0220

Appendix B. MEAN VELOCITY PROFILES

"Fully-developed" flow

$K_p \simeq -0.00831$, pump speed $\simeq$ 1790 rpm, V_b = 17.23 cm/sec
$Re = 2V_b s/\nu \simeq 1.25 \times 10^4$, $Re_s \simeq u_c s/\nu = 7410$.

y(mm)	$\bar{u}$(cm/s)	u^+	y^+
0	0	0	0
3.773	5.74	5.49	6.56
6.492	9.29	8.88	11.29
9.556	11.94	11.42	16.61
14.556	14.25	13.62	25.31
19.489	15.23	14.56	33.88
29.508	16.87	16.13	51.30
39.3	17.53	16.76	68.3
49.3	18.24	17.43	85.7
59.3	18.78	17.96	103.1
69.3	19.36	18.51	120.5
89.3	20.00	19.12	155.3
109.3	20.39	19.49	190.0

Appendix B. MEAN VELOCITY PROFILES (Cont'd.)

"Fully-developed" flow

$K_p \simeq -0.011$, pump speed $\simeq$ 1350 rpm, V_b = 12.82 cm/sec,
$Re = V_b 2s/\nu \simeq 9320$, $Re_s = u_c\, s/\nu \simeq 5600$.

y(mm)	$\tilde{u}$(cm/s)	u^+	y^+
0	0	0	0
3.805	3.79	4.73	5.07
6.477	6.01	7.49	8.63
8.964	7.53	9.40	11.94
14.717	10.26	12.81	19.60
19.241	11.04	13.78	25.63
29.099	12.54	15.64	38.76
39.4	13.15	16.42	52.5
49.4	13.69	17.08	65.8
59.4	14.16	17.67	79.1
69.4	14.45	18.04	92.4
89.4	15.12	18.87	119.1
109.4	15.39	19.20	145.7

Appendix B. MEAN VELOCITY PROFILES (Cont'd.)

Laterally converging (spatially accelerated) flows

$K_p \simeq -0.0108$, $V_b \simeq 19.48$ cm/sec,
$Re = V_b 2s/\nu \simeq 1.43 \times 10^4$, $Re_s = u_c s/\nu \simeq 8290$.

y(mm)	$\bar{u}$(cm/s)	u^+	y^+
0	0	0	0
5.000	9.39	8.09	9.64
10.000	14.38	12.39	19.28
14.020	16.76	14.44	27.03
27.7	19.04	16.40	53.4
55.2	20.95	18.04	106.4
82.7	22.07	19.01	159.5
110.2	22.64	19.50	212.5

$K_p \simeq -0.0201$, $V_b = 12.88$ cm/sec,
$Re = V_b 2s/\nu \simeq 9530$, $Re_s = u_c s/\nu \simeq 5600$.

y(mm)	$\bar{u}$(cm/s)	u^+	y^+
0	0	0	0
5.339	4.99	6.29	7.09
10.339	8.50	10.71	13.73
14.320	10.49	13.21	19.02
28.1	12.56	15.81	37.3
55.6	14.14	17.81	73.8
83.1	14.92	18.79	110.4
110.6	15.23	19.1?	146.9

Appendix C. Computer program TAU2.FOR

As described in Section 7, the technique for determination of the mean wall shear stress, from a single mean velocity measurement and the pressure gradient, was modified to account for the convective terms in the streamwise momentum equation. To accomplish the calculations, Fortran program TAUW.FOR [McEligot, 1984, Appendix B] was revised to TAU2.FOR which is provided here. A listing of the program follows, and then copies of the interactive iterative input statements and an example of the typical output. The bases of the program are described in Section 7.

Program listing

```
                                                          19-Mar-1990 18:08:31
 VAX FORTRAN V4.8-276                Page    1
                                                          19-Mar-1990 17:39:33
 DISK$DISK2:[LEHMANN.OLDVAX]TAU2.FOR;9

CCCCCCCCCCCCCCCCCCCCCCCCCCCCCCCCCCCCCCCCCCCCCCCCCCCCCCCCCCCCCCCCCCCCCCCCCCCCCCCC
C
C            D. M. McELIGOT    bei    H. ECKELMANN                    19 Mar 1990
C                                                                          1745
C                File TAU2.FOR
C
C           Calculation of wall shear stress with acceleration correction
C
CCCCCCCCCCCCCCCCCCCCCCCCCCCCCCCCCCCCCCCCCCCCCCCCCCCCCCCCCCCCCCCCCCCCCCCCCCCCCCC
C
C    PROGRAM TO DEDUCE WALL SHEAR STRESS
C                  WITH VAN DRIEST MODEL
C       HUFFMAN & BRADSHAW VERSION (JFM, 1972)
C
COUT       DOUBLE PRECISION Y1,Y2, Y3, F1,F2,F3,E,G,K,YL, YM, U1,U2,U3, KP,D
      IMPLICIT INTEGER*4 (I-N), REAL*8(A-H,O-Z)
      REAL*8 K, KP
      CHARACTER*9 TAG, ZEIT*8
      DIMENSION CI(1000)
C
      K = 0.4
      YL0 = 26.0
      A = 0.0
      IP = 2
      ICOR = 0
C
      CALL TIME(ZEIT)                                  ! Find system time
      CALL DATE(TAG)                                   ! Find system date
      WRITE(7,*)
      WRITE(7,11102) ZEIT, TAG
11102 FORMAT(/ '                           Start of calculation at ',
     +        A8,' on ',A9,/ )
      WRITE(7,11101)
11101 FORMAT(/
     +' ***************************************************************'//
     +'           D. M. McELIGOT    bei    H. ECKELMANN               '//
     +' ***************************************************************'//)
C
10    WRITE(7,*) 'DATA REDUCTION FOR WALL SHEAR STRESS'
```

Program listing (Cont'd.)

```
0040          WRITE(6,*) 'TEMP(C)? TOLERANCE?'
0041          READ(5,*)  T, EPS
0042          WRITE(6,*) 'DZ PROBABLY NEGATIVE'
0043          WRITE(6,*) 'DZ(MM OIL)? DX(CM)?'
0044          READ(5,*) DZ, DX
0045     C
0046     C       OIL PROPERTIES (REICHARDT,1953;ECKELMANN,1970)
0047          RO = 0.8358 - 0.000685*(T - 20.)
0048     C         GM/CC
0049          XMU = 4.99 - 0.13375*(T - 24.91)
0050     C         CENTIPOISE
0051          XMU = 0.001*XMU
0052     C         KG/M.SEC
0053          XNU = 10.*XMU/RO
0054     C         CM2/SEC

0055     C

0056          DZ = 0.1*DZ

0057     C         CM OIL
0058          WRITE(7,*) ' DZ = ',DZ,' CM, DX = ',DX,' CM'
0059          WRITE(7,*) ' TEMP = ',T,' C, RHO = ',RO,' GM/CM3'
0060          WRITE(7,*) ' VISC = ',XMU,' KG/M.SEC,  KIN VISC = ',XNU,
0061         +           ' CM2/SEC'
0062     C

0063     C         START LOOP FOR NEW DATA POINT

0064     C
0065     30   WRITE(6,*) ' Apply acceleration correction (Y=1,N=0)? >'
0066          READ(5,*) ICOR
0067          WRITE(6,*) ' YI(MM) ? UI(CM/SEC) ? N ?'

0068          READ(5,*)  YI, UI, N
0069          WRITE(6,*) ' Estimate of u,cl(cm/sec) ? >'
0070          READ(5,*) UCL
0071          WRITE(7,*) ' ICOR = ',ICOR,', u,cl(cm/sec) = ',UCL
0072          J = 1

0073          YI = 0.1*YI

0074     C         CM

0075          DCM = (YI - A)/N

0076          UICM = 0.0

0077          UT2M = 0.0

0078          IPRO = 0
0079          XCR = ICOR
0080          DO 35  I = 1, N
0081             CI(I) = 0.0D00
0082     35   CONTINUE
0083     C

0084     C         FIRST ESTIMATE

0085     C

0086          UT2 = 1. - (0.5*980.7*DZ*YI*YI)/(XNU*DX*UI)

0087          UT2 = UT2*XNU*UI/YI
```

Program listing (Cont'd.)

```
0088    C
0089    C          START OF ITERATION LOOP
0090    C
0091    40    CONTINUE
0092          UT = SQRT(UT2)
0093          UT3 = UT*UT2
0094          KP = 980.7*XNU*DZ/(UT3*DX)
0095          IF(KP.LT.(-0.0249))  KP = -0.0240
0096          CF = 2.0 * UT2 / UCL**2
0097          D = DCM*UT/XNU
0098          YM = YI*UT/XNU
0099          IC = 0
0100          A = 0.0
0101          Y1 = 0.0
0102          U1 = 0.0
0103          F1 =  1.0
0104    C
0105    C          APPROXIMATION OF HUFFMAN A+
0106          YL = YL0 - 31.3*LOG(1. + (KP/0.025) )
0107    C
0108          UO = 0.0
0109          UO2 = 0.0
0110          WRITE(7,20) K, YL, KP, YM, N, IP, D
0111    20    FORMAT(1X,//10X,'MEAN VELOCITY PROFILE',//
0112         1   10X,'VAN DRIEST (HUFFMAN/BRADSHAW) MODEL',//
0113         2   5X,'KAPPA = ',F9.6,'  Y+,L = ',F9.4,'  K,P = ',1PE12.4/
0114         3   5X,'Y+,MAX = ',0PF9.4,'  N = ',I3,'  PRINT INT = ', I3,
0115         4   '  DY+ = ',1PE12.4,///
0116         5   6X,'Y+',7X,'U+',6X,'(U+ - Y+)/U+',
0117         6   2X,'(U+ - Y+)/Y+',2X,'(U+ - UC)/U+' /)
0118          WRITE(7,22) Y1, U1, UO, UO2
0119          N1 = N + 1
0120          NM1 = N - 1
0121          DO 55 I = 1,NM1,2
0122             IC = IC + 1
```

Program listing (Cont'd.)

```
0123              Y2 = Y1 + D
0124              Y3 = Y2 + D
0125    C
0126    C             VAN DRIEST MODEL USED
0127              E = K*Y2*(1. - EXP(-Y2/YL))
0128              E = E*E
0129              G = 1. + KP*Y2
0130           +      *(1.0-(XCR*CF*CI(I+1)/(2.0*Y2) ) )
0131    C234567
0132              F2 = (-1. + SQRT(1. + 4.*E*G))/(2.*E)
0133              E = K*Y3*(1. - EXP(-Y3/YL))
0134              E = E*E
0135              G = 1. + KP*Y3
0136           +      *(1.0-(XCR*CF*CI(I+2)/(2.0*Y3) ) )
0137              F3 = (-1. + SQRT(1. + 4.*E*G))/(2.*E)
0138    C
0139    C             SIMPSON'S RULE INTEGRATION
0140    C
0141              U3 = (D*(F1 + 4.*F2 + F3)/3.) + U1
0142    C
0143    C             CORRECTION FOR CONVECTIVE TERMS IN ACCELERATED FLOWS
0144    C
0145              IF(ICOR.NE.1)  GO TO 50
0146              U2 = (U1 + U3) / 2.0
0147              CI(I+1) = CI(I) + (U1*U1+U2*U2)*D/2.0
0148              CI(I+2) = CI(I+1) + (U2*U2+U3*U3)*D/2.0
0149    C
0150    50        CONTINUE
0151              U1 = U3
0152              Y1 = Y3
0153              F1 = F3
0154              IF(IPRO.NE.1)  GO TO 55
0155              IF(IC.NE.IP)  GO TO 55
0156              IC = 0
0157              UO = (U3 - Y3)/U3
0158              UO2 = (U3 - Y3)/Y3
0159              UC = Y3*(1. + 0.5*KP*Y3)
0160              UO3 = (U3 - UC)/U3
0161              WRITE(7,22)  Y3, U3, UO, UO2, UO3
0162    22        FORMAT(2X,F8.3,2X,F8.3,2X,1PE12.4,3(2X,E12.4) )
```

Program listing (Cont'd.)

```
0163     55    CONTINUE

0164           UO = (U3 - Y3)/U3

0165           UO2 = (U3 - Y3)/Y3

0166           UIC = U3*UT

0167           ERR = (UIC - UI)/UI

0168           WRITE(7,22) Y3, U3, UO, UO2

0169           WRITE(6,*) YI,UI,UT,Y3,U3,UIC
0170           WRITE(6,*) ' Convergence error(fraction) = ',ERR
0171           WRITE(6,*) ' Trial K,p = ', KP
0172           WRITE(7,*) ' ITERATION: y,meas(cm), u,meas(cm/sec), u,tau(cm/sec)'
0173           WRITE(7,*) YI,UI,UT
0174           WRITE(7,*) ' y,+(pred), u+(pred), UIC'
0175           WRITE(7,*) Y3,U3,UIC
0176           WRITE(7,*) ' Convergence error(fraction)  = ',ERR
0177           WRITE(6,*) 'MORE? (1=YES) '                  ! Iteration control
0178           READ(5,*) IA

0179           UT2P = ((UI-UIC)*(UT2-UT2M)/(UIC-UICM)) + UT2

0180           UICM = UIC

0181           UT2M = UT2

0182           UT2 = UT2P

0183           IF(IA.EQ.1)  GO TO 40
0184           UT = SQRT(UT2)
0185           UT3 = UT*UT2
0186           CF = 2.0 * UT2 / UCL**2
0187           KP = 980.7*XNU*DZ/(UT3*DX)
0188           WRITE(7,11103)
0189     11103 FORMAT(/' ************************************************'/)
0190           WRITE(7,*) ' ICOR = ',ICOR,',   u,tau(cm/sec) = ',UT
0191           WRITE(7,*) ' C,f(based on u,cl) = ',CF,
0192          +           ',  K,p = ', KP
0193           WRITE(7,*) '    (ICOR = 1 = acceleration correction included'
0194           WRITE(7,*) '          = 0 = not included )'
0195           WRITE(7,11103)
0196           WRITE(6,*)  'ANOTHER POINT? (1=YES)'

0197           READ(5,*)  IB

0198           IF(IB.EQ.1)  GO TO 30

0199           WRITE(6,*)  'NEW T OR DP ? (1=YES)'

0200           READ(5,*)  ID

0201           IF(ID.EQ.1)  GO TO 10
0202           WRITE(7,11102) ZEIT, TAG
0203           WRITE(7,11101)
0204     C
0205           STOP
0206           END
```

Typical interactive input from terminal

Unit 6 provides the prompts to the terminal screen and Unit 5 is the user's response at the terminal.

```
0039    10    WRITE(7,*) 'DATA REDUCTION FOR WALL SHEAR STRESS'
0040          WRITE(6,*) 'TEMP(C)? TOLERANCE?'
0041          READ(5,*)  T, EPS
0042          WRITE(6,*) 'DZ PROBABLY NEGATIVE'
0043          WRITE(6,*) 'DZ(MM OIL)? DX(CM)?'
0044          READ(5,*) DZ, DX



0063    C           START LOOP FOR NEW DATA POINT

0064    C
0065    30    WRITE(6,*) ' Apply acceleration correction (Y=1,N=0)? >'
0066          READ(5,*) ICOR
0067          WRITE(6,*) ' YI(MM) ? UI(CM/SEC) ? N ?'

0068          READ(5,*)  YI, UI, N
0069          WRITE(6,*) ' Estimate of u,cl(cm/sec) ? >'
0070          READ(5,*) UCL



0169          WRITE(6,*) YI,UI,UT,Y3,U3,UIC
0170          WRITE(6,*) ' Convergence error(fraction) = ',ERR
0171          WRITE(6,*) ' Trial K,p = ', KP



0177          WRITE(6,*) 'MORE? (1=YES) '                  ! Iteration control
0178          READ(5,*) IA



0196          WRITE(6,*)  'ANOTHER POINT? (1=YES)'

0197          READ(5,*)  IB

0198          IF(IB.EQ.1)  GO TO 30

0199          WRITE(6,*)  'NEW T OR DP ? (1=YES)'

0200          READ(5,*)  ID

0201          IF(ID.EQ.1)  GO TO 10
0202          WRITE(7,11102) ZEIT, TAG
0203          WRITE(7,11101)
0204    C
0205          STOP
0206          END
```

Typical output from interactive session

```
DATA REDUCTION FOR WALL SHEAR STRESS
 DZ =  -3.0000000000000000E-02 CM, DX =     174.7000000000000      CM
 TEMP =     25.08000000000000      C, RHO =    0.8323202000000000      GM/CM3
 VISC =    4.9672625000000000E-03 KG/M.SEC,  KIN VISC =    5.9679706199609238E-02
 CM2/SEC
 ICOR =             1, u,cl(cm/sec) =     15.25100000000000


         MEAN VELOCITY PROFILE

         VAN DRIEST (HUFFMAN/BRADSHAW) MODEL

    KAPPA =  0.400000  Y+,L =  104.1371  K,P =  -2.2940E-02
    Y+,MAX =   15.2958  N = 150  PRINT INT =   2  DY+ =   1.0197E-01


     Y+        U+       (U+ - Y+)/U+  (U+ - Y+)/Y+  (U+ - UC)/U+

    0.000     0.000     0.0000E+00    0.0000E+00
   15.296    11.833    -2.9268E-01   -2.2641E-01
 ITERATION: y,meas(cm), u,meas(cm/sec), u,tau(cm/sec)
  1.201900000000000        9.579000000000000       0.7595033691333739
 y,+(pred), u+(pred), UIC
  15.29577066462467        11.83262820706867       8.986920988971251
 Convergence error(fraction)  =  -6.1810106590327678E-02


         MEAN VELOCITY PROFILE

         VAN DRIEST (HUFFMAN/BRADSHAW) MODEL

    KAPPA =  0.400000  Y+,L =   82.1830  K,P =  -2.0847E-02
    Y+,MAX =   15.7916  N = 150  PRINT INT =   2  DY+ =   1.0528E-01


     Y+        U+       (U+ - Y+)/U+  (U+ - Y+)/Y+  (U+ - UC)/U+

    0.000     0.000     0.0000E+00    0.0000E+00
   15.792    12.076    -3.0769E-01   -2.3529E-01
 ITERATION: y,meas(cm), u,meas(cm/sec), u,tau(cm/sec)
  1.201900000000000        9.579000000000000       0.7841232469575866
 y,+(pred), u+(pred), UIC
  15.79159467317374        12.07598699939817       9.469062136185694
 Convergence error(fraction)  =  -1.1476966678599649E-02


         MEAN VELOCITY PROFILE

         VAN DRIEST (HUFFMAN/BRADSHAW) MODEL

    KAPPA =  0.400000  Y+,L =   79.0784  K,P =  -2.0414E-02
    Y+,MAX =   15.9025  N = 150  PRINT INT =   2  DY+ =   1.0602E-01


     Y+        U+       (U+ - Y+)/U+  (U+ - Y+)/Y+  (U+ - UC)/U+
```

Typical output from interactive session (Cont'd.)

```
   0.000      0.000     0.0000E+00     0.0000E+00
  15.902     12.112    -3.1?93E-01    -2.3834E-01
ITERATION: y,meas(cm), u,meas(cm/sec), u,tau(cm/sec)
 1.201900000000000        9.579000000000000       0.7896296084287344
y,+(pred), u+(pred), UIC
 15.90248824610853        12.11222110904989       9.564168411541314
Convergence error(fraction)  =  -1.5483441339060719E-03


        MEAN VELOCITY PROFILE

        VAN DRIEST (HUFFMAN/BRADSHAW) MODEL

   KAPPA =  0.400000  Y+,L =   78.6299  K,P =  -2.0347E-02
   Y+,MAX =   15.9197  N = 150  PRINT INT =   2  DY+ =   1.0613E-01


    Y+        U+       (U+ - Y+)/U+   (U+ - Y+)/Y+   (U+ - UC)/U+

   0.000      0.000     0.0000E+00     0.0000E+00
  15.920     12.119    -3.1366E-01    -2.3877E-01
ITERATION: y,meas(cm), u,meas(cm/sec), u,tau(cm/sec)
 1.201900000000000        9.579000000000000       0.7904848547073068
y,+(pred), u+(pred), UIC
 15.91971219990579        12.11859558323355       9.579566268868983
Convergence error(fraction)  =   5.9115656016590674E-05


        MEAN VELOCITY PROFILE

        VAN DRIEST (HUFFMAN/BRADSHAW) MODEL

   KAPPA =  0.400000  Y+,L =   78.6462  K,P =  -2.0350E-02
   Y+,MAX =   15.9191  N = 150  PRINT INT =   2  DY+ =   1.0613E-01


    Y+        U+       (U+ - Y+)/U+   (U+ - Y+)/Y+   (U+ - UC)/U+

   0.000      0.000     0.0000E+00     0.0000E+00
  15.919     12.119    -3.1358E-01    -2.3872E-01
ITERATION: y,meas(cm), u,meas(cm/sec), u,tau(cm/sec)
 1.201900000000000        9.579000000000000       0.7904534187114223
y,+(pred), u+(pred), UIC
 15.91907910490817        12.11889022361206       9.579418208242582
Convergence error(fraction)  =   4.3658862363722366E-05


        MEAN VELOCITY PROFILE

        VAN DRIEST (HUFFMAN/BRADSHAW) MODEL

   KAPPA =  0.400000  Y+,L =   78.6924  K,P =  -2.0357E-02
   Y+,MAX =   15.9173  N = 150  PRINT INT =   2  DY+ =   1.0612E-01


    Y+        U+       (U+ - Y+)/U+   (U+ - Y+)/Y+   (U+ - UC)/U+
```

Typical output from interactive session (Cont'd.)

```
   0.000     0.000    0.0000E+00    0.0000E+00
  15.917    12.118   -3.1347E-01   -2.3866E-01
ITERATION: y,meas(cm), u,meas(cm/sec), u,tau(cm/sec)
 1.2019000000000000       9.5790000000000000      0.7903646186512759
y,+(pred), u+(pred), UIC
 15.917290745026 97       12.11849922037130       9.578033014934551
Convergence error(fraction)  =  -1.0094843568733802E-04


        MEAN VELOCITY PROFILE



        VAN DRIEST (HUFFMAN/BRADSHAW) MODEL

   KAPPA =  0.400000  Y+,L =   78.6602  K,P =  -2.0352E-02
   Y+,MAX =   15.9185  N = 150  PRINT INT =   2  DY+ =   1.0612E-01


    Y+       U+      (U+ - Y+)/U+  (U+ - Y+)/Y+  (U+ - UC)/U+

   0.000     0.000    0.0000E+00    0.0000E+00
  15.919    12.119   -3.1355E-01   -2.3870E-01
ITERATION: y,meas(cm), u,meas(cm/sec), u,tau(cm/sec)
 1.2019000000000000       9.5790000000000000      0.7904266098460991
y,+(pred), u+(pred), UIC
 15.91853919649905       12.11872123327992       9.578959740091384
Convergence error(fraction)  =  -4.2029343997[illegible]8896E-06

**************************************************

 ICOR =            1,   u,tau(cm/sec) =   0.7904293028319327
 C,f(based on u,cl) =   5.3722896225529610E-03,  K,p =  -2.0351766221567797E-02
    (ICOR = 1 = acceleration correction included
          = 0 = not included )

**************************************************
```

REFERENCES CITED

Alfredsson, P.H., and A.V. Johannsson, 1984. J. Fluid Mech., 19, pp 325-345.

Alfredsson, P.H., A.V. Johannsson, J.H. Haritonidis and H. Eckelmann, 1988. Phys. Fluids, 31, pp 1026-1033.

Badri Narayanan, M.A., and V. Ramjee, 1969. J. Fluid Mech., 35, pp 225-241.

Bankston, C.A., and D.M. McEligot, 1970. Int. J. Heat Mass Transfer, 13, pp 319-344.

Berman, N.S., 1977. Ann. Rev. Fluid Mech.

Black, T.J., 1966. Proc., Heat Transfer and Fluid Mech. Inst., pp 366-386. Stanford University Press.

Black, T.J., 1968. NASA CR-888.

Blackwelder, R.F., and H. Eckelmann, 1978. Lecture Notes in Physics, 75, pp 190-204.

Blackwelder, R.F., and R.E. Kaplan, 1976. J. Fluid Mech., 76, pp 86-112.

Blackwelder, R.F., and L.S.G. Kovasznay, 1972. J. Fluid Mech., 53, pp 61-83.

Blake, W.K., 1986. Mechanics of Flow-Induced Sound and Vibration. Academic Press.

Bradshaw, P., 1967. J. Fluid Mech., 30, pp 241.

Bradshaw, P., 1969. J. Fluid Mech., 35, pp 387-390.

Brodkey, R.S., 1975. Personal communication at seminar by D.M. McEligot, Max Planck Inst. für Strömungsf., Göttingen, BRD, March.

Brodkey, R.S., 1990. Personal communication, Ohio State Univ.

Brooks, T.F., and T.H. Hodgson, 1981. J. Sound Vib., 78, pp 69-117.

Brown, G.L., and A.S.W. Thomas, 1977. Phys. Fluids Suppl., 20, pp 243-252.

Burton, T.E., 1973. Acoust. and Vibr. Lab., MIT, Rep. No. 70208-9.

Cantwell, B., 1981. Ann. Rev. Fluid Mech., 13, pp 457-515.

Chambers, F.W., 1985. Synthetically generated turbulent boundary layer development and structure. AIAA paper, pp 85-0534.

Chambers, F.W., H.D. Murphy and D.M. McEligot, 1983. J. Fluid Mech., 127, 403-428.

Chase, D.M., 1980. J. Sound Vib., 70, pp 29-67.

Chase, D.M., 1981. Tech Memo 21, Chase, Inc..

Corcos, G.M., 1963. J. Acoustical So. Amer., 35, pp 192-199.

Corcos, G.M., 1967. J. Sound Vib., 6, pp 59-70.

Corino, E.R., and R.S. Bordkey, 1969. J. Fluid Mech., 37, pp 1-30.

Dinkelacker, A., and T.H. Langeheineken, 1982. IUTAM Symposium, Marseille.

Donohue, G.L., W.G. Tiederman and M.M. Reischman, 1972. J. Fluid Mech., 56, p 559.

REFERENCES CITED (Cont'd.)

Eckelmann, H., 1970. Mitt. MPI für Strömungsf./AVA Göttingen Nr. 48 (English translation available).

Eckelmann, H., 1974. J. Fluid Mech., 65, pp 439-459.

Eckelmann, H., 1980. Personal communication, Max Planck Institut für Strömungsforschung, Göttingen, BRD.

Finnicum, D.S., and T.J. Hanratty, 1987. Rpt 7, Ch.E. Dept., U. Illinois.

Finnicum, D.S., and T.J. Hanratty, 1988. A.I.Ch.E. Journal, 34, pp 529-540.

Ffowcs Williams, J.E., 1982. J. Fluid Mech., 125, pp 9-25.

Hahn, M., 1976. AIAA paper 76-335.

Handler, R.A., R.J. Hansen, L. Sakell, S.A. Orszag and E. Bullister, 1983. Phys. Fluids, 27, p 549.

Hanratty, T.J., 1988. Personal communication, Univ. Illinois.

Harder, K.J., and W.G. Tiederman, 1989. Influence of wall strain rate, polymer concentration and channel height upon drag reduction and turbulent structure. Report PME-FM-89-1, Purdue Univ.

Haritonidis, J.H., and A.V. Johansson, 1985. Pers. Comm. from M.T. Landahl, MIT.

Hendricks, E.W., 1988. Draft manuscript, Naval Research Laboratory.

Hoyt, J.W., and A.C. Fabula, 1964. 5th. Symp., Naval Hydrodynamics.

Huffman, G.D., and P. Bradshaw, 1972. J. Fluid Mech., 53, pp 45-60.

Hwang, Y.F., and F.E. Geib, 1983. ASME WAM Paper, Boston.

Johansson, A.V., and P.H. Alfredsson, 1982. J. Fluid Mech., 122, pp 295-314.

Johansson, A.V., J.-Y. Her and J.H. Haritonidis, 1987. J. Fluid Mech., 175, pp 119-42.

Jones, W.C., and B.E. Launder, 1972. J. Fluid Mech., 56, pp 337-351.

Julien, H.L., W.M. Kays and R.J. Moffat, 1969. Tech. Rpt. HMT-4, Thermosci Div., Mech. Engr. Dept., Stanford Univ.

Kim, H.T., S.J. Kline and W.C. Reynolds, 1971. J. Fluid Mech., 177, pp 133-166.

Kim, J., P. Moin and R. Moser, 1987. J. Fluid Mech., 177, pp 133-166.

Kim, J., and P.R. Spalart, 1987. Phys. Fluids, 30, pp 3326-8.

Kline, S.J., W.C. Reynolds, F.A. Schraub and P.W. Rundstadler, 1967. J. Fluid Mech., 30, pp 741-773.

Kobashi, Y., H. Komoda and M. Ichijo, 1984. Turbulence and Chaotic Phenomena in Fluids, Elsevier pp 461-466.

Kraichman, R.H., 1956. J. Acoust. Soc. Amer., 28, p 378.

REFERENCES CITED (Cont'd.)

Kreplin, H.P., and H. Eckelmann, 1979. J. Fluid Mech., 95, pp 305-322.

Landahl, M.T., 1967. J. Fluid Mech., 29, pp 441-459.

Landahl, M.T., 1980. A theoretical model for coherent structures in wall turbulence. ICHM/IUTAM Meeting, Dubrovnik, October 1980.

Landahl, M.T., 1975. J. Acoust. Soc. Amer., 57, pp 824-831.

Langeheineken, T., 1981. Mitt. Nr70, MPI Strömingsf.

Launder, B.E., and W.P. Jones, 1969. J. Fluid Mech., 38, pp 817-831.

Leehey, P., 1985. ONRL Report R-5-85, London.

Lim, K.B., 1971. Thesis, Dept. Mech. Eng., Univ. Adelaide.

Loyd, R.J., R.J. Moffat and W.M. Kays, 1970. Tech. Rpt. HMT-13, Thermosci. Div., Mech. Engr. Dept., Stanford Univ.

Luchik, T.S., and W.G. Tiederman, 1987. J. Fluid Mech., 174, pp 529-552.

Martini, K., P. Leehey and M. Moeller, 1984. Acoust. and Vibr. Lab., MIT, Rpt. No. 92828-1.

McEligot, D.M, 1963. Ph.D. thesis, Stanford Univ.

McEligot, D.M, 1984. Bericht 109/1984, Max Planck Inst. Für Strömungsf., Göttingen, BRD.

McEligot, D.M, 1985. Lec. Notes Physics, 235, pp 292-303.

McEligot, D.M, 1985. GOULD-OSD-771-HYDRO-BP-85-15 (Proprietary).

McEligot, D.M, 1986. Adv. Transport Processes, 4, pp 113-200.

McEligot, D.M, 1986. High Temperature Heat Exchangers (Ed.: Y. Mori et al.), New York: Hemisphere, pp 60-86.

McEligot, D.M., C.W. Coon and H.C. Perkins, 1970. Int. J. Heat Mass Transfer, 13, pp 431-433.

McEligot, D.M., L.W. Ormand and H.C. Perkins, 1966. J. Heat Transfer, 88, pp 239-245.

Meng, J.C.S., and J.A. Lovett, 1985. GOULD-OSD-771-HYDRO-CR-85-02.

Moretti, P.M., and W.M. Kays, 1965. Int. J. Heat Mass Transfer, 8, pp 1187-1202.

Moin, P., and P.R. Spalart, 1988. Advances in Turbulence (Ed.: W.K. George and R. Arndt), New York: Hemisphere, pp 11-38.

Murphy, H.D., 1979. Ph.D. thesis, Univ. Arizona. Also Report LA-7906-T, available from the National Technical Information Service.

Murphy, H.D., F.W. Chambers and D.M. McEligot, 1983. J. Fluid Mech., 127, pp 379-401.

REFERENCES CITED (Cont'd.)

Murphy, H.D., M. Coxon and D.M. McEligot, 1978. J. Fluid Engr., 100, pp 477-484.

Narasimha, R., and K.R. Sreenivasan, 1979. Adv. Appl. Mech., 19, pp 221-309.

Nikolaides, C., 1984. Ph.D. thesis, Univ. Illinois.

Offen, G.R., and S.J. Kline, 1974. J. Fluid Mech., 62, pp 223-239.

Panton, R.L., and J.H. Linebarger, 1974. J. Fluid Mech., 65, 261-287.

Patel, V.C., 1965. J. Fluid Mech., 23, pp 185-208.

Patel, V.C., and M.R. Head, 1968. J. Fluid Mech., 34, pp 371-392.

Perkins, K.R., and D.M. McEligot, 1975. J. Heat Transfer, 97, pp 589-593.

Perry, A.E., K.L. Lim and S.M. Henbest, 1987. J. Fluid Mech., 177, 437-466.

Randolph, M., 1983. Diplomarbeit, Böttingen.

Randolph, M., 1988. Ph.D. thesis, Univ. Göttingen, BRD.

Rao, K.N., R. Narasimha and M.A. Badri Narayanan, 1971. J. Fluid Mech., 48, pp 339-352.

Rodi, W 1980. Turbulence Models and Their Application in Hydraulics. IAHR, Delft.

Schloemer, H.H., 1967. J. Acoust. Soc. Amer., 42, pp 93-113.

Schubert, G., and G.M. Corcos, 1967. J. Fluid Mech., 29, pp 113-135.

Sharma, L.K. and W.W. Willmarth, 1980. Study of turbulent structure with hot wires smaller than the viscous length. University of Michigan, manuscript in preparation for J. Fluid Mech.

Shehata, A.M., 1984. Ph.D. thesis, Univ. Arizona.

Simpson, R.L., 1979. Proc., 2nd. Int. Symp. Turb. Shear Flow.

Simpson, R.L., M. Ghodbane and B.E. McGrath, 1987. J. Fluid Mech., 177, pp 76-335.

Spalart, P.R., 1986. J. Fluid Mech., 172, pp 307-328.

Spalart, P.R., 1990. Personal communication, NASA Ames Research Center.

Sreenivasan, K.R., A. Prabhu and R. Narasimha, 1983. J. Fluid Mech., 127, pp 251-272.

Strickland, J.H., and R.L. Simpson, 1975. Phys. Fluids, 18, pp 306-308.

Subramanian, C.S., S. Rajagopalan, R.A. Antonia and A.J. Chambers, 1982. J. Fluid Mech., 123, pp 335-362.

Thomas, A.S.W., and M.K. Bull, 1983. J. Fluid Mech., 128, pp 283-322.

Tiederman, W.G., T.S. Luchik and D.G. Bogard, 1985. J. Fluid Mech., 156, pp 419-437.

van Driest, E.R., 1956. J. Aerospace Sci., 23, pp 1007-1011 and 1036.

REFERENCES CITED (Cont'd.)

Wallace, J.H., R.S. Brodkey and H. Eckelmann, 1977. J. Fluid Mech., 83, pp 673-693.

Wallace, J.H., H. Eckelmann and R.S. Brodkey, 1972. J. Fluid Mech., 54, pp 39-48.

Wells, C.S. and J.G. Spangler, 1967. Phys. Fluids, 10, p 1890.

White, J.B., and W.G. Tiederman, 1990. The effect of adverse pressure gradient on turbulent burst structure in low-Reynolds number equilibrium boundary layers. Report PME-FM-90-2, Purdue Univ.

White, W.D., and D.M. McEligot, 1970. J. Basic Eng., 92, pp 411-418.

Willmarth, W.W., 1975. Adv. Appl. Mech., 15, pp 159-254.

Zakkay, V., V. Barra and K. Hozumi, 1979. AGARD-CP-271.

DISTRIBUTION LIST

Mr. V.J. Monacella, Code 1505
Scientific Officer
ONR Applied Hydrodynamics Research Program
David Taylor Research Center
Bethesda, MD 20084-5000

Mr. James A. Fein, Code 1215
Program Manager
Applied Hydrodynamics Research Program
Office of Naval Research
800 North Quincy Street
Arlington, VA 22217

Dr. E.P. Rood, Jr., Code 1132F
Office of Naval Research
800 N. Quincy Street
Arlington, VA 22217

Dr. M.M. Reischman, Code 1132
Office of Naval Research
800 North Quincy Street
Arlington, VA 22217

Dr. Spiro G. Lekoudis, Code 1132F
Office of Naval Research
800 North Quincy Street
Arlington, VA 22217

Mr. Edward Comstock (SEA-55W3)
Naval Sea Systems Command
Washington, DC 20362

Dr. T. Peirce (SEA-63R31)
Naval Sea Systems Command
Washington, DC 20362

Library (SEA-99612)
Naval Sea Systems Command
Washington, DC 20362

Dr. T.S. Momiyama (AIR-0931)
Research and Technology Directorate
Naval Air Systems Command
Washington, DC 20361-0931

Defense Technical Information Center
Bldg. 5, Cameron Station
Alexandria, VA 22314

Dr. P.Henrik Alfredsson
Department of Mechaniks
Royal Institute of Technology
S-10044 Stockholm
SWEDEN

Dr. J.L. Altman, Dept. 721, Bldg. 2
Westinghouse Electric Corporation
Naval Systems Division
18901 Euclid Avenue
Cleveland, OH 44117

Dr. Win Aung, Director
Division of Mechanics, Structures and
Materials Engineering
National Science Foundation
1800 G Street NW
Washington, DC 20550

Dr.Henry P. Bakewell Code 3241
New London Laboratory, Bldg .80
Naval Underwater Systems Center
New London, CT 06320

Dr. R.F. Blackwelder
Aerospace Engineering
University of Southern California
Los Angeles, CA 90089

Dr. Wm. K. Blake, Code 1905
David Taylor Research Center
Bethesda, MD 20084-5000

Prof. Peter Bradshaw
Thermosciences Division,
Mechanical Engineering Department
Stanford, CA 94305-3030

Prof. R.S. Brodkey
Dept. Chemical Engineering
Ohio State University
Columbus, OH 43210

Dr. Dennis Bushnell, Head
Viscous Flow Branch, High-Speed Aerodynamics
NASA Langley Research Center
Hampton, VA 23365

DISTRIBUTION LIST (Cont'd.)

Prof. Frank W. Chambers
Mechanical or Aerospace Engineering
Oklahoma State University
Stillwater, OK 74078-0545

Prof. C.F. Chen
Aero. Mechanical Engineering Department
University of Arizona
Tucson, AZ 85721

Dr. S. Deutsch
Applied Research Laboratory
Pennsylvania State University
P.O. Box 30
State College, PA 16801

Dr. S.C. Dickinson, Head, Code 8214
Fluid Mechanics Branch
Naval Underwater Systems Center
Newport, RI 02841

Dr. R.B. Duffy
Energy and Systems Technology
Idaho National Engineering Laboratory
P.O. Box 1625
Idaho Falls, Idaho 83415

Prof. Dr. F. Durst
Lehrstuhl für Strömungsmechanik
Universitat Erlangen-Nurnberg
Cauerstraße 4
D-8520 Erlangen
WEST GERMANY

Dr. Helmut Eckelmann
Max-Planck-Institut für Strömungsforschung
Postfach 2853
D-3400 Göttingen
WEST GERMANY

Prof. Robt. E. Falco
Mechanical Engineering Department
Michigan State University
East Lansing, MI 48824-1326

Dr. Charles L.S. Farn, Manager
Heat Transfer & Fluid Dynamics
Science and Technology Center
Westinghouse Electric Corporation
1310 Beulah Road
Pittsburgh, PA 15235

Prof. John F. Foss
Mechanical Engineering Department
Michigan State University
East Lansing, MI 48824-1326

Dr. Robt. A. Handler, Code 4430
Naval Research Laboratory
Washington, DC 20375-5000

Prof. T.J. Hanratty
Chemical Engineering
1209 West California St. - Box C-3
University of Illinois
Urbana, IL 61801

Prof. J.H. Haritonides 37-467
Aero. Engineering Dept.
Massachusetts Institute of Technology
Cambridge, MA 02139

Dr. Eric W. Hendricks, Code 634
Naval Ocean Systems Center
271 Catalina Blvd.
San Diego, CA 92152-5000

Dr. Larry E. Hochreiter
Consulting Engineer
Westinghouse NES
P.O. Box 355
Pittsburgh, PA 15230

Dr. T.T. Huang
David Taylor Research Center
Carderock Laboratory
Bethesda, MD 20084

Dr. Julian C.R. Hunt
Department of Applied Mathematics and
Theoretical Physics
University of Cambridge
Silver Street
Cambridge CB3 9EW
ENGLAND

Dr. Arne V. Johansson
Department of Mechaniks
Royal Institute of Technology
S-10044 Stockholm
SWEDEN

DISTRIBUTION LIST (Cont'd.)

Dr. Howard Julian
Mechanical Engineering Department
New Mexico State University
Box 3001/Dept. 3450
Las Cruces, NM 88003-3001

Prof. N. Kasagi
Mechanical Engineering Department
University of Tokyo
Bunkyo-ku, Tokyo, 113
JAPAN

Prof. Matthew D. Kelleher
Mechanical Engineering
U.S. Naval Postgraduate School
Monterey, CA 93940

Dr. John Kim
Computational Fluid Mechanics Branch
NASA Ames Research Center
Moffett Field, CA 94035

Prof. S.J. Kline
Mechanical Engineering Department
Stanford University
Stanford, CA 94305

Prof. M.T. Landahl
Aeronautics Department, Room 33-219
Massachusetts Institute of Technology
77 Massachusetts Avenue
Cambridge, MA 02139

Prof. B.E. Launder
Mechanical Engineering
University of Manchester
Institute of Science and Technology
P.O. Box 88
Manchester, M60 1QD
ENGLAND

Prof. Patrick Leehey 3-264
Acoustics and Vibrations Laboratory
Mechanical Engineering
Massachusetts Institute of Technology
Cambridge, MA 02139

Dr. M.A. Leschziner
Mechanical Engineering Dept.
University of Manchester
Institute of Science and Technology
P.O. Box 88
Manchester M60 1QD
ENGLAND

Prof. R.C. Lessmann
Mechanical Engineering
University of Rhode Island
Kingston, RI 02881

Prof. H.W. Liepmann
Aeronautics Department
California Institute of Technology
Pasadena, CA 91125

Dr. J.A. Lovett, Room ESB-104
Corporate Research and Development Center
Bldg. K-1
General Electric Company
P.O. Box 8
Schenectady, NY 12301

Prof. J.L. Lumley
Aeronautical Engineering
Cornell University
Ithaca, NY 14853

Mr. Peter Madden, Dept. 721, Bldg. 2
Westinghouse Electric Corporation
Naval Systems Division
18901 Euclid Avenue
Cleveland, OH 44117

Dr. James McMichael
Aerospace Sciences/Fluid Mechanics
Air Force Office of Scientific Research
Bolling AFB
Washington, DC 20322

Prof. M.V. Morkovin
Mechanical Engineering
Illinois Institute of Technology
3300 S. Federal
Chicago, IL 60616

Dr. Donald M. McEligot
P.O. Box 4008
Middletown, RI 02840

DISTRIBUTION LIST (Cont'd.)

Prof. C.L. Merkle
Dept. of Mechanical Engineering
Pennsylvania State University
University Park, PA 16802

Prof. R.J. Moffat
Mechanical Engineering Department
Stanford University
Stanford, CA 94305

Dr. R.F. Mons (MS 9105)
Westinghouse Oceanic Division
P.O. Box 1488
Annapolis, MD 21404

Dr. H.D. Murphy (MS D450)
MEE-DO
Los Alamos National Laboratory
Los Alamos, NM 87545

Prof. Ronald L. Panton
Mechanical Engineering Dept.
University of Texas
Austin, TX 78712-1063

Prof. H.C. Perkins
Aero. Mechanical Engineering Department
University of Arizona
Tucson, AZ 85721

Dr. Michael Randolph
DFVLR/AVA
Bunsenstrasse 7
D-3400 Göttingen
WEST GERMANY

Prof. Eli Reshotko
Mechanical and Aerospace Engineering
Case Western Reserve University
Cleveland, OH 44106

Dr. Steven K. Robinson
Viscous Flow Branch, High-Speed Aerodynamics
NASA Langley Research Center
Hampton, VA 23365

Prof. D.O. Rockwell
Mechanical Engineering Department
Lehigh University
Bethleham, PA 18015

Mr. Richard E. Ryan, Manager (M/S EB1)
Missile Launching and Handling
Marine Division
Westinghouse Electric Corporation
P.O. Box 3499
Sunnyvale, CA 94088-3499

Dr. H.H. Schloemer (Code 2133)
Naval Underwater Systems Center
New London Laboratory, Bldg. 44
New London, CT 06320

Prof. William R. Sears
Aero. Mechanical Engineering Department
University of Arizona
Tucson, AZ 85721

Dr. Robert J. Simoneau
Turbine Cooling
NASA Lewis Research Center
21000 Brookpark Road
Cleveland, OH 44135

Dr. Helmut Sobiezcky
DFVLR/AVA
Bunsenstrasse 7
D-3400 Göttingen
WEST GERMANY

Prof. Roger L. Simpson
Department of Aerospace and Ocean Engineering
Virginia Polytechnic Institute
and State University
Blacksburg, VA 24061

Prof. C.R. Smith
Mechanical Engineering Department
Lehigh University
Bethleham, PA 18015

Prof. A.J. Smits
Mechanical and Aerospace Engineering
Princeton University
Princeton, NJ 08544

Dr. Philippe R. Spalart
Computational Fluid Mechanics Branch
NASA Ames Research Center
Moffett Field, CA 94035

DISTRIBUTION LIST (Cont'd.)

Prof. K.R. Sreenivasan
Mechanical Engineering Department
Yale University
New Haven, CT 06510

Prof. William G. Tiederman
School of Mechanical Engineering
Purdue University
W. Lafayette, Indiana 47907

Prof. J.D.A. Walker
Mechanical Engineering Department
Lehigh Univeristy
Bethleham, PA 18015

Dr. William A. von Winkle (Code 31)
Naval Underwater Systems Center
New London Laboratory, Bldg. 36
New London, CT 06320

Prof. James M. Wallace
Mechanical Engineering
University of Maryland
College Park, MD 20742

Prof. Frank M. White
Mechanical Engineering Department
University of Rhode Island
Kingston, RI 02881

Prof. J.H. Whitelaw
Mechanical Engineering
Imperial College
Exhibition Road
London SW7 2BX
ENGLAND

Prof. W.W. Willmarth
Aeronautical Engineering
University of Michigan
Ann Arbor, MI 48104

Prof. I. Wygnanski
Aero. Mechanical Engineering Department
University of Arizona
Tucson, AZ 85721